FACULTY OF SCIENCE
UNIVERSITY OF COPENHAGEN

University of Copenhagen
The Niels Bohr Institute

A Thesis Presented for the Degree of
Cand. Scient. in Physics

Pore theory in pure lipid membranes

From soft perforation to oscillating reversible electrical breakdown under voltage clamp conditions

by

Klaus Bruun Pedersen
(110383 - xxxx)

Supervisor:
Thomas Heimburg

Copenhagen, 2010

The thesis is submitted to fulfill the requirements for the M.Sc. in Biophysics at the Niels Bohr Institute, Faculty of Science, University of Copenhagen, Denmark. The experimental work was conducted at the Niels Bohr Institute, University of Copenhagen from September 2009 to May 2010.

Acknowledgments

First of all I would like to thank Thomas Heimburg for supervision and inspiration. The experimental work of this thesis was been carried out in the Membrane biophysics group at NBI. I would like to thank everybody in the group. In particular I owe Andreas Blicher and Katrine Rude Laub a great, big thanks for preparing and developing the experimental setup. I would like to thank everybody at the C-floor for academic as well as social inputs. Thanks to Ninna Struck Rossen, Pia Cordsen, Niels Bjerre, Anders Kyrstng and Simone Hald for comments and proof-reading. Finally a much deserved thanks to my family, friends and kannibalgangen for moral support.

Resumé

Iontransport over cellemembraner forklares i litteraturen og i lærebøger som transport via proteinkanaler. Elektroporation er en sjælden undtagelse. Elektroporation er et reversibelt elektrisk nedbrud af membranen. Membranen bliver gjort kortvarigt gennemtrænglig for ioner og molekyler ved hjælp af en elektrisk spændingspuls, der danner porer i membranen. Grundet de høje spændinger, der benyttes ved elektroporation bliver poreteorierne inden for feltet ikke benyttet i biologisk regi. I dette speciale undersøger jeg elektriske strømme gennem membraner (Proteinfri *black lipid membranes*) under *voltage clamp* forhold i faseovergangen. Jeg finder proteinkanal-lignende strømme, reversible elektriske nedbrud samt oscillerende reversible elektriske nedbrud af membranen.

Teoretisk såvel som eksperimentielt finder jeg, at den spændig, der skal til for at skabe reversible elektriske nedbrud af membranen mindskes, når membranen befinder sig i dennes faseovergang. Derfor foreslår jeg, at andre electriske fænomener såsom proteinkanal-lignende strømme og oscillerende reversible elektriske nedbrud kan forklares ved de samme poremodeller, der beskriver elektroporation.

Jeg diskuterer to poremodeller med henblik på, at forklare proteinkanal-lignede strømme og oscillerende reversible elektriske nedbrud gennem en negativ feedback mekanisme i spænding/poreradius forholdet. Jeg konkluderer at begge fænomener kan forklares ved hjælp af de to poremodeller

Abstract

The movement of ions through the cell membrane is in the literature and in textbooks explained by the action of protein ion channels. An exception is the field of *electroporation*. Electroporation is a temporary reversible electrical breakdown induced by lipid channels in the membrane. The lipid channels are caused by large trans membrane voltages, hence the pore models of electroporation are not considered relevant for voltages in the biological regime.

In this thesis I investigate currents through membranes (protein free *black lipid membranes*) under voltage clamp conditions in the phase transition. I find *channel-like events*, *electroporation events* and *oscillating reversible electrical breakdown*.

Theoretically and experimentally, I find that the voltage required for electroporation events such as reversible and irreversible electrical breakdown is lowered in the phases transition of the membrane. I propose, that other electrical phenomena, such as channel-like events and oscillating reversible electrical breakdown, can be explained by the pore models of electroporation.

I discuss the ability of two different pore models, to account for channel-like events and oscillating reversible breakdown through a negative feedback mechanism in the voltage-pore radius relation. I conclude that both events can be explained by the investigated pore models.

Contents

Motivation

Simple models with deep explanatory power are compelling. Classical Newtonian mechanics predicts the trajectory of falling bodies with divine precision. In three equations it unites the physics of apples falling from trees with the astronomical principles of the sun and stars moving in the sky.
The notion of congruence in the principles behind the diverse range of phenomena in life, and the notion of order in a chaotic world is what drove me to study physics.

Biophysics is an emerging scientific field. The field is biology but the approach and the concepts are transfered from physics.
The physical approach can impudently be summarized in the following quote:

"Everything should be made as simple as possible, but not simpler."

-Albert Einstein

To describe the data of a given experimental phenomenon, a model is proposed based on some simplifying assumptions. If the model succeeds in describing the data, the model is good.
In the contrary case, the model is dropped or modified. By adding more variables the system can gain extra degrees of freedom and increased explanatory power.
There is a pending danger in the last step. Any phenomenon can be adequately described with enough variables. Hence, a model should not only be judged on its explanatory power, but also on its simplicity.

In biochemistry, the principles are many and the applicability is often narrow. The equations in textbooks are specific and their genesis is opaque. In most cases, the equations are derived from thermodynamics, but the derivations and the underlying assumptions are often left behind.

The basic abstraction of thermodynamics is the division of the world into systems. The systems under consideration are chosen to reflect a given problem and assigned a number of variables. The system is controlled by these variables and other variables are assumed to be constant. Depending on how the system is controlled, a state function is chosen, which describes the equilibrium state of the system in a useful manner.
In chemical processes the pressure is often taken to be constant, hence the Gibbs free energy is a commonly used function of state in biochemistry.
The laws of thermodynamics are rules regarding the interaction of systems. They are the simple first principles from which everything else is deduced.It is here the beauty resides.

"The 2nd law of thermodynamics has the same degree of truth as the statement that if you throw a tumblerful of water into the sea, you cannot get the same tumblerful of water out again."

James Clerk Maxwell

"Books are not made to be believed, but to be subjected to inquiry."

William of Baskerville
("The Name of the Rose" by Umberto Eco.)

Objectives

In this thesis I will give an introduction into the thermodynamic description of the membrane and deduce some relevant physical properties of the membrane. In the light of these properties I will discuss the membrane permeability for ions and especially lipid channels.

A *black lipid membrane* (BLM) is a simplified version of a real biological membrane. The movement of ions across a BLM can be studied as a current, when a constant voltage is upheld across the membrane. This technique is called *voltage clamp*.
My focus in the present thesis is the movement of ions across a BLM observed under voltage clamp conditions.

Experimentally and through comparison with theory I will respond to the following objectives:

- BLMs have been shown to exhibit quantized conductance changes with magnitude and opening times identical to the conductance of protein ion channels.
  I will confirm the findings of channel-like events in BLM and present and discuss two models for voltage induced lipid ion channels in BLMs.
- Reversible electrical breakdown is a phenomenon used in electroporation. A membrane is made temporarily permeable to drugs, probes and electrons by a large applied voltage pulse. Under certain conditions this phenomenon was found to oscillate. I will propose a qualitative electrical pore model for the oscillating phenomenon of reversible electrical breakdown.
- Finally, I will substantiate that the mechanism for channel-like events is the same as for the reversible electrical breakdown.

Chapter 1

The membrane

The purpose of this chapter is to provide essential knowledge of the biological membrane relevant for this thesis.
I will briefly present a thermodynamic description of the membrane and deduce some physical properties of the membrane that are relevant for the following chapters.

1.1 The membrane - A cell component

Cells are the basic building blocks of life. *Cellula* is Latin for *small room*. The walls confining the cell are essentially an arrangement of lipids. A barrier that is as essential to the cell as walls are to a room. It separates the cell interior from its surroundings and makes it possible to maintain high concentrations of important matter.
The biological cell membrane has the form of a sphere and is composed of lipids and proteins neatly arranged into a *bilayer matrix* (see figure 1.1). The bilayer matrix was first described by Singer and Nicholson in 1972 [Singer and Nicolson, 1972].
The formation of the bilayer matrix is not a result of an active process involving enzymes and other proteins, it is the result of a spontaneous phenomenon that requires only water and lipids.
The lipids are amphiphilic molecules consisting of a hydrophilic head group and a number of hydrophobic tails. Each tail is a long chain of CH_2-groups that mixes very poorly with water. A lipid freely dispersed in water corresponds to a state of high interaction free energy. Therefore, a conformation of evenly distributed lipids in water is very unlikely. The more probable states are those which reduce the lipid tail/water-surface. The bilayer matrix conformation is one of these probable states. Two layers of lipids are arranged parallel to each other with tail-to-tail with the lipid head groups of each layer facing the water. In this manner, the lipid tail are shielded from the water (see figure 1.1). Other examples of low energy conformations are micelles, tubes, etc.

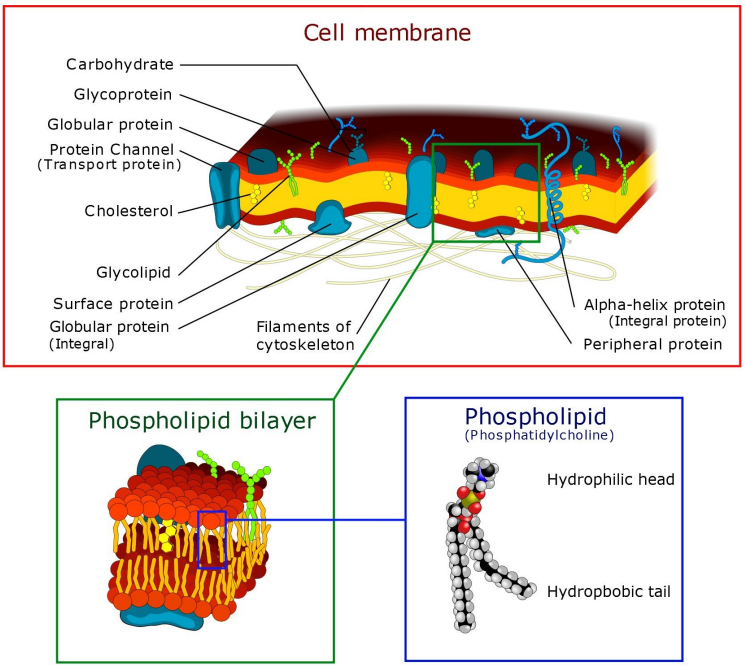

Figure 1.1: *Typical picture of a cell membrane. From wikipedia.org*

Besides a great variety of lipids, a cell membrane contains proteins. The proteins can either bind to, be partly embedded in, or penetrate the membrane.
The membrane confines the cell interior but it is not impermeable. Small, uncharged, polar molecules and gases can diffuse through it. Larger molecules and ions cannot pass, they require a specific membrane transport protein to cross the membrane.

The membrane has not played an important role in classical molecular biology. It has been viewed as a passive insulating barrier which of course is essential to prevent diffusion and to preserve an electrical potential. More complex phenomena such as *gated channeling* have been associated with membrane proteins due to their more complex nature.
As I will describe in the following section, biological membranes are dynamic entities with physical properties that provides much complexity.

1.2 Thermodynamics of the membrane

As described in the previous section, biological membranes are complex entities. The experiments in this thesis, on the other hand, are performed on BLMs. BLMs are typically composed of 1 - 3 different lipids, no proteins and no cytoskeleton. It is appropriate

to ask:
Have I simplified the system too much in order to say anything about the complex biological membrane? Do the results obtained have any biological relevance?
Yes, they do. The basic structure of amphiphilic molecules arranged in a bilayer is the same and the cellmembrane share a lot of properties with the BLM. The thickness and the capacitance are similar [Haydon, 1971, Weaver and Chizmadzhev, 1996]. Furthermore the simplification allows us to isolate the properties of lipid membranes and rule out the actions of proteins and other membranebound substances.

1.2.1 Phases of the membrane

The BLM can exhibit different phases. The transitions between these phases are controlled by a number of thermodynamic variables such as temperature, pressure, pH, electrical field strength, etc. The transitions are associated with a nonlinearity in the first derivatives of some of the systems thermodynamic variables. Up until the transition the increase in temperature is approximately proportional to the energy uptake. When energy is added to the system, the temperature increases linearly. In the transition, energy can be added or removed from the system without effecting the temperature. The excess energy is used to alter the subconfigurations of the system.
Four states of the membrane are defined:

- L_c - Liquid Crystalline phase (low temperatures)
- L_β - Gel phase
- P'_β - Ripple phase
- L_α - Fluid phase (high temperatures)

I will only be concerned with the main transition referring to the shift from P'_β to L_α since this transition is in the proximity of biological temperature regime and since it is the transition of highest excess energy. The phases below this transition will be denoted *gel*-state as opposed to the *liquid*-state above the transition.

Information about the transitions can be derived from the attributes of the subcomponents of the membrane; mainly the lipid tails. It is here the excess energy is absorbed. A lipid tail can bend in all its C-C-joints. Each saturated C-C-joint has 3 possible configurations. One trans and two gauche (see figure 1.2). If the joint is unsaturated the double-bond between the carbon atoms disables bending.

The state of a lipid with gauche configurations have a higher internal energy and the state is therefore less probable when the temperature is low. At higher temperatures

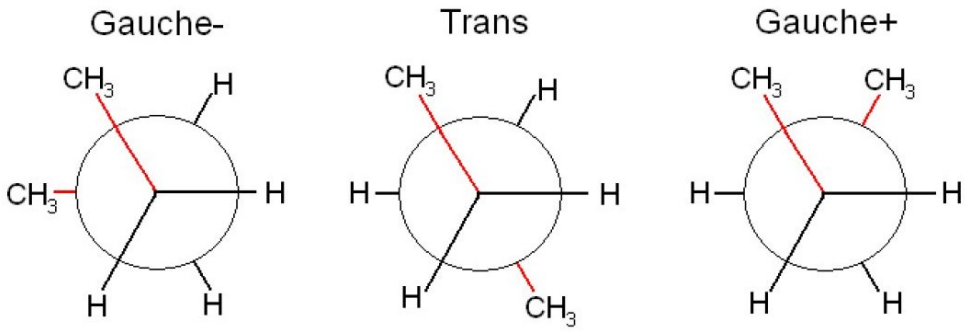

Figure 1.2: *The three possible configurations. The gauche configuration corresponds to a +/- 120° bending of the lipid-tail. The gauche configurations cost more free energy than the trans configuration and is thus only accessible under high temperatures.*

the two gauche configurations become accessible as the energy gab between trans- and gauche configurations becomes negligible. Each configuration will then be accessed approximately $1/3$. of the time which results in $1/3$. trans- and $2/3$. gauche configurations. The gauche configuration corresponds to a +/- 120° bending of the lipid-tail. This prompts a shorter but broader lipid-tail. Moving from gel to liquid, the membrane area may increase with as much as 26% [Leirer et al., 2009] and the thickness with as much as -16% [Heimburg, 2008]. Hence, the micro states of the lipid tails affects macro states of the membrane. In the transition, other mechanical properties of the membrane are also drastically altered.

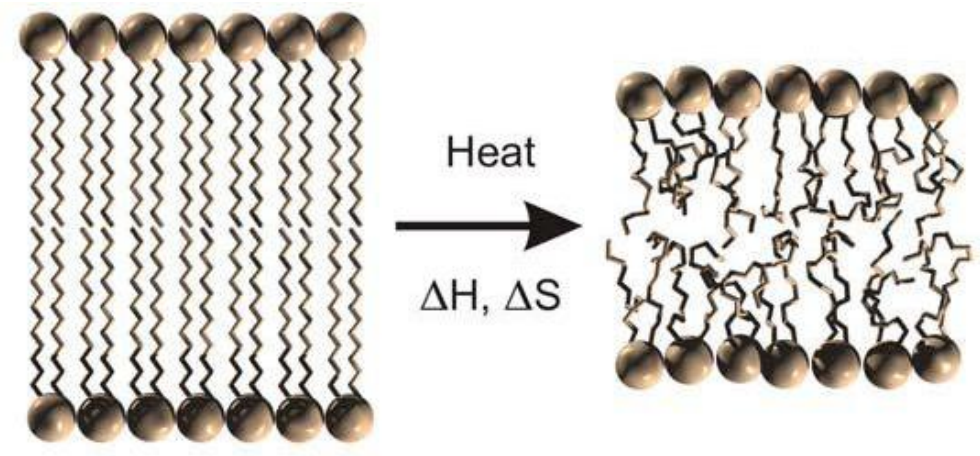

Figure 1.3: *The effect of lipid tail configurations on the state of the membrane [Blicher et al., 2009].*

1.2.2 Locating the phase transition

As stated above, I will only be concerned with the two states liquid and gel. The associated phase transition, melting transition or main transition will from this point just be denoted *the transition*. In the following pages I will deduce an expression for the heatcapacity as a function of temperature.

I will regard a membrane consisting of a single lipid species.
In order to make thermodynamic calculations on the membrane, I will make some justified, simplifying assumptions:

- A lipid can exist in two states gel (g) or liquid (l)
- Each state is associated with an enthalpy (H_g and H_l)
- The probability of any given state of a lipid is dependent on the temperature and independent of other lipids
- At the melting temperature T_m both states are equally likely.
  ($P_l(T_m) = P_g(T_m) = 0.5$)

Comparison with experimental data will reveal whether the assumptions are reasonable.
The probability P_l of a lipid being in the state l can be obtained from the canonical ensemble,

$$P_l = \frac{\Omega_l e^{\frac{-H_l}{k_b T}}}{Z}, \tag{1.1}$$

where Ω_l is the degeneracy of the state l, k_b is the Boltzmann constant, T is the temperature and Z is the partition function.
I only have two possible states, hence Z becomes:

$$Z = \Omega_g e^{\frac{-H_g}{k_b T}} + \Omega_l e^{\frac{-H_l}{k_b T}}. \tag{1.2}$$

I write out P_l and express it in terms of the equilibrium constant K;

$$K \equiv \Omega_l/\Omega_g \cdot e^{\frac{-\Delta H}{k_b T}} = e^{\frac{-(\Delta H - T\cdot\Delta S}{k_b T}}), \tag{1.3}$$

where $\Delta S = k_b \ln(\Omega_l/\Omega_g)$ is the entropy change. P_l becomes

$$P_l = \frac{\Omega_l e^{\frac{-H_l}{k_b T}}}{\Omega_g e^{\frac{-H_g}{k_b T}} + \Omega_l e^{\frac{-H_l}{k_b T}}} = \frac{\Omega_l/\Omega_g \cdot e^{\frac{-\Delta H}{k_b T}}}{1 + \Omega_l/\Omega_g e^{\frac{-\Delta H}{k_b T}}} = \frac{K}{1+K}. \tag{1.4}$$

I obtain P_g from $P_l + P_g = 1$ since the system is confined to two states,

$$P_g = \frac{1}{K+1}. \tag{1.5}$$

The membrane excess heatcapacity is defined as

$$c_p = \frac{\delta\langle\Delta H\rangle}{\delta T}\Big|_p. \tag{1.6}$$

The mean enthalpy change $\langle\Delta H\rangle$ is the enthalpy change times the probability of the state l (from gel to liquid)

$$\langle\Delta H\rangle = \Delta H \cdot P_l = \Delta H \frac{K}{1+K}. \tag{1.7}$$

Using the van't Hoff law ($\frac{d\ln K}{dT} = \frac{\Delta H}{RT^2}$) on equation 1.3 and inserting into equation 1.7 I obtain the heat capacity as a function of temperature,

$$c_p = \frac{K}{(1+K)^2} \cdot \frac{\Delta H^2}{RT^2}. \tag{1.8}$$

1.2.3 Cooperativity and domain formation

In the previous section I have obtained an expression for the heat capacity as a function of temperature for a membrane composed of a single lipid species (See equation 1.8) The heat capacity is easy to measure as a function of temperature using Differential Scanning Calorimetry (DSC). The excess enthalpy of the transition can be obtained by fitting the c_p-function to experimental data.
As I will show later in this paper, a lot of other membrane properties are closely related to the c_p-profile. Hence, a lot of interesting information can be obtained from equation 1.8.

Are the assumptions I made in order to obtain equation 1.8 justified?
Not quite. The c_p-peak of the transition is much more narrow in experiments than obtained fromequation 1.8. This discrepancy is due to lipid *cooperation*. When a lipid changes state from gel to liquid it becomes shorter. If the states of the surrounding lipids are unaltered, the difference in height exposes part of the hydrophilic tails of the neighboring gel-lipids. The state of each lipid affects the neighbors. This effect causes cooperativity in the transition and an epidemic change of states across the membrane over a short range in the transition.
The cooperativity can be accounted for by assuming a cooperative unit size n. The cooperativity alters the energy and the entropy of the system as follows:

$$\begin{aligned} \Delta H &\rightarrow n\Delta H \\ \Delta G &\rightarrow n\Delta G \\ \Delta S &\rightarrow n\Delta S \end{aligned} \tag{1.9}$$

and is a measure for how cooperative the lipids act in transition [Heimburg, 2010a].
The number of carbon atoms in the lipid tail varies between different species. This number determines the length of the lipid tail. When a lipid is composed of more than a single lipid species the varying lipid lengths lower the cooperativity. Moreover the extra

C-*C*-bonds increases the melting temperature [Lewis and Engelman, 1983].
In the case of two-lipid membranes the lipids may arrange and form coexisting domains of gel and liquid lipids. Multi lipid membranes consequently have broader transitions than membranes composed of a single lipid species.

The state of a membrane is not only a function of temperature. The internal energy of each lipid depends on other thermodynamic variables such as pH, pressure, voltage, chemical potential, etc. A high lateral pressure in the membrane will favor the gel state since it takes up less space. This shifts the transition to higher temperatures.
Other impurities such as organic solubles and membrane bound proteins also affect the transition [Fidorra, 2004].
Anesthetic compounds dissolve well in the membrane and have been shown to shift the transition [Græsbøll, 2006].

1.2.4 Elasticity of the membrane

I have obtained the heat capacity of a membrane and shown that the c_p-profile has its maximum in the transition.
In the following, I will relate the area and volume compressibility to the heat capacity of the membrane. In this manner I can show what influence the temperature has on compressibility and the ability to bend for the membrane.

The volume compressibility is defined as [Ebel et al., 2001]

$$\kappa_T^V = -\frac{1}{\langle V\rangle}\frac{d\langle V\rangle}{dp}\Big|_T, \tag{1.10}$$

where p is the pressure and $\langle V\rangle$ is the thermodynamic average of the volume calculated from the different volume states and their respective energies,

$$\langle V\rangle = \frac{\Sigma_i V_i \exp(-H_i/RT)}{\Sigma_i \exp(-H_i/RT)}. \tag{1.11}$$

By carrying out the differentiation of equation 1.10 and inserting equation 1.11 I obtain the compressibility expressed as fluctuations in volume,

$$\kappa_T^V = \frac{\langle V^2\rangle - \langle V\rangle^2}{\langle V\rangle \cdot RT}. \tag{1.12}$$

Similarly, I can obtain expressions for the area compressibility with area fluctuations,

$$\kappa_T^A = \frac{\langle A^2\rangle - \langle A\rangle^2}{\langle A\rangle \cdot RT}. \tag{1.13}$$

To obtain a similar expression for the heatcapacity I insert the thermodynamic average $\langle H\rangle$ into the heat capacity function (equation 1.6 again),

$$c_p = \frac{d\langle H\rangle}{dT}\Big|_p, \tag{1.14}$$

to obtain an expression in terms of the fluctuations in enthalpy [Hill, 1960],

$$c_p = \frac{\langle H^2 \rangle - \langle H \rangle^2}{RT^2}. \tag{1.15}$$

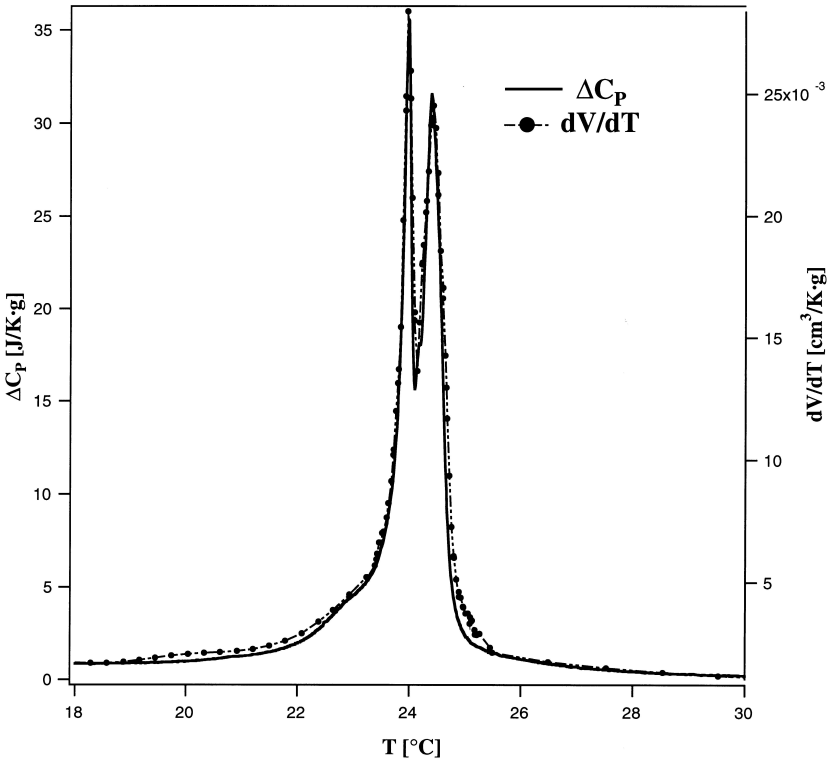

Figure 1.4: *Compressibility and heatcapacity as functions of temperature [Ebel et al., 2001].*

I define the volume of the membrane as a function of temperature;

$$V(T) = V_0(T) + \Delta V(T). \tag{1.16}$$

The first term on the right hand side of equation 1.16 accounts for the linear volume increase as a function of temperature and the second term is the non-linear area increase in the membrane transition. These assumptions are justified by the constant offset of dV/dT in figure 1.4 [Ebel et al., 2001].
Under these assumptions, the compressabilities are,

$$\kappa_T^V = -\frac{1}{V} \cdot \frac{dV_0}{dp}\Big|_T - \frac{1}{V} \cdot \frac{d(\Delta V(T)}{dp}\Big|_T = \kappa_{T,0}^V + \Delta\kappa_T^V \tag{1.17}$$

and

$$\kappa_T^A = -\frac{1}{A} \cdot \frac{dA_0}{dp}\Big|_T - \frac{1}{A} \cdot \frac{d(\Delta A(T)}{dp}\Big|_T = \kappa_{T,0}^A + \Delta\kappa_T^A. \tag{1.18}$$

The heat capacity can be expressed in a similar manner,

$$c_p = \frac{dH_0}{dT}\Big|_p + \frac{\Delta H(T)}{dT}\Big|_p = c_{p,0} + \Delta c_p. \tag{1.19}$$

It has been shown that the volume expansion and the heatcapacity are proportional functions in the proximity of the transition. The relation holds for various lipid mixtures [Anthony et al., 1981, Heimburg, 1998, Ebel et al., 2001] (See figure 1.4).
The excess heat capacity and the excess area- and volume change obey the relations,

$$\Delta V(T) = \xi_V \Delta H(T), \tag{1.20}$$

$$\Delta A(T) = \xi_A \Delta H(T). \tag{1.21}$$

The constants ξ_V $[m^3/J]$ and $\xi_A = 8,9$ $[m^2/J]$ are found experimentally [Heimburg, 2008]. They are roughly the same for different lipid mixtures.
From equations 1.17 - 1.21 I can calculate the excess compressabilities (for calculations see [Heimburg, 1998]).

$$\Delta\kappa_T^V = \frac{\xi_V^2 T}{V} \cdot \Delta c_p \tag{1.22}$$

and

$$\Delta\kappa_T^A = \frac{\xi_A^2 T}{A} \cdot \Delta c_p \tag{1.23}$$

I have obtained expressions for the area- and volume compressabilities. These functions are proportional to the heatcapacity. Consequently, I have a way of measuring the changes in the compressibility of the membrane.
c_p has a pronounced maximum in the transition, hence the membrane is also highly compressible in this regime.

1.2.4.1 Curvature

What consequences does the dramatic increase in membrane area- and volume compressibility during the transition have? In the following, I will describe how the increased compressibility can lower the free energy of bending the membrane.

The lipid bilayer is not merely a 2-dimensional *layer*. In the case of a cell membrane, it forms a sphere. Under certain conditions (pH, ionic strength, lipid concentration, etc.) lipids will form odd looking shapes as described in section 1.1.
It requires free energy to bend a membrane but it also requires energy to have the tails of the border-lipids exposed to water. This balance produces a complex energy landscape with numerous local energy-minima resulting in the different shapes.
When a membrane is bend the outer layer is expanded and inner layer is compressed. For an isotropic membrane, the bending modulus was thoroughly described by Helfrich in 1973 [Helfrich, 1973], Evans in 1974 [Evans, 1974] and many others.

The following calculations are from [Heimburg, 2010a, Helfrich, 1973, Evans, 1974].

The membrane can be regarded a lyotropic *liquid crystal* since the lipids are arranged parallel to the surface normal. A lipid in the membrane may diffuse in the plane but its orientation in the z-plane is determined by the amphiphilic nature of the lipids.

I regard a membrane in a coordinate system with z being parallel to the surface normal n while x and y are parallel to the plane.
The energy of curvature for a lipid vesicle may be written as

$$G = \oint_A \frac{1}{2} k_s \Big(\frac{\delta n_x}{\delta x} + \frac{\delta n_y}{\delta y} - c_0 \Big)^2 dA + \oint_A k_{ss} \Big(\frac{\delta n_x}{\delta x} \cdot \frac{\delta n_y}{\delta y} - \frac{\delta n_x}{\delta y} \cdot \frac{\delta n_y}{\delta x} \Big) dA, \tag{1.24}$$

where the area A is the closed surface of the membrane. k_s and k_{ss} are bending moduli with dimensions of energy. $\frac{\delta n_i}{\delta j}$ is a parameter for how much the surface normal n changes i-direction when n is parallel-displaced in the j-direction. Hence, the first term where $i = j$ describes the energy of the *splay* and the second term where $i \neq j$ describes the *saddle splay* of the membrane. c_0 is the spontaneous curvature of the membrane caused by chemical or physical differences on the two sides of the membrane. It allows for splay in the equilibrium if the conditions of the two sides vary.
For a sphere the saddle splay is zero but in other configurations it plays a role. An example involving saddle splay is the donut shape that can be obtained through the fusion of two poles of a vesicle.

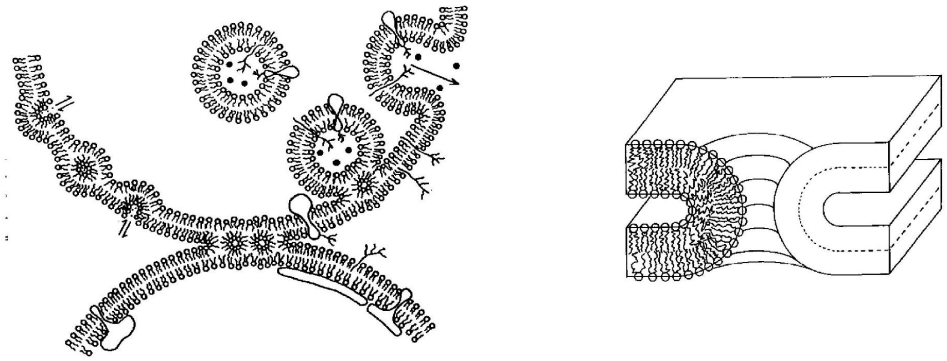

Figure 1.5: *The curvature in membrane fusion and. In the fusion process the membrane presumably exhibits a saddle node curvature [Heimburg, 2010a].*

The saddle splay energy of a vesicle with h donut-holes is given by

$$G_{ss} = \oint_A k_g \Big(\frac{\delta n_x}{\delta x} \cdot \frac{\delta n_y}{\delta y} - \frac{\delta n_x}{\delta y} \cdot \frac{\delta n_y}{\delta x} \Big) dA = k_{ss} 4\pi (1 - h). \tag{1.25}$$

1.2.4.2 Fluctuation and relaxation

The last physical property of membranes I will describe and relate to the transition, is the relaxation time.
The enthalpy of a membrane fluctuates around a mean enthalpy. The magnitude of the fluctuations are proportional to the temperature. When the system is brought out of balance by a small perturbation, it is quickly driven back to equilibrium by entropy forces. The rate with which the system is driven back to equilibrium depends on the magnitude of the perturbation and the relaxation time of the system.

Relaxation times in membranes were first investigated by Tsong and Kanehisa in 1977 through perturbations in pressure and volume. Experimentally they found the relaxation time of a membrane to be at a maximum in the transition [Tsong and Kanehisa, 1977].
Grabitz et al. [Grabitz et al., 2002] developed a model for the relaxation time in membranes. After a perturbation in pressure the relaxation time was measured and compared to calculations.
They assumed that fluctuations in enthalpy could be described by a normal distribution. Further, they assumed the two-state model for lipid melting described in section 1.2.2.
The following calculations are from [Seeger et al., 2007] and [Grabitz et al., 2002].
Consider a fluctuation in the enthalpy of the system,

$$\alpha = H - \langle H \rangle. \tag{1.26}$$

I assume that the distribution of perturbations α is Gaussian around $\langle H \rangle$

$$P(\alpha) = \frac{1}{\sigma\sqrt{2\pi}} \cdot e^{-\frac{\alpha^2}{2\sigma^2}}, \tag{1.27}$$

where the variance is

$$\sigma^2 = \langle H^2 \rangle - \langle H \rangle^2 \tag{1.28}$$

The Gibbs free energy depends linearly on $P(\alpha)$ [Lee and Kosterlitz, 1991]. Consequently, the entropy of the system can be approximated by a *well function* [Seeger et al., 2007]

$$S(\alpha) = -\frac{R\alpha^2}{2\sigma^2}, \tag{1.29}$$

where R is the gas constant.
In linear non equilibrium thermodynamics, the forces of the system are described by derivatives of the entropy with respect to the perturbations in the system variables.
Hence, the thermodynamic force X resulting from the perturbation α is

$$X(\alpha) = \frac{\delta S(\alpha)}{\delta \alpha} = -\frac{\alpha R}{\sigma^2} \tag{1.30}$$

The time evolution of the perturbation is described by the Onsager equation,

$$\frac{d\alpha}{dt} = L \cdot X(\alpha) = -L\frac{R\alpha}{\sigma^2} \tag{1.31}$$

where L is a *phenomenological constant*.
Integration of the phenomenological equation 1.31 yields

$$\alpha(t) = \alpha_0 \exp(-\frac{LR}{\sigma^2}t). \tag{1.32}$$

This function describes the exponential decay of a perturbation. The relaxation time can be obtained directly

$$\tau = -\frac{\sigma^2}{LR}. \tag{1.33}$$

From equations 1.28, 1.15 and 1.33 I can obtain an expression for the relaxation time τ as a function of the heat capacity,

$$\tau = \frac{T^2}{L}c_p. \tag{1.34}$$

This result was verified in simulations by Seeger et al. and Grabitz et al. [Seeger et al., 2007, Grabitz et al., 2002]. It tells us that the relaxation times are related to the heat capacity in a direct manner just as the compressabilities are.

Chapter 2

Membrane permeability

In this chapter, I will describe the movement of molecules and especially ions across a membrane. I will start by deducing an expression for the current flows of different ions across a membrane and the resulting potential of equilibrium.
Subsequently, I will describe the prevalent discipline used to describe ion- and molecule transport across membranes; Channelomics.
Finally, I will present a model for lipid channels that does not directly involve proteins. This model builds on the various physical properties of the membrane that I have outlined in chapter 1.

The membrane of a cell confines the organelles but it is not impermeable. Cells need a supply of sugar, amino acids, oxygen, etc. for maintenance. Further they need to get rid of waste substances.
Each molecule has its own affinity for crossing the membrane. Though most textbooks state that *membranes are impermeable to ions*, the truth is not that simple. Impermeable should not be interpreted similarly to *people can not walk through brick walls*. A better resemblance would be flies in a greenhouse with a small piece of glass missing. Most of the time the flies will ricochet off the glass but once in a while a fly escapes.

In the following, I will deduce the Goldman-Hodgkin-Katz equation that describes the current fluxes across a membrane and how the fluxes of different ions are coupled.
The movement of charges in an electric field is governed by Ohm's law. The flux of an ion with charge z, mobility μ in a potential U,

$$J_{field} = \sigma \cdot E = -\mu z[C]\frac{dU}{dx}. \tag{2.1}$$

From Fick's diffusion equation, I have the flux associated with diffusion

$$J_{diff} = -D\frac{dC}{dx}. \tag{2.2}$$

If I insert the Einstein relation $D = \frac{kT}{e}\mu$ describing the relation between friction and diffusion, I obtain an expression of the coupled flux;

$$\begin{aligned} J &= J_{diff} + J_{field} \\ J &= -\frac{\mu}{N_A}\left(z[C]\frac{dU}{dx} + \frac{RT}{F}\frac{d[C]}{dx}\right). \end{aligned} \tag{2.3}$$

This is closely related to the Nernst-Planck equation,

$$I = -\frac{\mu}{N_A}\left(z^2F[C]\frac{dU}{dx} + zRT\frac{d[C]}{dx}\right). \tag{2.4}$$

If I assume that the voltage change across the membrane is constant, I can write: $\frac{dU}{dx} = \frac{dU}{d}$, where d is the membrane thickness.
I will now make a definition, that by first glance may seem arbitrary, but eventually will turn out practical:

$$y = I - \frac{\mu}{N_A}z^2F[C]\frac{\Delta U}{d} \tag{2.5}$$

and consequently:

$$y = -\frac{zRT\mu}{N_A}\frac{d[C]}{dx}. \tag{2.6}$$

In the stationary state the net current is constant. I differentiate equation 2.5 with respect to x. and $\frac{dI}{dx}$ vanishes:

$$\frac{dy}{dx} = \frac{\mu z^2F\Delta U}{N_A l}\frac{d[C]}{dx}. \tag{2.7}$$

Next, I isolate $\frac{d[C]}{dx}$ from equation 2.7 and insert into 2.6:

$$y = \frac{zRT\mu N_A l}{N_A\mu z^2F\Delta U}\frac{dy}{x}y = \frac{RTd}{zF\Delta U}\frac{dy}{dx}. \tag{2.8}$$

I isolate dx,

$$dx = \frac{RTd}{zF\Delta U}\frac{dy}{y} \tag{2.9}$$

and make an integration across the membrane (from $x = 0$ to $x = d$)

$$\int_d^{x=0} dx = \int_{[C]_{x=0}}^{[C]_{x=d}} \frac{RTd}{zF\Delta U}\frac{dy}{y}. \tag{2.10}$$

I carry out the integration and obtain

$$d = \frac{RTd}{zF\Delta U}\ln\left(\frac{I - \frac{\mu z^2F\Delta U}{d}\beta[C]_{out}}{I - \frac{\mu z^2F\Delta U}{d}\beta[C]_{in}}\right), \tag{2.11}$$

where $[C]_{in} = \beta[C]_{x=0}$ is the concentration of ions *inside* and $[C]_{out} = \beta[C]_{x=d}$ is the concentration of ions *outside*.

I isolate I and obtain an expression for the current across a membrane for a single ion species

$$I = PzF\xi\Big(\frac{[C]_{in} - [C]_{out}\exp(-\xi)}{1 - \exp(-\xi)}\Big), \tag{2.12}$$

where $P = \frac{\beta\mu RT}{Fd}$ and $\xi = \frac{zF\Delta U}{RT}$ are constants.
Different ions have different affinities for crossing the membrane. This can cause the gradient of one ion to be large and as a consequence drive other ions across their gradients because of the electric field induced by the first ion.
I assume that only the ions sodium, potassium and chloride are present. In equilibrium when no net current flows ($I = I_{Na} + I_K + I_{Cl} = 0$).
The resting potential can be calculated;

$$\Delta U_{rest} = \frac{RT}{F}\ln\Big(\frac{P_{Na}[Na]_{out} + P_K[K]_{out} - P_{Cl}[Cl]_{in}}{P_{Na}[Na]_{in} + P_K[K]_{in} + P_{Cl}[Cl]_{out}}\Big). \tag{2.13}$$

This equation is called the *Goldman-Hodgkin-Katz voltage relation*. It is a very important equation for molecular biology and biophysics. It relates the potentials of different ions given their permeabilities.

2.1 Membrane Transport Proteins

Proteins are long chains of amino acids that fold up as complex entities. The sequence of amino acids uniquely determine the structure of the protein. The shape also depends on the thermodynamic state of the surroundings and it is highly coupled to the function of the protein. Especially membrane proteins are highly dependent on the membrane in which they are embedded. This makes them difficult to study as isolated entities. If they are studied without a membrane, they do not work. If they are observed in their natural complex environment, one cannot make unambiguous statements about their functions.

Protein channels play a major role in biology and biochemistry. They are held accountable for the movement of various molecules and ions across the, otherwise impermeable membrane. For each type of ion and molecule there is a specific protein channel. The widespread approach to study protein channels is by means of *channel blockers*. Channel blockers are agents that interfere with specific channel proteins and block them. The subsequent lack of channel activity is taken as a proof for the function of the protein channel. For ion channels, the opening and closing of a channel is measured as step-changes in conductance measured with patch clamp technique (see figure 2.1). The discipline is called *channelomics*.

The proteins spanning the membrane are called integral proteins. They consist of a number of subunits and are believed to govern the flow of ions across the membrane. They are ion-specific and can access multiple states (open/closed). The states can be *gated* by voltage, ligands, light, etc. meaning that changes within these parameters control the state of the protein. The voltage-gated sodium- and potassium channels are as

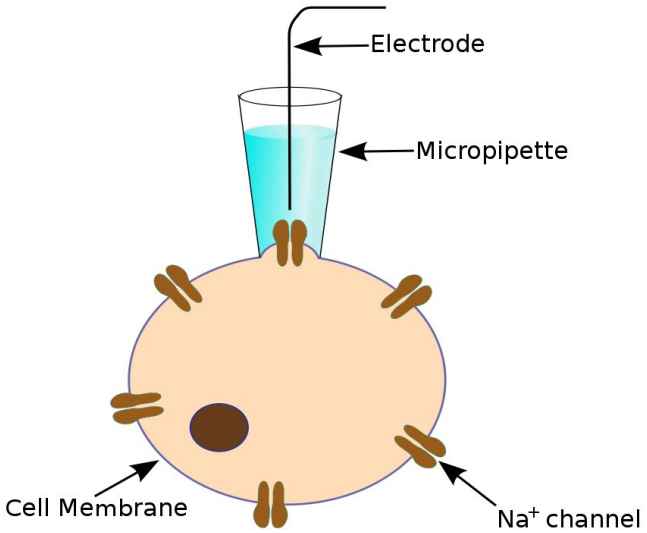

Figure 2.1: *Single protein channel recording with patch clamp technique. From wikipedia.org*

an example crucial components in the Hodgkin-Huxley model for describing nerve action [Hodgkin and Huxley, 1952](see section 2.1.1).

There is a large number of such membrane transport proteins. They can be divided into classes depending on the nature of their transportation. In the following I will briefly describe the processes of some of these classes.

Simple diffusion is a passive process in which an ion or molecule diffuses through a membrane transport protein without chemical binding.

Facilitated diffusion is the process where a protein speeds up diffusion of an ion or molecule across the membrane by lowering the energy cost required to cross the membrane. This process involves binding and is often denoted *carrier mediated transport*. It is a passive process that does not consume energy and can therefore not transport ions or molecules against a gradient.

Primary active transport is the process where energy in the form of ATP is consumed to transport an ion or molecule against its chemical or electrical gradient. Examples include the $Na^+/K^+ - ATPase$ that uses ATP to pump potassium ions in and sodium ions out of the cell against their gradients to regulate membrane potential.

Secondary active transport is also a process where ions or molecules are transported against a gradient but in this case the free energy is not delivered by ATP but by a coupled transport process. The coupled transport process must have sufficient free excess

energy to drive the primary process. Examples include the $Na^+/Ca^{2+} - exchanger$ that drives calcium out of the cells. The coupled process that delivers the excess free energy, is the movement of sodium in the other direction, down its gradient. This process is also called *counter transport* (See figure 2.2).

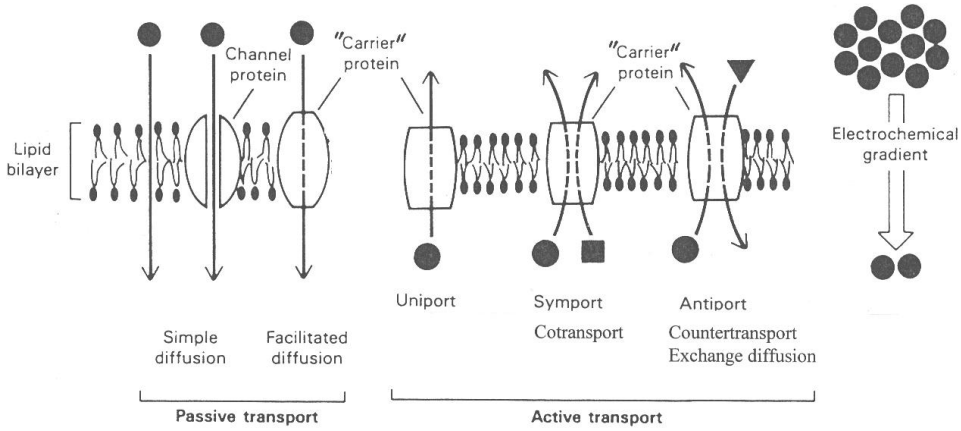

Figure 2.2: *Schematic drawing of membrane transport proteins. From wikipedia.org.*

Most membrane transport proteins are gated by external parameters. Ligand-gated channels operate similar to a lock for which a specific ligand functions as the key. Voltage-gated ion channels open/close due to the movement of a charged gating-unit within the ionchannel when the membrane potential is shifted past a threshold. Some MTPs have been suggested to be temperature-gated, functioning by changing to a high entropy conformation with raising temperature and hereby changing the protein conformation to an open state [Caterina et al., 1997].

2.1.1 Ion channels as a key component in the Hodgkin-Huxley model

As an example of how ion channels are believed to operate, I have chosen to describe the protein dominated model of *Hodgkin* and *Huxley* (HH-model).

Voltage-gated ion-channels play a central role in the dominating model for nerve signaling. It is called the HH-model and was proposed in 1952 by Alan Lloyd Hodgkin and Andrew Huxley [Hodgkin and Huxley, 1952] (they received a Nobel prize for their work in 1963).
The model is essentially electrical and describes the signal as a *traveling action potential* along the axon. The axon is the long, pipe-like part of a nerve cell or neuron. It transmits signals between the central nervous system and dendrites from all parts of the body. Ion-translocating proteins maintain and restore a resting potential across the membrane of

about $-70mV$. The resting potential is a weighted average over the Nernst-potentials of the different ions present. It can be calculated from the Goldman-Hodgkin-Katz relation (See equation 2.13).

The resting potential is dominated by the potassium concentrations since the permeability for these ions are high due to open potassium specific ion channels (the instantaneous conductance for potassium is independent of voltage).
When a local depolarization of the membrane potential is generated at the axon near the dendrite the voltage-gated sodium channels opens up. This is the beginning of a complicated chain of events called a traveling action potential. The voltage-gating of the sodium- and potassium channels are controlled by 3 species of gating particles (denoted n,m and h). The potassium channel contains 4 particles of species n and the sodium channel contains 3 particles of species m and one of species h.
The three particles each have access to two different states in the ion channel (active/inactive). In order to be in an 'open' state, a channel must have all four particles in an *active* state.
The time and voltage dependencies of the gating particles can be described qualitatively as follows:

- n is slow and activates on depolarization
- m is fast and activates on depolarization
- h is slow and activates on polarization

This combination of time and voltage dependencies allows for a traveling action potential:

When the membrane is depolarized passed the critical action potential (about -45 mV, the fast m-particles move in an active state and the sodium channels open up. Sodium flows into the axon and the membrane is further depolarized.
Soon after the slow gating particles starts moving causing potassium channels to open (n) and sodium channels to close (h). Consequently the membrane becomes permeable to potassium-ions solely and a resting potential is restored.

The HH-model is a complex model has been very successful. After more than half a century it is still the dominating model for describing the travelling action potential.
This is somewhat surprising. The model was merely an attempt to describe the phenomena empirically. In the original article from 1952, the authors wrote:

"*The agreement must not be taken as evidence that our equations are anything more than an empirical description of the time-course of the changes in permeability to sodium and potassium. An equally satisfactory description of the voltage clamp data could no doubt have been achieved with equations of very different form, which would*

probably have been equally successful in predicting the electrical behavior of the membrane." [Hodgkin and Huxley, 1952]

They use a large number of variables to create freedom in the model. The following quotes are also from the original paper of Hodgkin and Huxley:

"A useful simplification is achieved by supposing that g_K [the potassium conductance] *is proportional to the fourth power of a variable which obeys a first order equation.*" [Hodgkin and Huxley, 1952]

and

"*...we might suppose that it* [the sodium conductance] *is determined by two variables, each of which obeys a first-order equation.*" [Hodgkin and Huxley, 1952]

2.2 Lipid ion channels

It was taken as evidence for the existence and function of the acetylcholine receptor when Neher and Sakmann in 1976 recorded quantized currents in frog muscle with voltage clamp [Neher and Sakmann, 1976].
In 1974, two years before the famous experiment of Neher and Sakmann, Yafuso et. al. [Yafuso et al., 1974] described the same quantized events. Only, these data were obtained from pure lipid membranes. The paper described the different phenomena observed with voltage clamp experiments.

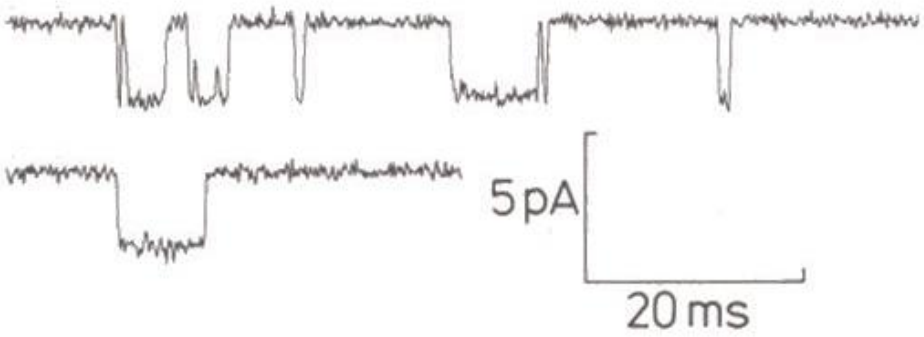

Figure 2.3: *Single channel recording of acetylcholine recepter. The channel is closed when the trace is up and open when the trace is down. From www.unmc.edu/physiology/Mann/mann3b.html#N_13_*

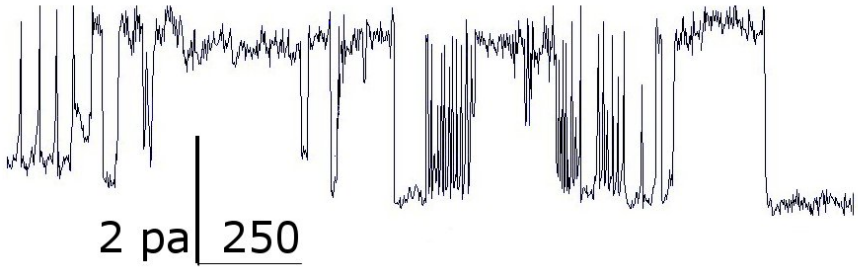

Figure 2.4: *Voltage clamp on a BLM (DPPC/DLPC − 1 : 4). As in the case of the acetylcholine recepter there are quantized conductance steps. In pure lipid membranes they are called channel-like events.*

- With small voltages ($U < 70\ mV \sim$ biological regime) they observed high resistance and stable conductance.
- They observed a transition of the membrane over longer time scales ($min < T < hour$) with a trans membrane voltage of 70 mV. The new state had dramatic increase in the noise and the fluctuations of the current. The state of the membrane return to the initial low-noise/low-conduction state but most often the *noise-state* was an indication of imminent rupture.
- They observed *step-functions* in the apparent multilevel conductance states under certain conditions. They suggested that these quantized current steps were pores formed in the lipid membrane. The quantized nature of the conductivity represented the opening and closing of a single pore.

The degree of stochastic behavior and randomness associated with the observations together with the fact that the phenomena had only been observed in lipid films of *aged oxidized cholesterol* may have caused lack of interest in the findings.

Moreover the scene was set for the discovery of the protein ion channel. The action of protein ion channels had been quantitatively described for a long time. It seemed far fetched that the membrane in itself should even have an open/close mechanism. The proteins with their opaque complexity, on the other hand, allowed for a much needed degree of freedom in models such as the HH-model described in section 2.1.1.

The experiments with pure lipid membranes were later made by others using more regular lipids and in 1980 Antonov et al. [Antonov et al., 1980] showed that the quantized action was highly correlated with the transition of the lipid membrane (described in section 1.2.2). It had already been indicated in 1973 by Paphadjopoulos et al. that membrane ion-leakage is increased in the transition [Papahadjopoulos et al., 1973]. The fact that channel-like events could be induced was new.

The membrane itself can account for quantized currents under voltage conditions of biological regime and Antonov had found a gating parameter that allowed the current events to be regulated.
The findings of pure lipid membranes did not get much attention from biologist and biochemists and for many it remained a secret. The following is an example of how unknown lipid channels remained for scientists. In 1989 Woodbury rediscovered lipid ion channels by accident and urged other scientists to be careful when studying protein channels:
"In the original experiments that led to this work... the subsequent conductance jumps that followed the liposome addition were thought to represent a rich diversity of channel proteins just waiting to be studied. However, this thought was abandoned, when control experiments using liposomes without protein gave similar results." [Woodbury, 1989]

A number of different models have been proposed as mechanisms for currents through pure lipid membranes:

1. Simple diffusion
2. No-pass transport
3. The interface model
4. The hydrophilic pore model

In the following I will briefly describe these models.

1. Simple diffusion
The simplest proposed mechanism for describing the movement of ions through a membrane is by means of simple diffusion. The solubility of ions in the hydrophobic core is very low. Hence, the rate for ion diffusion across the membrane is very small.
The movement of a charge from a medium with a high dielectric constant such as water, to one with a low dielectric constant such as lipid is unlikely. The energy of a unhydrated ion (radius 0.2 nm) to leave water ($\epsilon_w = 78$) and enter the hydrocarbon interior of a lipid bilayer ($\epsilon_l = 2$) was approximated by Parsegian in 1969 to be 160 $\frac{kJ}{mol}$ [Parsegian, 1969]. This energy barrier was much too large to account for transport of ions across a membrane. The Born energy is calculated as the energy to move a charged sphere located far from a sheet into the middle of the sheet. For a sheet with the properties of a membrane ($\epsilon_w = 80$, thickness: $d = 6\ nm$) and a sphere with the properties of an monovalent ion ($\epsilon_l = 2$, radius: $r = 0.2\ nm$) [Weaver and Chizmadzhev, 1996].

$$W_b \approx \frac{e^2}{8\pi\epsilon_0 r}\left(\frac{1}{\epsilon_m} - \frac{1}{\epsilon_w}\right) \approx 65kT \tag{2.14}$$

Here, e is the elementary charge of the ion, e_0 is the dielectric constant for vacuum.
This result suggests that electrochemical diffusion across the membrane is highly improbable. Since the probabilities of each ion is independent of the others, the mechanism

can at most account for small leak currents and not quantized events since the movement of ions across the membrane in the case of quantized currents is highly correlated.
Under voltage clamp conditions the ions are driven towards the membrane and an electromechanical force is exerted on the membrane. Thus the energy barrier is lowered but not nearly enough.
Further, Parsegian showed that a dielectric defect in the membrane greatly reduces the energy barrier [Parsegian, 1969].

2. No-pass transport
The mechanisms behind the second model are based on a *no-pass* idea. A file/line of water molecules pass through an opening in the membrane. Ions in the file/line will be transported across due to a assumption that water can not pass the ion. The model was proposed by Levitt [Levitt, 1984] and Finkelstein [Finkelstein, 1987] in the 1980-ties.

3. Interface model
The third and fourth model are pore models. The pores of the third model are hydrophobic and are believed to form primarily around the interfaces of the domains (see 1.2.3). In the interfaces alternating lipid sizes may expose part of the hydrophobic tail to the water and hereby lowering the energy cost associated with a pore. Permeability in the interphases however, can not account for all of the action. [Nagle and Scott, 1978]

When a membrane is near the phase transition the lipids fluctuate between the fluid and the solid state and consequently the density of the local lateral tension fluctuates as well. The lateral density fluctuations open short-living cavities in the head group region of the bilayer. Cavities into which ions enter and pass through the BLM.
This property also accounts for higher permeability in the membrane melting transition since the areas of domain interfaces are in a maximum under such conditions.
The orientation of the pore lipids will be parallel to the surface norm in the narrow pore: A reorientation of the lipids would yield a deformation of the molecular order and repulsive interactions between the hydrophobic parts of the tilted pore lipids [Rand, 1981, Israelachvili and Pashley, 1984, Glaser et al., 1988]. The free energy associated with the hydrophobic pore grows injectively with pore size and no local energy minima exists. Hence, all pores of this nature are unstable and result from thermal fluctuations in the membrane.

The energy has been calculated as the area of hydrophobic interaction between lipid tail and water together with an interaction factor σ_0. The area of interface tension equals the circumference $2\pi r$ of the pore times the thickness d of the membrane. [Petrov et al., 1980]

$$E_0 = 2\pi r \cdot d \cdot \sigma_0(r) \tag{2.15}$$

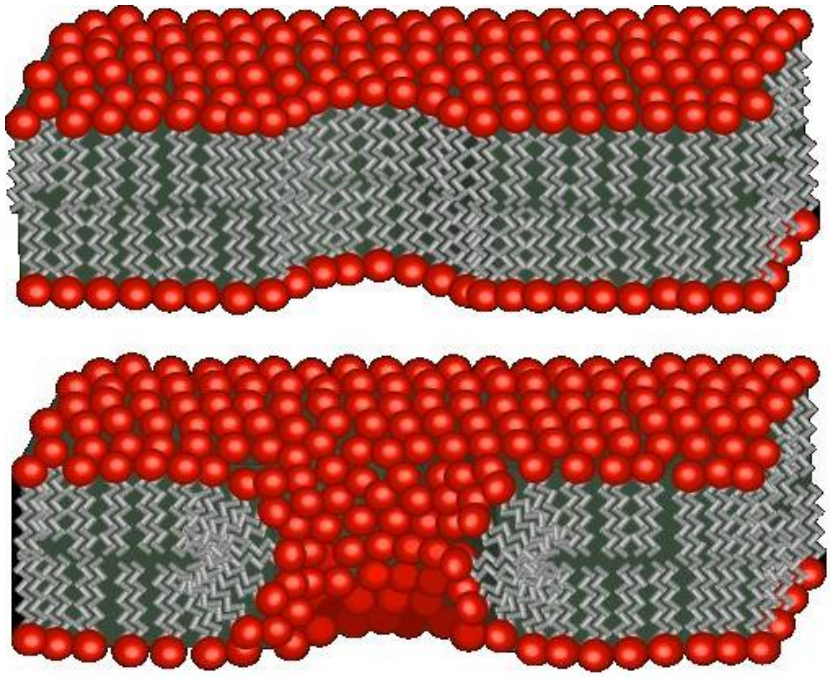

Figure 2.5: *Top: A hydrophobic pore. Thermal fluctuation, may cause temporal defects or holes in the membrane. Bottom: A hydrophilic pore. The border lipids are tilted in a conformation that lowers the free energy by shielding the lipid tails. From wikipedia.org*

For small values of r, σ_0 is reduced due to the small volume of water between the hydrophobic layers, which causes hydrophobic attraction [Israelachvili and Pashley, 1984]. Excess energy cost due to change in water structure near the interface is reduced when the affected area is overlapped by two hydrophobic areas. The characteristic length of the structure change is $\rho \sim 1$ *nm*

For larger values of r σ_0 converges to a finite value $\sigma(\infty)$ (see figure 2.6 A). A qualitative description was proposed by Marcelja et al. in 1977 [Marcelja, 1977]:

$$\sigma_0(r) = \sigma(\infty) \cdot \frac{I_1(r/\rho)}{I_0(r/\rho)} \tag{2.16}$$

I_0 and I_1 are modified Bessel functions of zeroth and first order respectively. The reduced interface tension and the energy of the hydrophobic pore is plotted as a function of radius in figure 2.6.

The hydrophobic pores-theory is a good description of thermal fluctuations leading to increased permeability in the transition of membranes but it does not account for pores with lifetimes of the order of seconds [Wunderlich et al., 2009].

4. Hydrophilic pore model

The fourth model suggests hydrophilic pores. In this model, the lipids on the pore edges

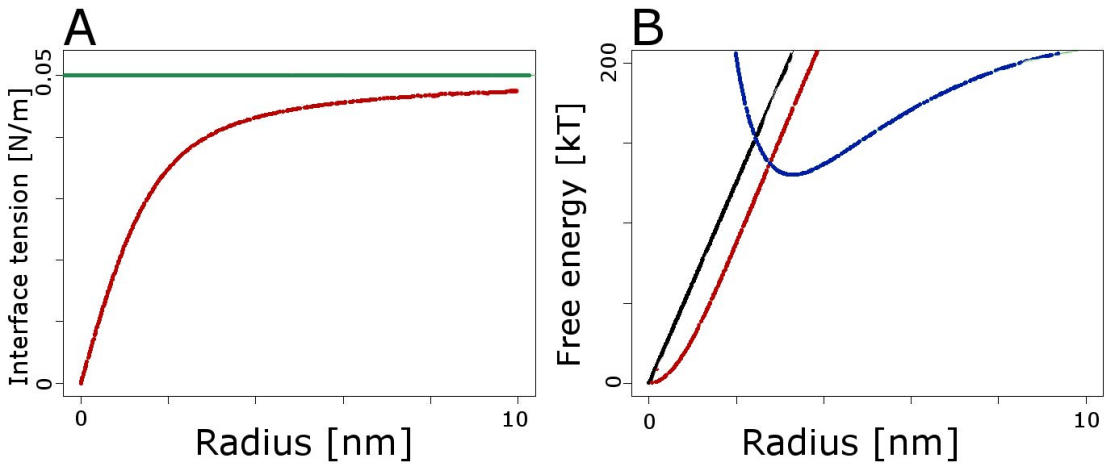

Figure 2.6: *A) Red: The Interface tension as a function of pore radius. Green: the interface tension at large radius. B) Pore energies. Black: Hydrophobic pore without consideration of hydrophobic interaction. Red: hydrophobic pore. Blue: hydrophilic pore.*

are tilted so they shield the hydrophobic parts. Hence, the hydrophobic interaction is reduced.

The free energy of a hydrophilic pore was described by Taupin [Taupin et al., 1975] and Litster [Litster, 1975] simultaneously. They proposed a model consisting of two terms.

$$E_i(r) = 2\pi\gamma r - \pi\sigma r^2 \tag{2.17}$$

The contribution from the first term accounts for the energy of the pore edge γ which increases linearly with pore radius. The second term is the lateral tension σ produced by the displaced lipids corresponding to the area πr^2 of the abandoned pore.
If the membrane is compressed the lateral tension will be negative, and the term will promote the closing of a pore. The forming of a pore can even influence the tension [Blicher et al., 2009]. If the membrane is stretched the lateral tension is positive, and the term promotes the opening of a pore. In the latter case, equation 2.17 is a parabola with a maximum pore energy E_c at some finite positive radius r_c. r_c is an unstable critical radius,

$$r_c = \frac{\gamma}{\sigma}. \tag{2.18}$$

For values of r lower than r_c the energy increases with r. For values larger than r_c the energy declines (se figure 2.7. Thus, when r_c is reached the pore may either contract and vanish or grow until rupture of the membrane. Litster proposed that the unstable

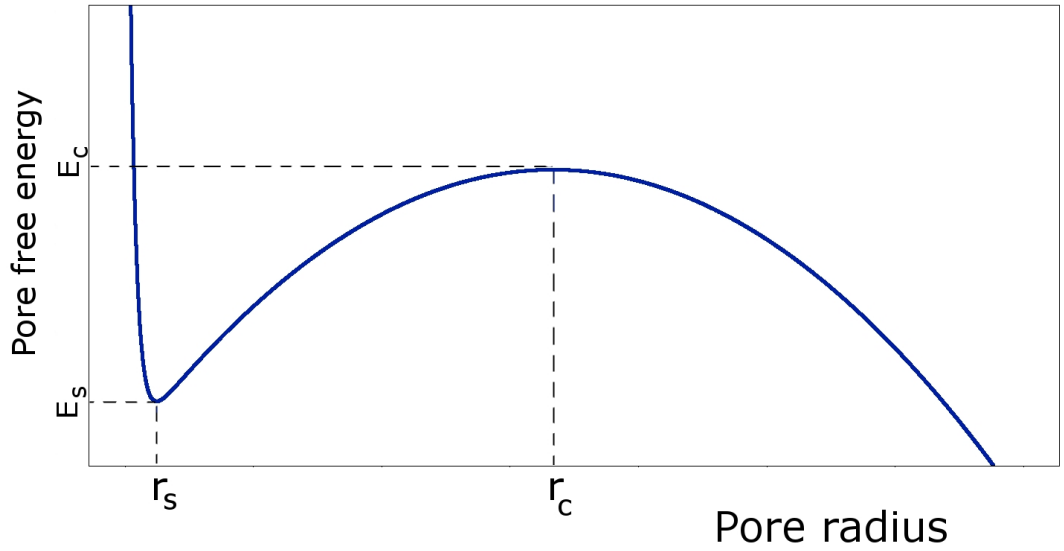

Figure 2.7: *Schematic drawing of the Abidor free energy. The first minimum in free energy is a stable radius r_s. The free energy maximum is the unstable radius r_c.*

radius r_c could be stabilized by the dynamical flow of water and solubles through the pore [Litster, 1975]. Hereby, he could account for stable pores with a finite radius.
If the membrane is compressed the energy of equation 2.17 is an ever growing function of r. Hence, r_c vanishes.

Equation 2.17 describes the hydrophilic pore, but it is not valid for small pore sizes ($r \ll h$). The shielding of the hydrophobic lipid tails requires a pore of a certain size. The diameter of a hydrophilic pore must be large enough so the lipids on the edges can rearrange to form the hydrophilic pore [Abidor et al., 1979, Glaser et al., 1988].
The lipid heads on the edge of the pore and the lipid tails are squeezed for small values of r. At this point the energy rises steeply.
To my knowledge, the actual form of the contribution to the energy as r approaches zero is not given in the literature. I assume that non-linear elastic properties arise from the squeezing of the border lipids head groups and that this energy only dependent on r in the following manner:

$$E_h = k_1 \cdot e^{-k_2 r}. \tag{2.19}$$

In this description of the energy of small radius ($r < 1\ nm$), the constants k_1 and k_2 are chosen so E_h rises steeply when r approaches 0 and vanishes at a characteristic length of about 1 nm. The characteristic length was found experimentally [Wintherhalter and Helfrich, 1987].

$$E_i(r) = k_1 \cdot e^{-k_2 r} + 2\pi\gamma r - \pi\sigma r^2. \tag{2.20}$$

Hence, an intermediate step is inevitable. Small hydrophobic pores must precede the hydrophilic pores.
Figure 2.6 shows the energies of the hydrophobic and the hydrophilic pores. For small pores a hydrophobic formation will be favorable (the red curve), but for larger pores the hydrophilic pore is favorable (blue curve).
This two-state model for pore formation can account for stable pores of a certain size (see figure 2.6 B).
A hydrophobic pore grows to a semi stable size due to thermal fluctuations, whereupon it may close again or change formation to a hydrophilic pore. In the latter case, it falls into a local energy minimum E_s of the stable radius r_s.

Chapter 3

Electroporation

When an electrical potential is applied across the membrane the properties of ion permeability change. It is well established that voltage can induce permeability in membranes through *electroporation*. Electroporation or reversible electrical breakdown is a technique for inducing permeability in a cell. It is among other things used in molecular biology to load a cell with probes, drugs or DNA.
Upon applying a short voltage pulse of 200-500 mV for a period in the order of milliseconds, the membrane quickly charges as a capacitor and after a short delay the permeability and the conductance soars. The technique was first invented by Neumann and Rosenheck in a famous paper from 1972 but the mechanisms are still not fully understood [Neumann and Rosenheck, 1972].

The applied voltage used for electroporation is most often delivered in the form of an unipolar rectangular pulse. The duration ranges from tens of microseconds up to milliseconds. In the first few microseconds after the onset of the pulse, the voltage is build up across the membrane and the membrane is charged like a capacitor. This voltage persists until the end of the pulse. Within milliseconds a steep increase in electrical conductivity and permeability of the membrane arises.

Just as most literature solely holds proteins responsible for the movement of ions across membranes in biological voltage regime ($U < 150\ mV$), there is widespread agreement in the literature that electroporation is a lipid based phenomenon.
The physical mechanisms behind electroporation is still disputed. Most scientists however, favor models of electrically induced pores.

In the following, I will discuss some non-pore models and subsequently present two of the favored models of electrically induced pores.

The first proposed model treated the electrical breakdown literally as a breakdown of the membrane. The membrane was viewed as an *elastic capacitor* and the membrane was stretched by the electromechanical force of the ions and stretched until a critical point of rupture [Crowley, 1973, Weaver and Chizmadzhev, 1996, Chen et al., 2006].
When quantities such as elasticity and capacitance were known, the model predicted a critical voltage at which the membrane would burst. This however, did not correspond very well with experimental facts [Weaver and Chizmadzhev, 1996].
As the voltage is elevated, the membrane is stretched. Consequently, the model predicts the capacitance to change as the membrane becomes thinner (the capacitance is inversely proportional to the membrane thickness).
According to experimental findings, this is not true [Weaver and Chizmadzhev, 1996].
Further, the predicted critical voltage of membrane rupture was about a factor of ten too high [Chen et al., 2006].

In 1989, Needham and Hochmuth proposed a model of isotropic surface expansion of a membrane. They suggested that deformation of the membrane and subsequent breakdown was an intrinsic property of the membrane material. Thus, the criterion for breakdown was the same regardless of whether the membrane was expanded to the point of breakdown by an isotropic tension or an electro compressive stress. Both the stress and the compressive tension stored elastic energy in the membrane.
They used a micro-pipet technique to place a lipid vesicle between two electrodes. With this setup, they could determine the critical field strength for membrane breakdown as a function of applied membrane tension. The membrane tension and the electro compressive forces stored energy in the membrane and a critical point was found where the stored energy exceeded the critical energy. This model predicts a shift in critical voltage as a function of membrane compressibility [Needham and Hochmuth, 1989].

3.1 Pore models of Electroporation

The pore models for describing electroporation are found in various versions. Common for versions of this model is that the membrane has more properties than *being an elastic capacitor*.

Neumann and Rosenheck first described the technique of electroporation in 1972. In 1982 Neumann was first again to suggest the hydrophilic pore model of section 2.2 as the underlying mechanism for the electroporation phenomenon. Neumann et al. proposed a model stating that the electrical field effect on the ionic-polar head groups was responsible for the rearrangements of lipids leading to hydrophilic pores [Neumann et al., 1982].
In the following, I will present some of the established models.

3.1.1 The Abidor pore model

The dependence of the hydrophilic pore on the voltage was described by Abidor et al. in 1979. They estimated the voltage contribution to the free energy as the capacitative energy of a cylindrically shaped defect in the membrane.
The specific capacitance of the pore is [Abidor et al., 1979]:

$$C_{lw} = (\frac{\epsilon_w - \epsilon_l}{d})\epsilon_0, \tag{3.1}$$

where ϵ_w and ϵ_l are the permittivities of water and lipid respectively, and d is the membrane thickness.
The Abidor free energy of a pore with a voltage across the membrane is [Abidor et al., 1979]

$$E_{Ab}(r, U) = k_1 \cdot e^{-k_2 r} + 2\pi\gamma r - \pi\sigma r^2 - \frac{\pi}{2} C_{lw} \cdot U^2 r^2. \tag{3.2}$$

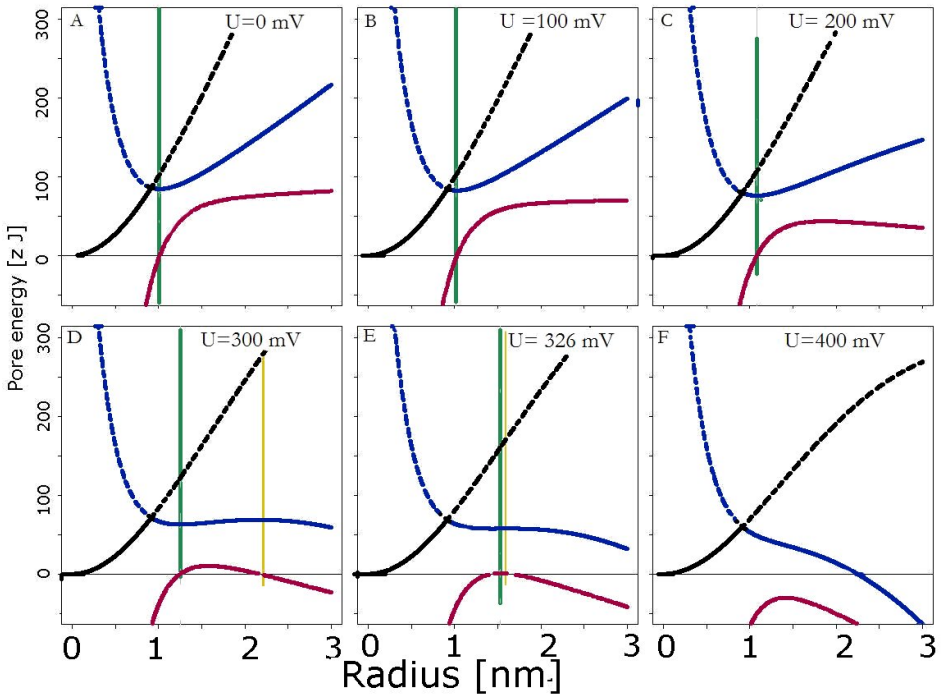

Figure 3.1: *Black: hydrophobic pore. Blue: hydrophilic pore. Red: dE_{Ab}/dr. Green and yellow: $dE_{Ab}/dr = 0$. Figure A-F shows the Abidor energy of increased voltage. As voltage is increased, the stable radius (green line) increases from $\sim 1nm$ to $\sim 1,5nm$. The unstable radius (yellow line) migrates from $\sim 10nm$ to $\sim 1,5nm$ where it bifurcates with the stable radius. There are no stable radii for higher voltage.*

This model builds on the pore free energy of equation 2.20.
The voltage acts on the lateral tension where it adds a negative contribution. Hence, the term lowers the free energy and promotes the opening of a hydrophilic pore.
For $U = 0$ the Abidor free energy obviously reduces to equation 2.20. For higher values of $|U|$ the critical radius r_c is significantly lowered (see figure 3.3), while the stable radius is increased (see figure 3.2). Eventually r_c and r_s collide and both points lose their stability in a *bifurcation*.

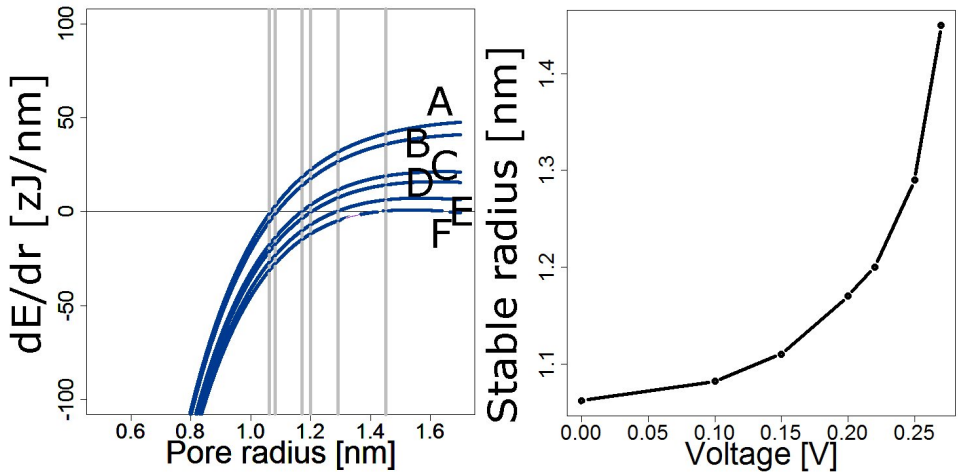

Figure 3.2: *Left: dE_{Ab}/dr as a function of radius (blue) and $dE_{Ab}/dr = 0$ which corresponds to r_s (grey) for different valtages: A) $U = 0$; B) $U = 0.1$; C) $U = 0.2$; D) $U = 0.22$; E) $U = 0.25$; F) $U = 0.27$. Right: r_s as a function of U. When the voltage is increased r_s grows.*

I carry out a differentiation on equation 3.2 with respect to radius to find r_c and r_s;

$$\frac{dE(r,U)}{dr} = -k_1 k_2 \cdot e^{-k_2 r} + 2\pi\gamma - (2\pi\sigma + \pi C_{lw} \cdot U^2)r. \tag{3.3}$$

The equation $\frac{dE(r,U)}{dr} = 0$ is not easy to solve analytically. In figure 3.2, the numerical solution to the equation is illustrated for the stable radius r_s. For the stable radius r_s the exponential term is important but I can neglect it in the case of r_c since the exponential term approaches zero for $r > 1$ *nm*. The critical radius r_c becomes,

$$r_c(U) \approx \frac{\gamma}{\sigma + 0.5 \cdot U^2 C_{lw}}. \tag{3.4}$$

The behavior of r_c is illustrated in figure 3.3.

and the corresponding critical energy

$$E_{Ab,c}(U) \approx \frac{2\pi\gamma^2}{2\sigma + U^2 C_{lw}}. \tag{3.5}$$

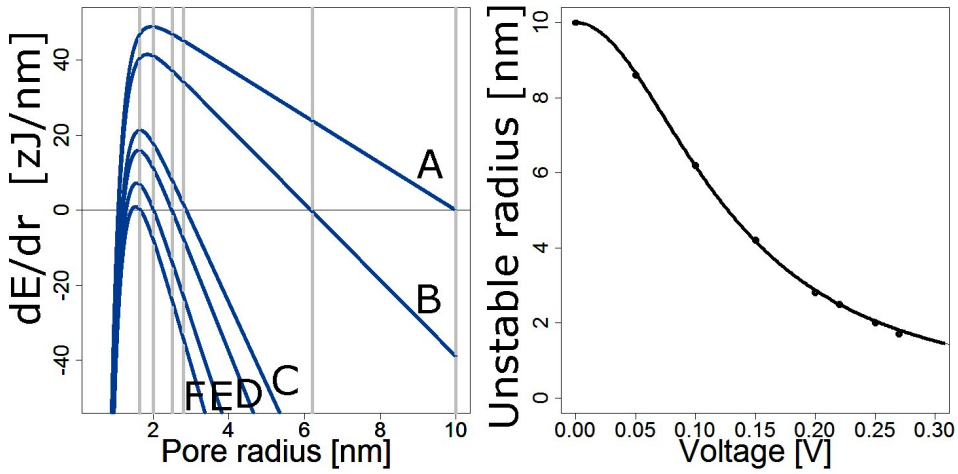

Figure 3.3: *Left:* dE_{Ab}/dr *as a function of radius (blue) and* $dE_{Ab}/dr = 0$ *which corresponds to* r_c *(grey) for different valtages: A)* $U = 0$*; B)* $U = 0.1$*; C)* $U = 0.2$*; D)* $U = 0.22$*; E)* $U = 0.25$*; F)* $U = 0.27$*. Right:* r_c *as a function of* U*. When the voltage is increased* r_c *decreases*

In the model of Abidor et al. the voltage contributes to the lateral tension and reduces the energy barrier ΔE that has to be overcome to form a pore. Moreover, the stable radius r_s of the system grows with increasing voltage and the critical radius r_c decreases. Eventually, at higher voltage the two radii annihilates and disappears in a saddlenode bifurcation. At this point, the forming of a hydrophilic pore would lead to eminent rupture of the membrane (see figure 3.1 A-F).

3.1.2 The Wintherhalter/Helfrich pore model

In 1987, Wintherhalter and Helfrich proposed a different model for the interaction of pores with an electric field [Wintherhalter and Helfrich, 1987].
They noted that when the pore radius is larger than that of a hydrated ion, the local voltage will collapse due to the conductance of the pore. They calculated the electric field of a conducting disc and the *Maxwell stresses* exerted by this electric field in an insulating medium.
They found a positive energetic contribution to the lateral tension and a additional energetic contribution to the edge energy. The Wintherhalter/Helfrich pore free energy is [Wintherhalter and Helfrich, 1987]

$$E_{wh}(r,U) = k_1 \cdot e^{-k_2 r} + 2\pi(\gamma - \frac{\epsilon_w \epsilon_0}{2\pi} U^2)r - \pi r^2(\sigma - \frac{\epsilon_l \epsilon_0}{2d} U^2). \tag{3.6}$$

In figure 3.4, the energies of pores exposed to different voltages are shown. As opposed to the Abidor energy (see figure 3.1), the stable radius r_s does not increase with

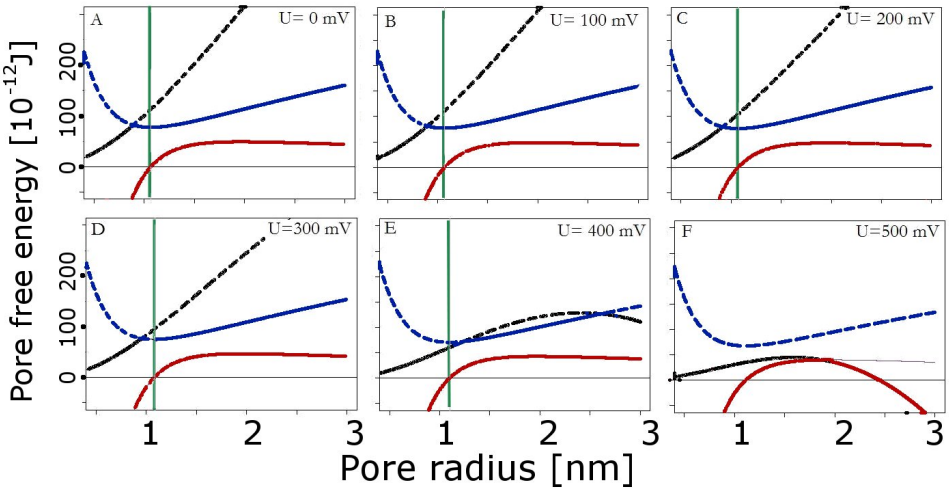

Figure 3.4: *The hydrophobic energy (E_0), the hydrophilic energy (E_{Ab}) and dE_{wh}/dr. Figure A-F shows the Wintherhalter/Helfrich energy of increased voltage.*

voltage. The critical radius can be found by differentiation in the same way as before;

$$r_c \approx \frac{\gamma - \epsilon_w \epsilon_0 U^2/2\pi}{\sigma - \epsilon_l \epsilon_0 U^2/2d}, \equiv \frac{\gamma_{eff}}{\sigma_{eff}}, \tag{3.7}$$

where γ_{eff} and σ_{eff} corresponds to the *effective* edge tension and lateral tension respectively.

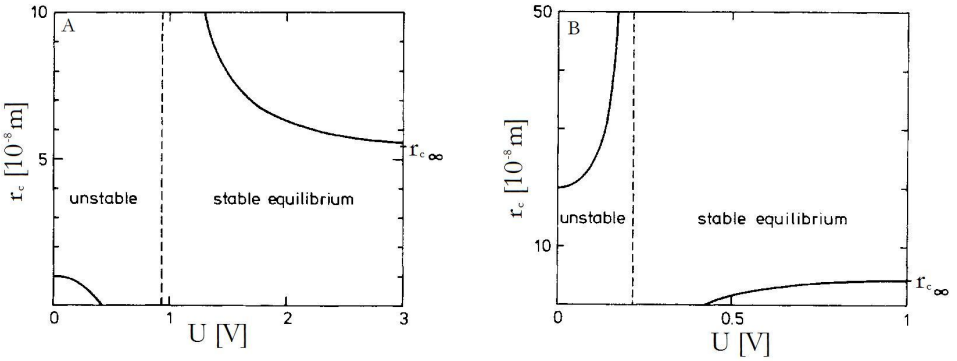

Figure 3.5: *r_c as a function of voltage. A: $\sigma = 2 \cdot 10^{-3}$ N/m and B: $\sigma = 0,1 \cdot 10^{-3}$ N/m [Wintherhalter and Helfrich, 1987].*

When U is elevated both γ_{eff} and σ_{eff} of equation 3.7 will approach and eventually pass through zero. If γ_{eff} reaches zero first $r_c \to 0$ and any existing pore will grow until

the membrane ruptures.
If σ_{eff} reaches zero first $r_c \to \infty$. r_c does not reappear before γ_{eff} also reaches zero.
When one of the parameters (σ_{eff} or γ_{eff}) is negative r_c is negative. There is no physical use of the negative radii.
In the case where both γ_{eff} and σ_{eff} are negative the nature of the critical pore radius r_c will evolve into a stable radius.
The two situations are plotted in figure 3.5. In *A*) γ_{eff} reaches zero first and in *B*) σ_{eff} reaches zero first. For elevated voltages the membrane can have stable pores of size r_c^{∞};

$$r_c^{\infty} = \frac{\epsilon_w d}{\epsilon_l \pi}. \tag{3.8}$$

The pore model of Wintherhalter/Helfrich considers the electrical contribution on the edge tension as well and predicts a stabilizing effect of pores on this account.
Other models have also been proposed which I will not include here. Some models are slight variations of the above described models and other models are utterly different [Sugar, 1979, Sugar and Neumann, 1984, Weaver and Chizmadzhev, 1996].

In 1993, Wilhelm et al. used the pore model of Wintherhalter and Helfrich [Wintherhalter and Helfrich, 1987] as a basis to describe the irreversible breakdown of a model. They neglected the electrical part of the surface tension ($\sigma_{eff} \approx \sigma$) since they assumed that this term was much smaller than the mechanical surface tension. When a pore was open, the expansion process was driven by the mechanical surface tension and the conductivity of the pores caused the membrane to discharge. They further assumed that the remaining potential was small, and hence, that the opening process was independent of the applied voltage [Wilhelm et al., 1993].

Joshi et al. found that the evolution of pores indeed is dependent, not only on the applied voltage, but also on the duration of the pulse. Through analysis of the Abidor pore free energy, they suggested that a large number of pores open up subsequent to the onset of a voltage pulse.

The elevated voltage causes r_s to increase and r_c to decrease. Eventually the two radii collide and both points loose their stability (see figure 3.1).
At this point a number of pores start expanding. When the pulse ends, r_s and r_c are reconstituted. If a pore radius has passed the critical radius ($r > r_c$), the pore will keep expanding and the membrane ruptures (irreversible electrical breakdown). If the all radii are below the critical radius at the end of the voltage pulse ($r < r_c$), the pores will close (reversible electrical breakdown).
Through simulations they showed that irreversible breakdown would lead to the formation of a few large pores, while a large number of smaller pores would appear in the case of reversible breakdown.
In figure 3.6, the energies of pores exposed to different voltages are shown (A) and the time evolution of these pores (B).

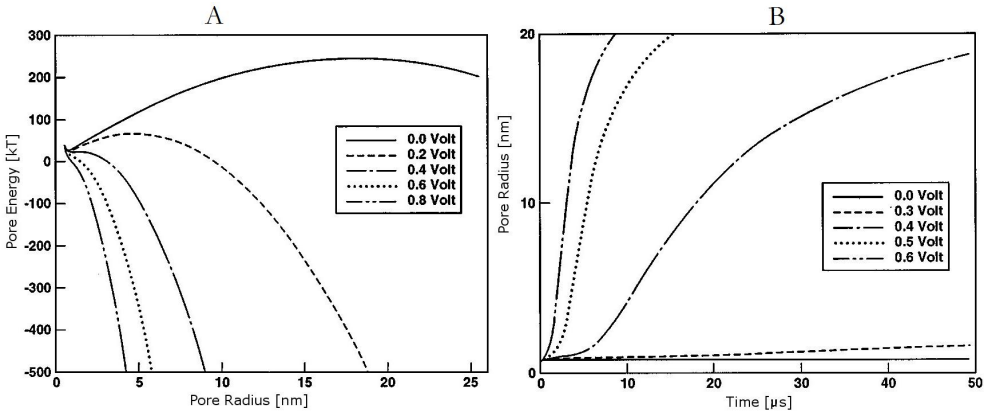

Figure 3.6: *Evolution of a voltage induced pore [Joshi and Schoenbach, 2000]*

In an article from 2001, Melikov et al. studied the conductance associated with single pores in unmodified BLMs under high voltage. In accordance with other data [Sowers, 1986, Weaver and Chizmadzhev, 1996, Joshi et al., 2002, Böckmann et al., 2008, Melikov et al., 2001] they observed a lag-time in the conductance from pores subsequent to a applied voltage. Melikov et al. suggested that the voltage affected the formation of the lipids and created non conducting prepores in the membrane (see figure 3.8) [Melikov et al., 2001].
The existence of the pre-pore state was substantiated by experiments with two consecutive pulses of high voltage ($U = 400\ mV$) separated by a pause with lower voltage (50 mV). The conductance behavior of the second voltage step depended on the duration of the pause.
In the case of a short pause ($\Delta t < 250\ ms$), the application of the second voltage pulse yielded an immediate upsurge in conductance (i.e. no lag-time detectable).
In the case of a longer pause ($\Delta t > 500\ ms$), the lag-time of the second voltage pulse was similar to that of the first step.

They proposed that after the end of the first pulse, the open pore quickly turned into a non conductive, silent pore. The prepore was ready to reopen in response to a second pulse. The prepore is a meta stable structure and without a second pulse it reseals with a relaxation time of the order of $100 - 1000\ ms$ [Melikov et al., 2001]
In accordance with Joshi et al., Melikov et al. proposed that in the case of irreversible breakdown, few pores are formed before the first one of them reaches a critical radius and starts irreversible expansion leading to rupture of the membrane. In contrast, during reversible breakdown a large population of pores have formed during the voltage pulse before the onset of membrane rupture [Melikov et al., 2001].

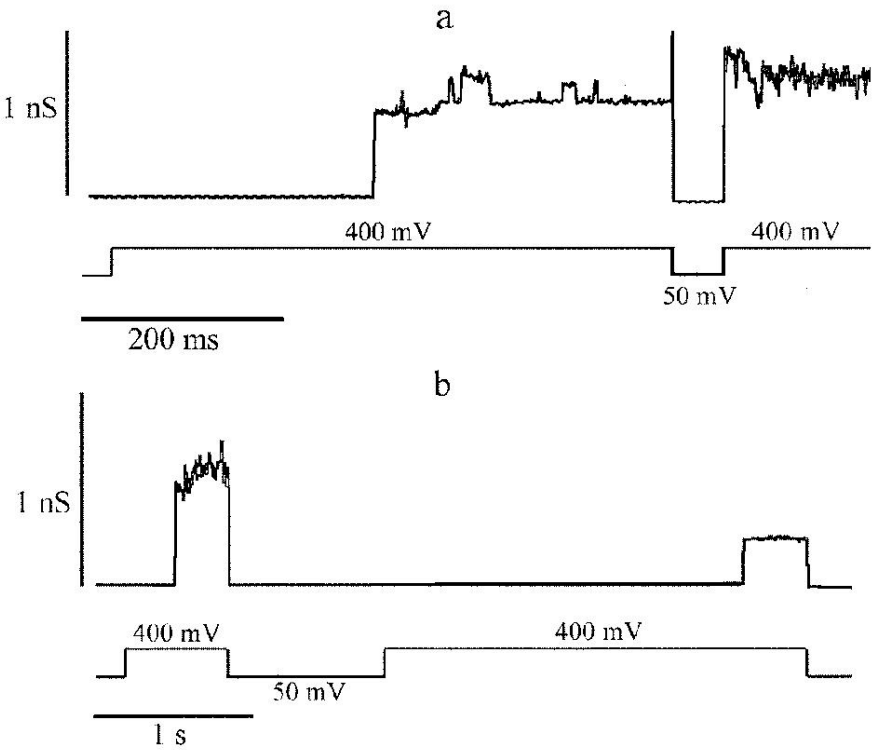

Figure 3.7: *Pore formation in BLM. Reopening of a meta stable non conducting prepore [Melikov et al., 2001]*

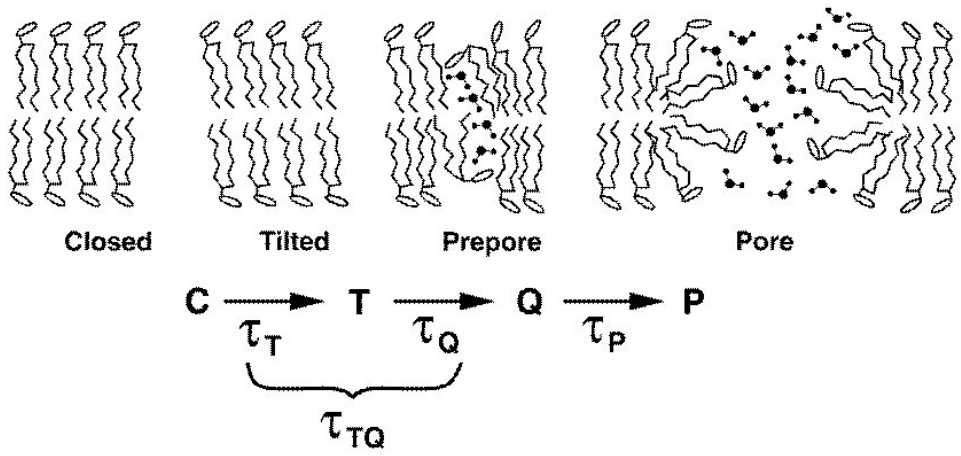

Figure 3.8: *From prepore to hydrophilic pore [Böckmann et al., 2008]*

Through simulations, Böckmann et al. found supporting evidence for such prepores. They found that the lag-time decreases with increasing field strength and requires two

intermediate preparation steps. They suggested two intermediates: a state with modified head group orientation (T) and a prepore state (Q) with a closed water lipid file across the membrane (see figure 3.8) [Böckmann et al., 2008].
The dependence of the lag-time on the voltage has been used to distinguish different pore theories [Weaver and Chizmadzhev, 1996].

In 2005, Antonov et al. showed electroporation can be performed on BLMs exposed to voltage of biological relevance ($U < 150\ mV$) when the membrane is in the transition [Antonov et al., 2005]. They denoted the technique *soft perforation*.
They further noted that the blocking of the conductance with polyethyleneglycol (PEGs - used for the calibration of the lipid pore size) was very similar to the blocking of protein channels.
They proposed that soft perforation could supersede electroporation because the damage exerted on the cell organelles could be minimized. Using low voltages in the transition could compensate for the high voltages of electroporation.

Chapter 4

Oscillating reversible electrical breakdown

The oscillatory reversible electrical breakdown of BLM was described in section 6.
To my knowledge, this phenomenon has not been reported in the literature and the physics has not been described.

In the following, I will discuss the phenomenon in the light of the outlined models for pore formation in electroporation and propose a qualitative model for the phenomenon based on the pore models by Abidor and Wintherhalter/Helfrich.

4.1 Basics of a model for oscillations

The pore model of Abidor [Abidor et al., 1979] has one stable pore radius at small radius and one unstable pore radius at larger radius. The stable radius of size $r_s \approx 1\ nm$ corresponds to the shift from the hydrophobic to the hydrophilic energy function and the unstable radius $r_c \approx 18\ nm$ is the maximum of the quadratic energy function.
When the voltage pulse is applied r_s grows and r_c decreases. Eventually they collide and the system loses stability (see section 3.1), consequently the pores expand until the end of the pulse.
At the end of the pulse the stability is reestablished and the pores either shrink back to r_s or expand until membrane rupture, depending on the duration and strength of the pulse.
This model was used to describe the reversible electrical breakdown of electroporation by Joshi and Schoenbach [Joshi and Schoenbach, 2000, Joshi et al., 2002] but can it also account for oscillating reversible electrical breakdown?
In the model described above, the reversibility relies on *the end of the voltage pulse*. In my experiments however, the voltage is kept constant. The oscillating system of a volt-

age clamped membrane is *self-regulating*. Hence, I propose the following self-regulating system involving the pore radius and the local voltage in the vicinity of the pore:
The voltage induces the opening of pores in the membrane (in the same manner as the Joshi/Schoenbach model). When the pores are open, the membrane is in a highly conducting state and as a consequence, the local voltage collapses in the regions near the pores. Subsequently the pores start to close again.
This qualitative model describes the correlation between the local radius of a pore and the local voltage near the pore when the voltage far from the membrane is held constant. Further, it includes a negative feedback mechanism for the relation between the local voltage and the radius (see figure 4.1).

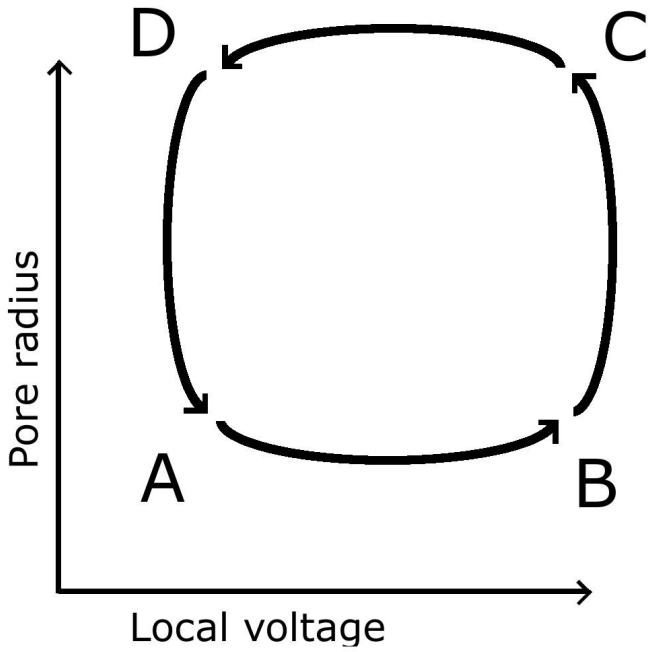

Figure 4.1: *Schematic model for oscillating reversible electrical breakdown.**A:** The pore is small and the local voltage increases across the membrane. **B:** The pore starts to open in response to the increasing local voltage. **C:** The local voltage collapses due to the large conducting pore. **D:** The pore starts to close due to the low local voltage.*

In the following I will examine the possibilities of oscillations by examining the phase plane of U and r.
First, I must obtain differential equations coupling U and r.

$$\begin{aligned} \dot{U}(r,U) &= \frac{dU}{dt}(r,U) \\ \dot{r}(r,U) &= \frac{dr}{dt}(r,U) \end{aligned} \tag{4.1}$$

The rate change $\dot{U}(r,U)$ of the voltage in the vicinity of a pore is not known. I propose a Taylor series of 2. order:

$$\dot{U}(r,U) = k_1 + k_2 r + k_3 U + k_4 r^2 + k_5 U^2 + k_6 rU \tag{4.2}$$

If $r = r_0$ is constant, the local voltage should go towards an equilibrium voltage U_{eq} from both larger and smaller U:

$$\dot{U}(U_{eq} + dU, r_0) = -\dot{U}(U_{eq} - dU, r_0) \tag{4.3}$$

Hence, I demand that the quadratic terms in U cancel. This yields: $k_5 = 0$.
Further, I assume that $\dot{U}(r,U)$ is proportional to the area of the pore r^2 rather than the pore radius r. Hence $k_2 = 0$ and $k_6 = 0$ cancels.

The signs of the remaining constants can be determined by analyzing $\dot{U}(r,U)$ qualitatively at the points A, B, C and D in figure 4.1:

$\dot{U}(0,0)$ should be positive hence, k_1 is positive.
With $r = r_0$ being constant $\dot{U}(r,U)$ should be positive for small U and negative for large U. Hence k_3 should be negative.
$\dot{U}(r,U)$ should decrease with increasing pore area. Hence k_4 should be negative.

I rename the remaining constants so they have positive values for simplicity: $k_1 \equiv \kappa_1$, $k_3 \equiv -\kappa_2$ and $k_4 \equiv -\kappa_3$. Equation 4.2 becomes:

$$\dot{U}(r,U) = \kappa_1 - \kappa_2 U - \kappa_3 r^2 \tag{4.4}$$

The form of the rate change $\dot{r}(r,U)$ in the vicinity of the pore can be derived from the Abidor or the Wintherhalter/Helfrich pore free energy functions.

The pore free energy function describes the free energy as function of pore and voltage. I can assume that the rate is proportional to a force and hence, that the change in pore radius will be proportional to the gain in free energy:

$$\dot{r}(r,U) \propto -\frac{dE}{dr} \tag{4.5}$$

The rate change of the radius moves in response to the potential energy. The proportionality constant is a phenomenological constant that describes the inertia of the system.

4.2 Oscillations derived from the Abidor function

In this section I will examine the oscillatory properties of two differential equations coupling $\dot{U}$ and $\dot{r}$. The first equation for $\dot{U}$ was derived in the previous section. In the following, I will derive the second equation for $\dot{r}$ from the Abidor free energy function.

From equations 3.2 and 4.5 I obtain:

$$\dot{r}(r, U) = (-\kappa_4^{Ab} + \kappa_5^{Ab} r + \kappa_6^{Ab} r U^2) \cdot \kappa_7^{Ab} \tag{4.6}$$

where $\kappa_4^{Ab} = 2\pi\gamma$, $\kappa_5^{Ab} = 2\pi\sigma$, $\kappa_6^{Ab} = \pi C_{lw}$ and κ_7^{Ab} is a phenomenological constant.

I have neglected the exponential term of equation 3.2 since it is only relevant for very small pore radii. It would preclude the system from moving between $r = 0$ to $r = 1$.

Out of the 7 parameters in equations 4.4 and 4.6 3 of them are known and the sign is known for the 4 remaining parameters.
κ_1 has the dimension $[V/s]$. It is a driving force that restores the potential and measure for the applied voltage.
κ_2 has the dimension $[s^{-1}]$. It is a measure for how fast the voltage changes in response to the equilibrium voltage for a fixed radius.
κ_3 has the dimensions $[V/m^2 s]$. It is a measure for how the voltage rate change responds to a change in pore area.
The phenomenological constant κ_7 has the dimensions $[s/kg]$ and describes the inertia of the pore, i.e. how fast the pore radius changes in respond to changes in voltage and radius. Hence, κ_7 is related to the relaxation time and the lag time of the system.

In figures 4.2 and 4.3 I have plotted a vector field for the two equations in U, r-space. Each black arrow illustrates the initial change in U, r from that point.
The change is calculated by the linear approximation:

$$\begin{aligned} dU &= \dot{U} \cdot dt \\ dr &= \dot{r} \cdot dt \end{aligned} \tag{4.7}$$

The black arrows illustrate the direction of the flow in U, r-space with time.
The red and purple arrows corresponds to two different starting points P_1 and P_2. Each arrow is drawn in continuation of the previous arrow. The arrows illustrate the trajectory of a starting point (P_1 and P_2) in a period of time.

In appendix B I plotted variations of κ_1, κ_2 and κ_3 respectively to illustrate the influences of these parameters.

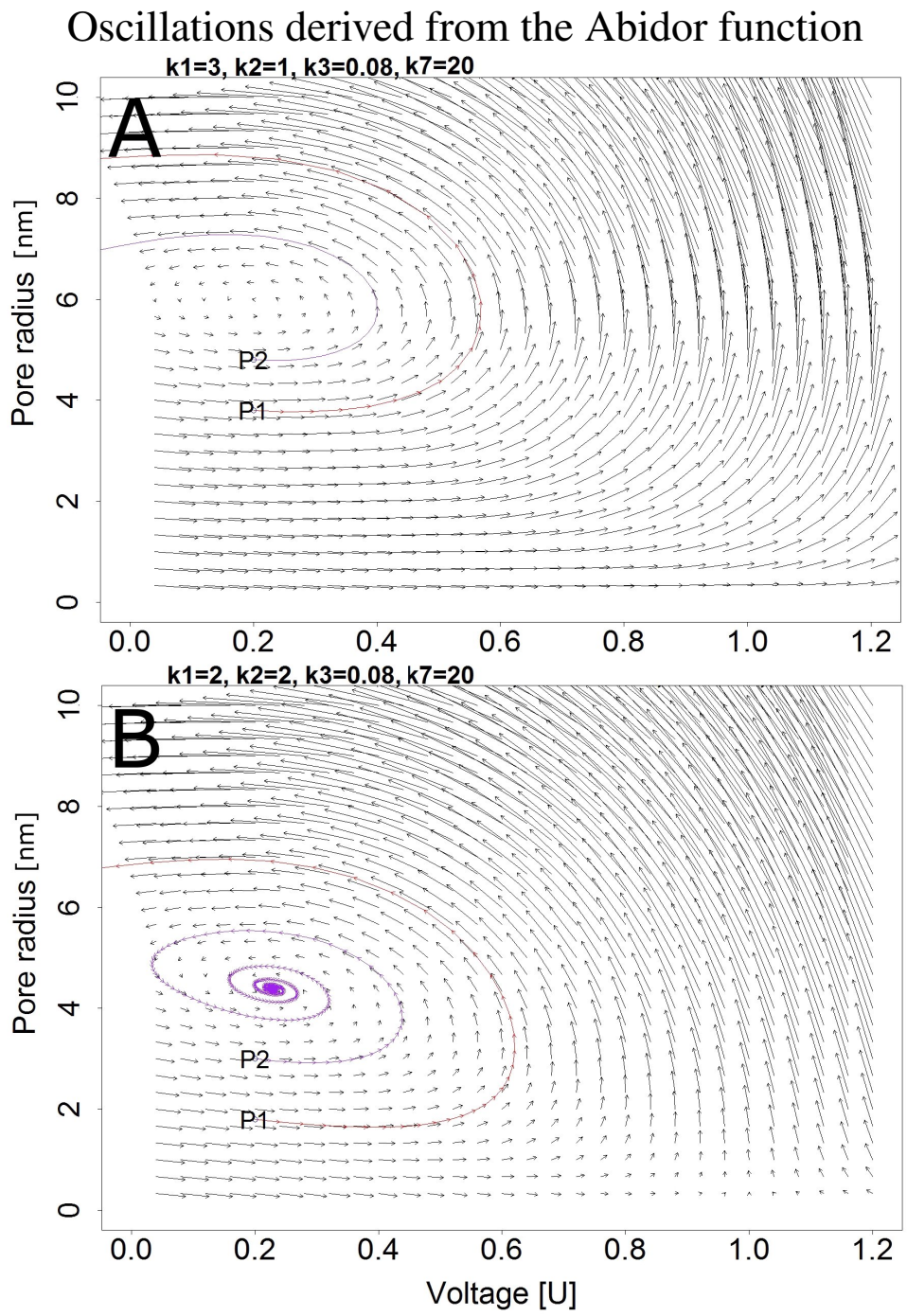

Figure 4.2: *In each figure (A-D) a vector field in the U, r-space is plotted. The black arrows are 1. order approximations to the change in U and r after a time step dt. The red and purple arrows illustrate the evolution of two starting points after n = 2000 time steps.* ***A Unstable spiral:*** *The starting points P_1 and P_2 circulates away from the unstable node P_u.* ***B stable spiral:****. The starting points circulate towards a stable node P_s. For* ***C*** *and* ***D*** *see figure 4.3. Plotted with R. For R-code see appendix A.*

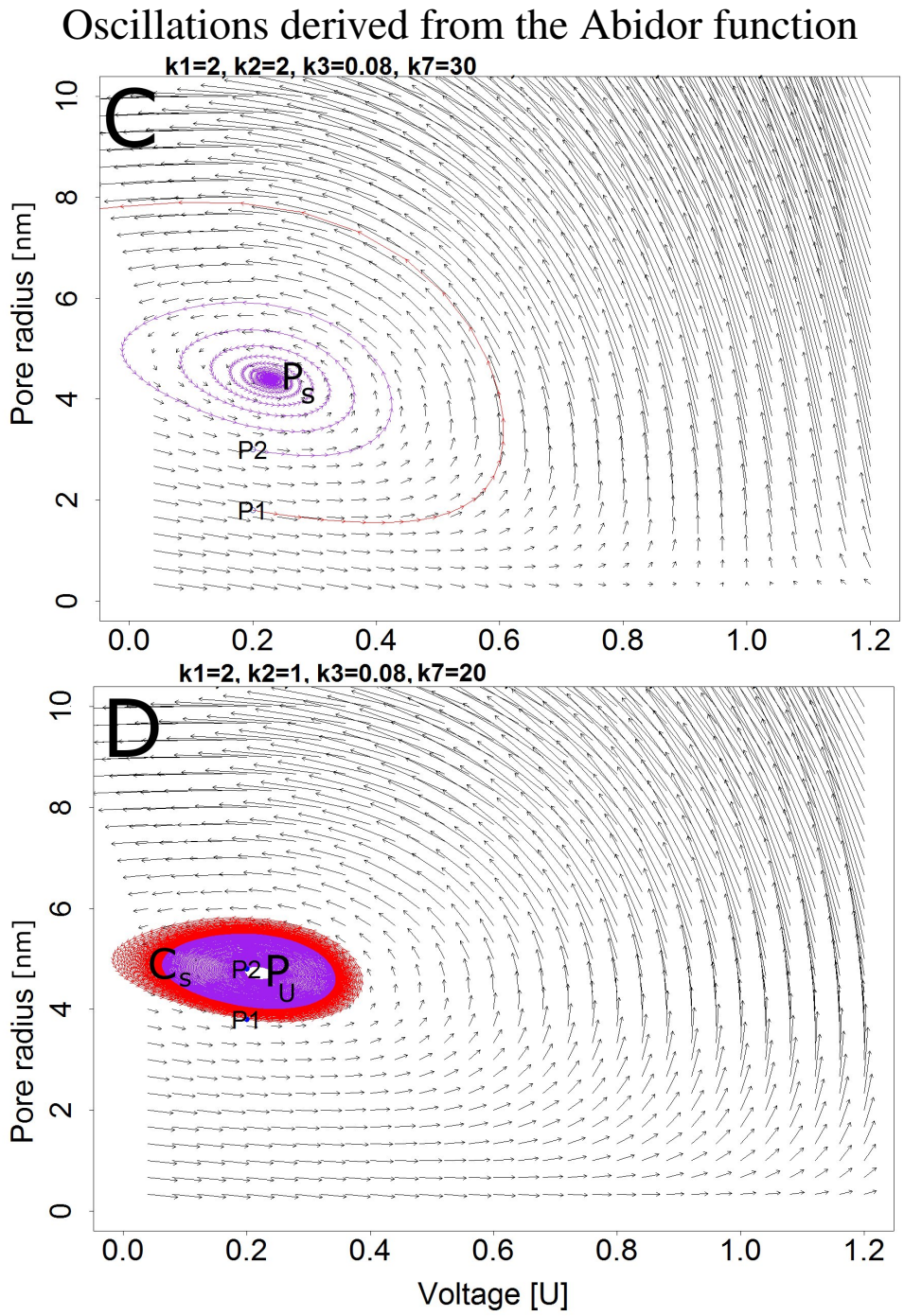

Figure 4.3: *Continued from figure 4.2.* ***C: stable spiral****: Like B but the attraction is less powerful.* ***D: Stable limit cycle****. A starting point outside the limit cycle P_1 circulates towards it and a starting point P_2 inside the limit cycle circulates towards it. This circulation is stable and will go on for as long as it has to.*

Figure 4.2 and 4.3 show 4 situations with different parameter values κ_1, κ_2, κ_3 and κ_7^{Ab}. Depending on these values the system yields different behavior.
The system can exhibit a *limit cycle*. A limit cycle is a closed path in the U, r-space that attracts the flow around it. Any starting point in the vicinity of the closed path will circle around it and converge towards it. Also starting points within the closed path will converge towards it (see figure 4.3 D). The limit cycles are stable oscillations of the system.

Other behaviors include stable spirals which are attracting points P_s in the U, r-space (see figure 4.2 and 4.3 B and C). After a number of time steps starting points in the vicinity of P_s will converge towards it. P_s corresponds to a stable pore in the system. When the system has reached this point both the radius and the local voltage stays constant.

Most starting points with small radius end up with a very large radius. The voltage grows very high before the pore starts to open. Once the pore opens, the voltage is so high that the pore radius rapidly grows without bounds.This scenario corresponds to irreversible electrical breakdown.

The only parameter in $\dot{r}(U, r)$ that acts to *close* a given pore, is the constant term $\kappa_4^{Ab} = 2\pi\sigma$. Hence neither U, nor r have any pore closing effects. The re-closing of the pore at low local voltage is a vital step in the oscillation process.

4.3 Oscillations derived from the Wintherhalter/Helfrich function

In the following, I will examine the properties of the system when the Wintherhalter/Helfrich pore model is used as basis for $\dot{r}(U, r)$.

I obtain $\dot{r}(U, r)$ from equations 3.6 and 4.5. I use the same expression for $\dot{U}$ as before (see equation 4.4).

$$\dot{r}(U, r) = (-\kappa_4^{Wi} + \kappa_5^{Wi} r + \kappa_6^{Wi} U^2 - \kappa_7^{Wi} r U^2)\kappa_8^{Wi} \tag{4.8}$$

where $\kappa_4^{Wi} = 2\pi\gamma$, $\kappa_5^{Wi} = 2\pi\sigma$, $\kappa_6^{Wi} = \epsilon_w\epsilon_0$, $\kappa_7^{Wi} = \frac{\pi\epsilon_l\epsilon_0}{d}$. equation 4.8 is a little different from 4.6. κ_6^{Wi} does not depend on r and an additional term κ_7^{Wi} promotes the closing of the pore. κ_8^{Wi} is the phenomenological constant with units of $[s/kg]$.

As before I construct a vector field in the U, r-space and plot the trajectories of different starting points. The result is shown in figures 4.4 and 4.5.

Only 4 out of the 8 parameters in equations 4.4 and 4.8 are known. The signs are known for the 4 remaining parameters, based on the suggested model.

The pore opening term κ_6^{Wi} is independent of r and the extra term κ_7^{Wi} depends on r and U^2 and promotes the closing of the pore.

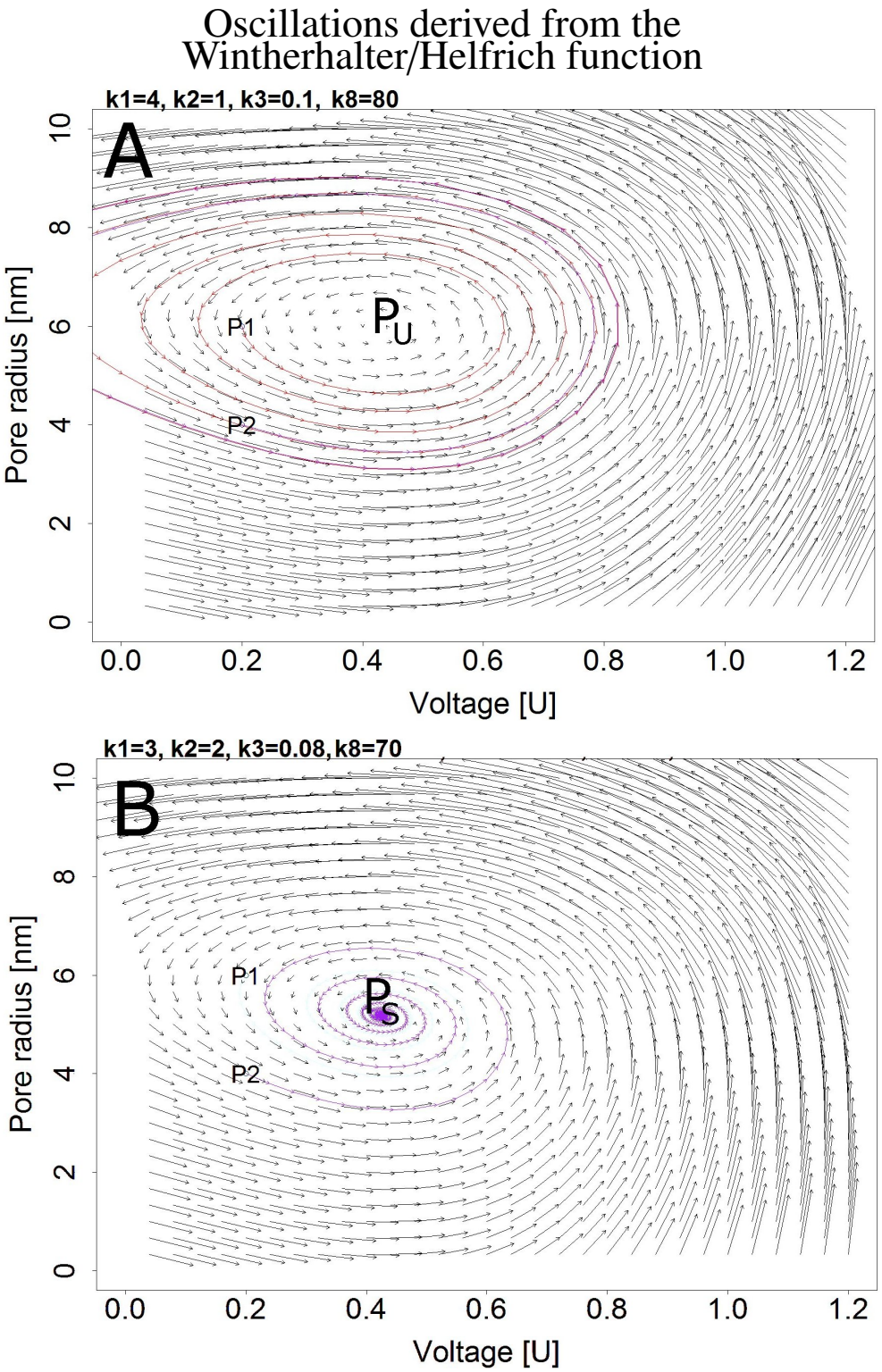

Figure 4.4: *In each figure (A-D) a vector field in the U, r-space is plotted. The black arrows are 1. order approximations to the change in U and r after a time step dt. The red and purple arrows illustrate the evolution of two starting points after n = 2000 time steps.* ***A Unstable spiral:*** *The starting points P_1 and P_2 circulates away from the unstable node P_u.* ***B stable spiral:****. The starting points circulate towards a stable node P_s. For* ***C*** *and* ***D*** *see figure 4.5*

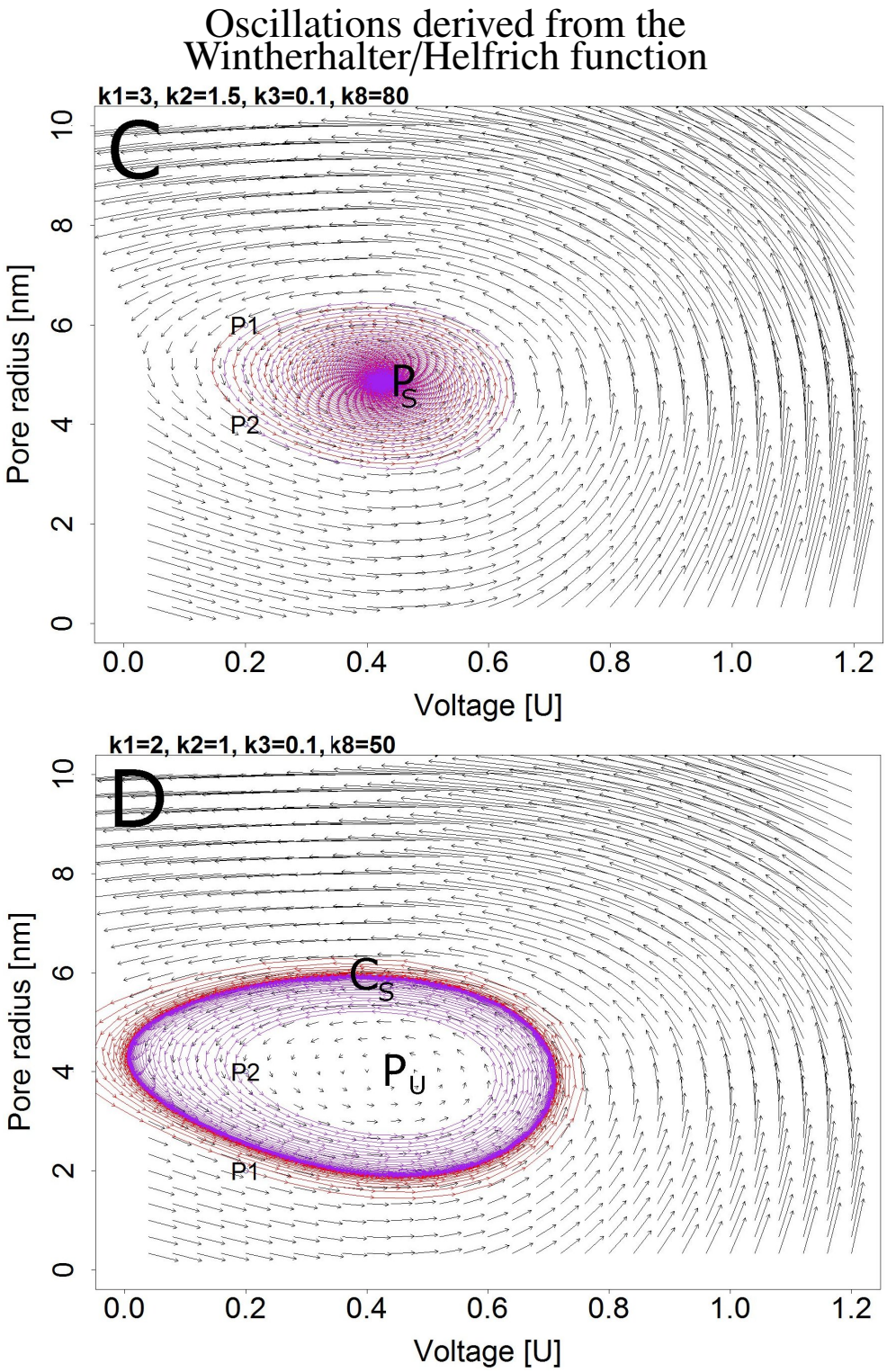

Figure 4.5: *Continued from figure 4.4.* ***C: stable spiral****: Like B but the attraction is less powerful.* ***D: Stable limit cycle****. A starting point outside the limit cycle P_1 circulates towards it and a starting point P_2 inside the limit cycle circulates towards it. This circulation is stable and will go on for as long as it has to.*

For different parameter values, this model produces unstable spirals, stable spiral and limit cycles. The system is very stable due to the extra closing term κ_7^{Wi}. Hence it is difficult to produce irreversible electrical breakdowns.

The models produced:

A) Unstable spirals

B) Stable spirals

C) Limit cycles

In terms of pore experiments on BLMs this can be interpreted as:

A) Irreversible electrical breakdown

B) Stable pores

C) Oscillating reversible electrical breakdown

For both the Abidor- and the Wintherhalter/Helfrich pore model I have 4 unknown parameters and my exploration of the parameter-spaces has been limited. To model can obtain predictive once the values of the remaining parameters have been estimated experimentally.

Chapter 5

Materials and methods

5.1 Lipids

The lipids for both calorimetric scans and voltage clamp experiments were 1,2-Dimyristoyl-*sn*-Glycero-3-Phosphocholine (DMPC), 1,2-Dilauroyl-*sn*-Glycero-3-Phosphocholine (DLPC) and 1,2-Dipalmtoyl-*sn*-Glycero-3-Phosphocholine (DPPC). The lipids were obtained from Avanti Polar Lipids and used without further purification. Lipids were properly sealed and stored in a freezer at $-18\ ^{\circ}C$ between experiments.

5.1.1 Sample preparation

In order to construct a sample containing a mixture of different lipids, the lipids were dissolved in chloroform and mixed in the desired molar concentration. In the organic solvent the lipids were stirred thoroughly in order to mix properly. The chloroform was evaporated with N_2 and the last residues were removed with a vacuum pump.
In the samples for tip-dipping experiments, the lipid mixture were diluted to the proper concentration with a mixture of hexane and ethanol (4:1).
Samples for calorimetric scans were mixed in a buffer of KCl and HEPES with pH of 6.9.
All the lipid ratios measures are calculated from molar ratios from the relations:

Lipid	Carbon groups	Meltingpoint ($^{\circ}C$)	Molar mass (g/mol)
DLPC	12	-2	621.83
DMPC	14	24	677.94
DPPC	16	41.5	724.05

Table 5.1: [Fidorra, 2004]

$$c = \frac{n}{V} \tag{5.1}$$

and

$$n = \frac{m}{M} \tag{5.2}$$

where c is the desired concentration, n is the number of mole, V is the volume, m is the mass and M is the molar mass.

5.2 Differential Scanning Calorimetry

The Differential Scanning Calorimetry (DSC) used was a *MicroCal Inc. VPVP-DSC*.
DSC is an experimental technique used to obtain information about transitions in a sample. The DSC-aperture contains two chambers. One chamber where the sample is injected and one control chamber where the buffer without sample is injected.
The two chambers are connected to a thermocouple that controls the temperature. Energy is added to each chamber at a rate so the temperature change over time is constant with a predefined rate ($5\ \frac{^\circ C}{hour}$).
The pressure in each chamber is kept constant.
The difference in the amount of heat added to the chambers is:

$$dQ = (P_{ch1} - P_{ch2}) \cdot dt \tag{5.3}$$

Where P_{ch1} and P_{ch2} are the power added to chamber 1 and 2 respectively in the time interval Δt.
The enthalpy is related to the energy as follows;

$$\begin{aligned} dH &= dQ + V \cdot dp \\ &= dQ. \end{aligned} \tag{5.4}$$

$V\Delta p$ cancels out since the pressure is kept constant. The excess energy added to the sample is the excess enthalpy. The heatcapacity can therefore be obtained directly from this result as follows:

$$c_p = \frac{dH}{dT} = \frac{dQ}{dT}. \tag{5.5}$$

Though the scan rate was only $5\ \frac{^\circ C}{hour}$, the system showed a slight delay in response to heat absorption. Each experiment was therefore composed of 4 consecutive temperature scans across the transition. Two up-scans and two down-scans. The transition was then found as an average over the four scans.

The data analysis was carried out in *Igor Pro* software with a program kindly provided by Andreas Blicher.

5.3 Tip-dipping

5.3.1 Pipet preparation

In this section I will describe the technique used to measure the conductance of a membrane under voltage clamp conditions.
The method of tip-dipping was first described by Hanke et al. in 1984. It is a relative easy method for forming BLMs for voltage or current clamp experiments [Hanke et al., 1984].
A membrane was formed on the tip of a pipet in an electrolyte solution. The cross membrane voltage was held constant by an electrode on each side and the current was measured.

The tip-dipping experiments were performed with a pipet having a tip with a radius in the order of micrometers. The pipet was constructed by pulling the ends of a heated glass pipe (Glass type 1BBL, diameter of 1.5*mm*, by *World Precision Instruments*.

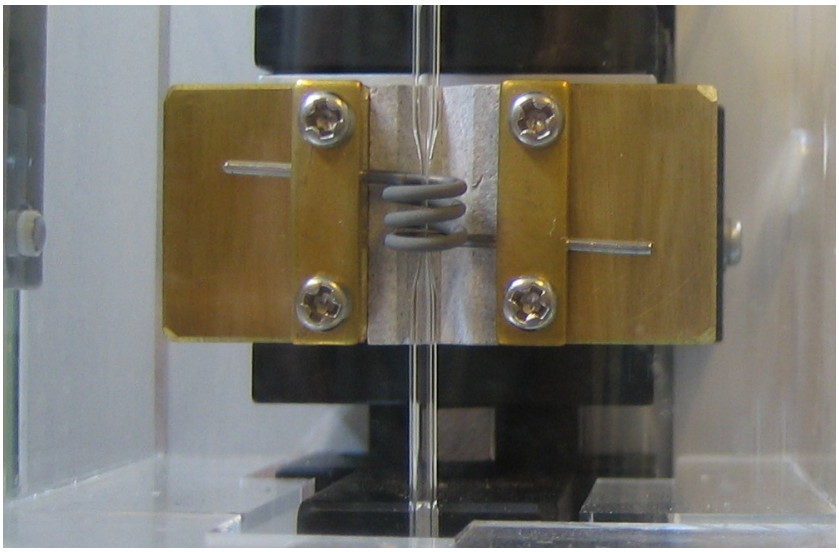

Figure 5.1: *The forming of a pipet from a glass pipe*

The pulling was performed vertically in two steps by a *Narshige PC10 heating instrument*.
Weights were attached to the bottom end of the pipe and a heating element surrounded the middle part of the glass pipe (see figure 5.1).
In the first step, the heating settings were set to 80%*. The pulling was blocked after a pull of 8*mm*. Subsequently the heater was lowered a distance of 4 *mm* to aim at the center of the stretched area.

*The heating level are on scale from 1 – 100%. The corresponding temperatures are not known to us.

In the second step the ends were pulled apart with a heating of 40%.
The pipet was at this stage not only narrow but sealed at the end. The tip was broken of using a glass heater as follows.
The pipet-tip was slowly moved into a small heated glass bulb (heating settings were 33%, see figure 5.2. After a rapid cooling the pipet was pulled out breaking off the sealed tip leaving the narrow tip of the pipet with a opening of approximately 1 μm.

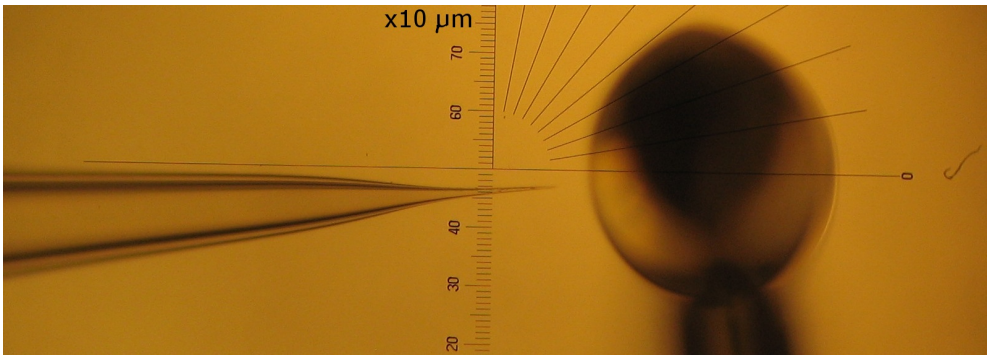

Figure 5.2: *The unsealing and polishing of a pipet*

In order to polish the tip, it was subsequently held at a short distance from the heated glass bulb (heating settings were 50%) for $3-5$ seconds and the distance was approximately 15 μm).

5.3.2 Tip-dipping

The tip-dip experiments were performed using voltage clamp. In voltage clamp experiments, the voltage is controlled across a system of capacitors and/or resistors and the resulting current is measured.

The pipet was filled with a buffer of 2 mM KCl and an electrode was placed into the non-tip end after assuring that no air bubbles were present. A Petri dish with the same buffer was prepared and placed under a movable device holding the pipet. The other electrode was placed in the Petri dish and both were connected to a computer.
The voltage across the two electrodes could then be controlled and the resulting current, be read by the *ClampEx* software on the computer.

When the unsealed tip was lowered into the buffer the system short circuited.

The experiments were performed using voltage clamp. In voltage clamp experiments, a voltage is controlled across a system of capacitors and/or resistors and the resulting current can be measured.

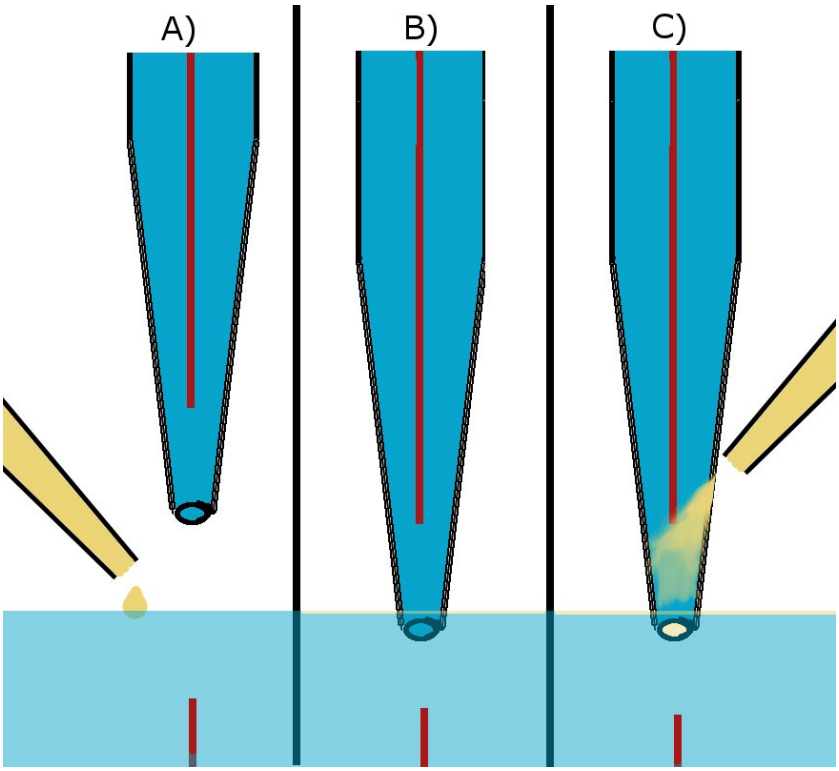

Figure 5.3: *Tip-dipping*

In our system, the membrane functions as a capacitor and the pores function as resistors:

$$I_m = \frac{dV_m}{dt} C_m + \frac{V_m}{R} \tag{5.6}$$

To form a BLM on the tip of the pipet, I proceeded as follows:

- A drop of lipid sample was dropped on the Petri dish-buffer to lower the surface tension prior to the first experiment (see figure 5.3 A).
- The pipet was lowered into the buffer in the Petri dish. As soon as the tip touched the surface, the current could freely run from the electrode in the tip through the tip to the other electrode and the system short circuited (see figure 5.3 B).
- Another droplet was then placed above the tip of the pipet. With a little luck, the drop ran down the tip and sealed the opening with a bilayer of lipids (a BLM). The success rate for this experiment was relatively high as described in [Hanke et al., 1984] (see figure 5.3 C).

The capacitance is defined: $C_m = \frac{Q_m}{U}$, where Q is the charge that builds up on the capacitor with the voltage U across the capacitor. If the capacitance does not change

over time, I can write:

$$C_m = \frac{I_m}{dU/dt} \tag{5.7}$$

When $\frac{dV}{dt}$ is constant. The capacitance can be directly obtained from the current.

In the beginning of each experiment, a *trial* voltage was applied across the newly formed membrane. The applied trial voltage had $\left|\frac{dU}{dt}\right| = constant$ (see figure 5.4). From the output current and $\frac{dU}{dt}$ the membrane capacitance could be obtained.
Ideally, the current should remain constant in the intervals where $\frac{dU}{dt} = constant$, assuming there are no pores or leaks in the membrane. This is of cause not entirely true. A small leak current will run across the membrane.
From the measured capacitance C_m, I can obtain the radius of the pipet, the thickness of the membrane or the relative permeativity of the lipid bilayer

$$C_m = \frac{\epsilon_0 \epsilon_l A_m}{d}, \tag{5.8}$$

where $\epsilon_0 = 8,85 pF/m$ is the vacuum permittivity, $\epsilon_l \approx 2$ is the relative permeativity of the lipid bilayer [Tien and Ottova, 2003]. A_m is the area of the membrane which corresponds to the area of the pipet tip and $d \approx 4\ nm$ is the thickness of the membrane. This value has been shown to change with as much as 65 % in the transition [Antonov et al., 2003].
A_m can obviously not be taken from the literature. I can estimate the radius of the pipet r_{pipet} under the microscope when the pipet tip is fire polished but the error of this estimation is in the order of $+/- 5\ \mu m$. Calculation from the capacitance yields (see equation 5.8):

$$r_{pipet} = \sqrt{\frac{C_m d}{\epsilon_0 \epsilon_r \pi}}, \tag{5.9}$$

where $r_{pipet} = \sqrt{A/\pi}$
For most experiments r_{pipet} was of the order of a micrometer.

In figure 5.3.2, the capacitative response from air is shown. This corresponds to the situation before the pipet is lowered into the buffer.

When the pipet is lowered into the buffer, the system immediately short-circuits (see figure 5.6 and figure 5.3 B).

When a membrane is formed subsequent to the drop of lipid sample, the capacitative current is detected, the capacitance of the formed membrane can be calculated from equation 5.7 and the experiment can begin (see figure 5.7).
A faraday net was layed over the experimental setup to reduce electrical disturbance from the surroundings.

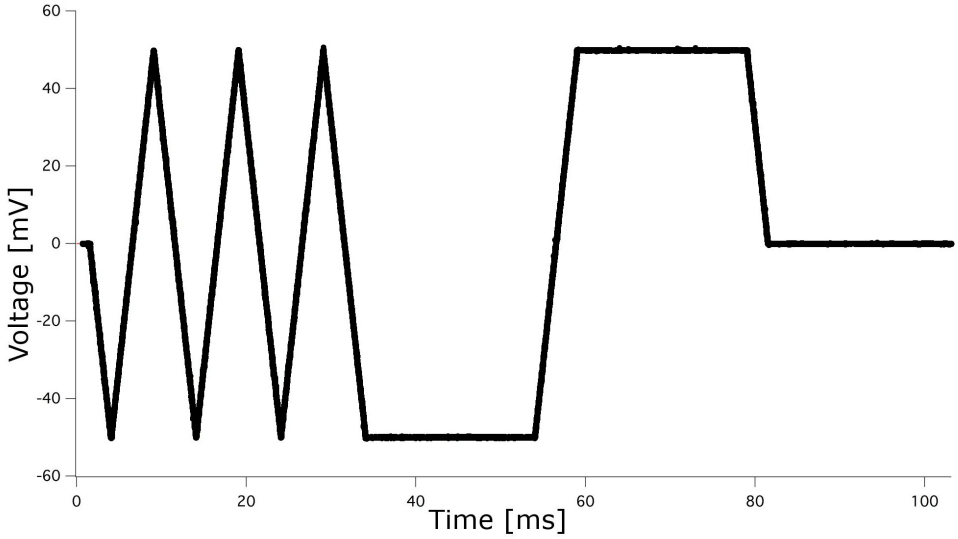

Figure 5.4: *The voltage input.* $\left|dU/dt\right|$ *is held constant.*

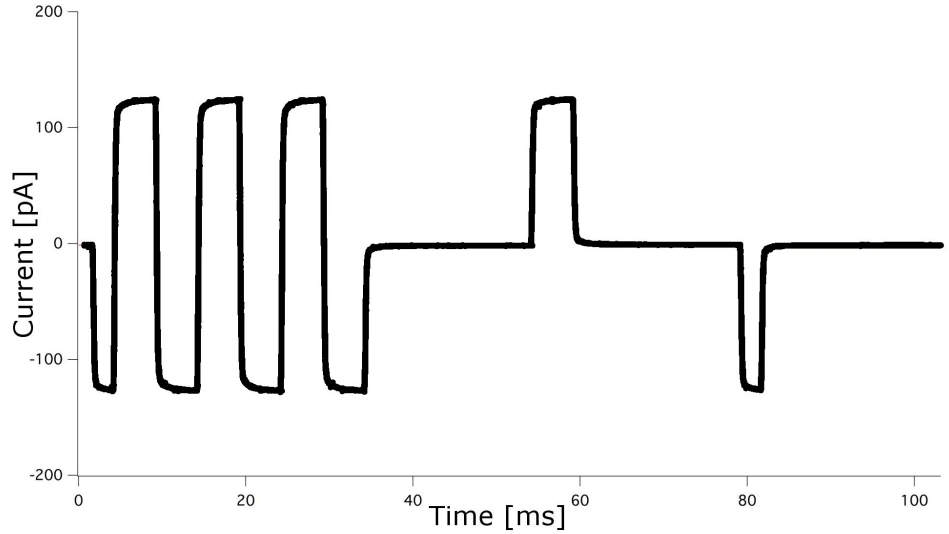

Figure 5.5: *The capacitative response from air*

In most experiments, the applied voltage was negative. The reason for negative voltage was that it seemed to work slightly better. If this was correct, it was most likely due to effects from asymmetry of the pipet tip.

The temperature of the buffer in the petri dish was controlled by a thermocouple. The aperture was calibrated and the temperature deviation within $5°C$ of room temperature was found to be:

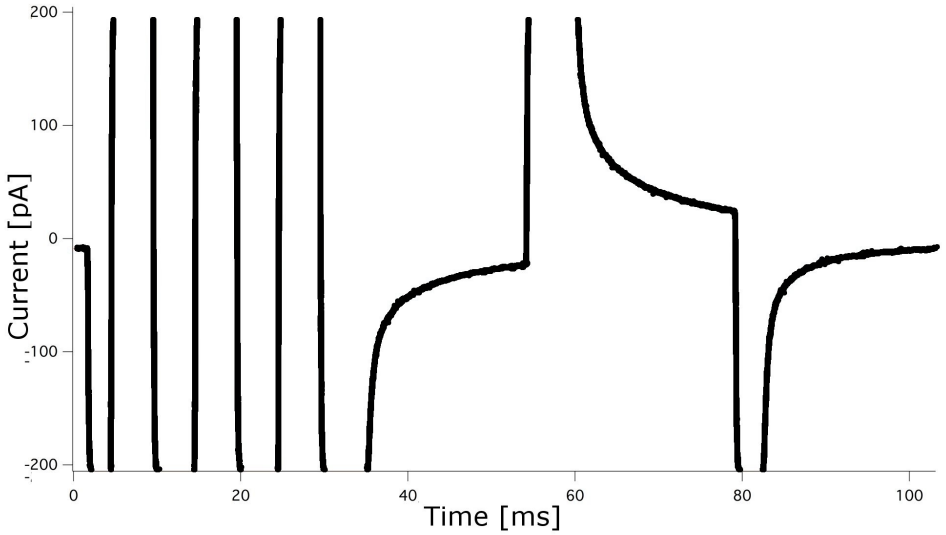

Figure 5.6: *The capacitative response from buffer: short-circuit.*

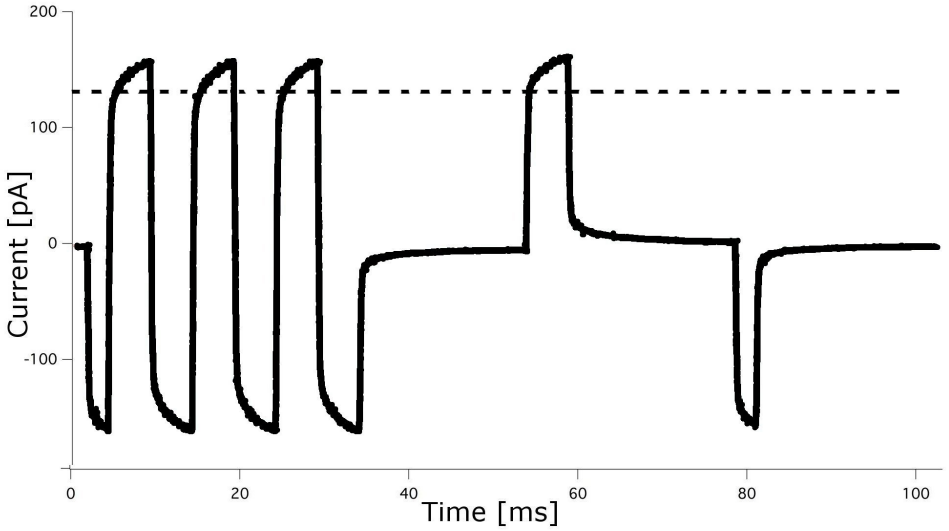

Figure 5.7: *The capacitative response from a BLM*

$$T = T_{thermocouple} +/- 0,5°C.$$

This is a large deviation, which means that the maximum of the transition could be difficult to predict.

Chapter 6

Results

6.1 Differential scanning calorimetry

Using DSC, I performed temperature scans to obtain the heat capacity profiles of various lipid mixtures.
The concerns were:

- To obtain a lipid mixture with a width large enough to enable control over the state of the membrane in the tip-dip experiments.
- To obtain a magnitude of the heat capacity profile large enough to get the desired effect of the transition (enhanced compressibility, prolonged relaxation times, etc.).
- To obtain a lipid mixture with a transition close to room temperature.
- To obtain a lipid mixture with good properties to form a stable membrane on the tip of a pipet fro the tip-dip experiments.

The last concern was not a property that could be studied with DSC. This property was investigated through *trial and error*.

For the lipid mixtures DPPC/DMPC (1:4) and DMPC/DLPC (4:1), I found the desired properties. Further, they were relatively well suited for forming BLM.

The transition of DMPC/DLPC (4:1) was 21.6 $^{\circ}C$ (see figure 6.1) and the transition of DPPC/DMPC (1:4) was 25.3 $^{\circ}C$ (not shown).

6.2 Tip-Dip experiments

An experiment starts with the forming of a BLM as described in section 5.3. The voltage is turned up to the desired level and the resulting current is measured as function of time.

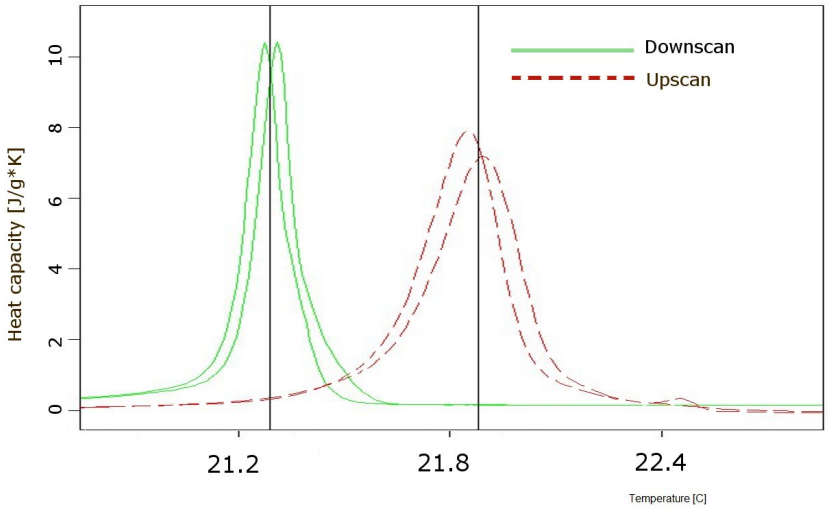

Figure 6.1: *Heat capacity profile of DMPC/DLPC (4:1). This lipid mixture has a transition at* 21.6 $^{\circ}C$. *The full width at half maximum is* $\sim$ 0.5 $^{\circ}C$.

The recordings are started and the trace may last from a few seconds to an hour depending on pipet, lipid mixture, voltage, etc.

When the voltage is applied a transient capacitative current runs across the membrane. The charges quickly build up on the membrane as a capacitor,

$$Q_m = C_m U\left(1 - exp(-\frac{t}{C_m R_m})\right) \tag{6.1}$$

where C_m is the membrane capacitance, R_m is the membrane resistance, U is the applied voltage and t is the time. The time constant $\tau_c = C_m R$ is of the order of milliseconds.

When the voltage is constant the only current running is the ionic current, which is due to the movement of ions across the membrane as a resistor. The current stabilizes at a baseline value I_m with a fixed conductance:

$$I_m = G_M \cdot U \tag{6.2}$$

where $G_m = 1/R_m$ is the membrane baseline conductance.
In figure 6.2, a voltage/current relationship for a BLM is shown. The slope of the graph is the conductance. The linear relation holds up until about 150 mV.

The observed conductive behavior depends on the voltage and the temperature. The voltage contributes to the energy of a pore as described in section 3.1 and the temperature affects the state of the membrane and consequently also the mechanical properties

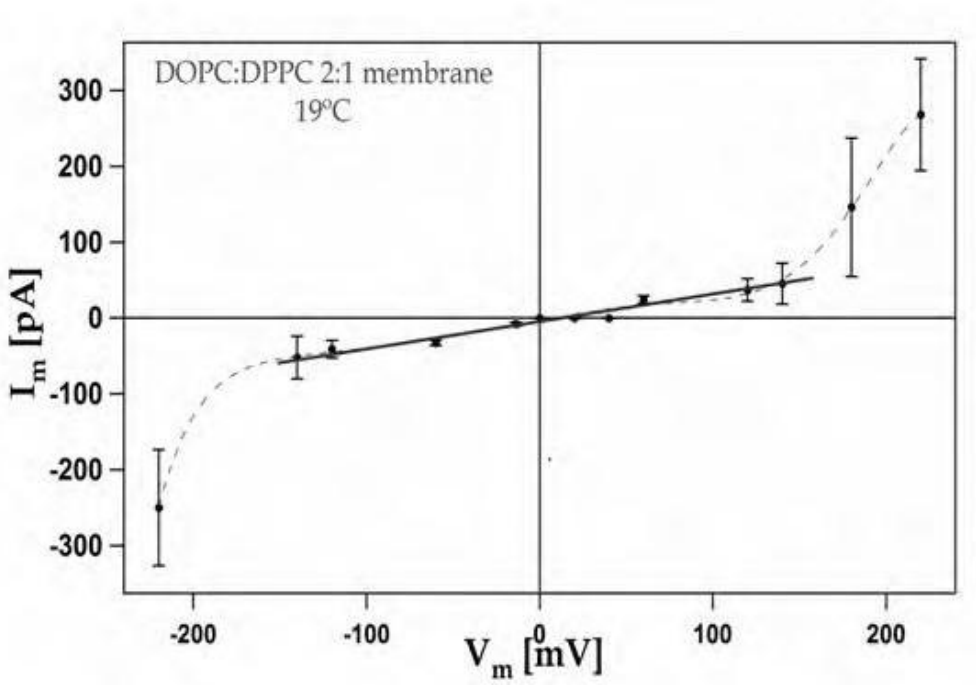

Figure 6.2: *Voltage/current relationship for a BLM (POPC:DPPC 2:1) [Wodzinska, 2008]*

including the energy of the pores.
Other factors such as pH, buffer concentration, lipid mixture, etc. also play a role but they are kept constant throughout the experiments.

I will in the following briefly describe some of the different phenomena I have observed during the many hours of experimenting.

- **Stable baseline**
  For low voltages ($|U| < 100\ mV$) the baseline was often stable with low conductance. The noise level of the conductance was approximately proportional to the input voltage but was very sensitive to disturbance such as people moving in the room, the arrangement of the faraday net, etc.
  For higher voltages ($|U| > 200\ mV$) the baseline could also be stable with a high noise level but typically only for a short period ($t < 20\ s$). The baseline could be stable for up to an hour for $|U| < 50\ mV$. Other states often succeeded the stable baseline state and other states could return to the stable baseline state.

- **Low conductance stable state**
  Low conductance states were states where the membrane showed little or no current response to a change in voltage. The membrane could withstand a voltage of

$|U| = 1000\ mV$ or more with a conductance of 20 pS (the aperture could not go higher).
This state was often seen in experiments performed with pipets that had been used for multiple traces. The low conductance was probably caused by more than one membrane on the tip of the pipet clocking it. The change to a low conductance state was irreversible and a new pipet had to be prepared.

- **Baseline drift**
  Baseline drift was a non-quantized conductance change. At constant voltage the current drifted toward higher or lower values for up to minutes.
  Baselinedrift was also seen in the cases where the voltage was altered. The subsequent response in the current had a delay. This equilibration process lasted a few seconds for small currents while it was slower for higher voltages. This was not a consequence of capacitative current building up since this time scale was in the order of milliseconds.
  For medium to high voltages ($|U| > 100\ mV$) the baseline drift indicated an unstable membrane and the phenomenon was often seen together with *baseline jumps*, *channel-like events*, spikes and oscillating reversible breakdown. It was often a sign of impending membrane rupture.

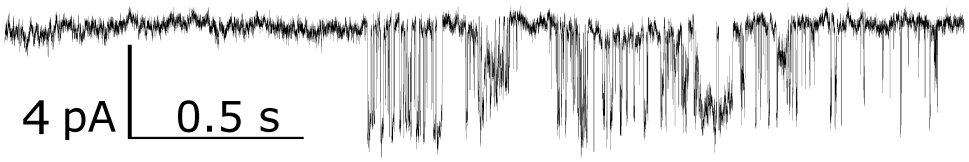

Figure 6.3: *Spikes. The spikes . BLM: DMPC-DLPC 4:1,* 21.6 °*C*, $U = -150\ mV$

- **Spikes**
  Spikes are short-lived conductance jumps of $G_s = 25 \pm 10\ pS$ to. They are of the same magnitude as channel-like event but with lifetimes of the order of milliseconds. Prepores/spikes were often observed in bursts of high activity and they often preceded other membrane activity such as channel-like events (for review on *channel-like event* and bursts see below).

- **Channel-like Events**
  Channel-like events are small, reversible, quantized conductance changes across a BLM with lifetimes from milliseconds to seconds. See figure 6.5 and 6.4.

channel-like event were observed with low- and high voltage and were often found in bursts of high activity lasting from 1 to 10 seconds often with multiple conductance levels and multiple time scales (see figure 6.7). Channel-like event could be induced by applying a voltage pulse (500 mV for 0.1 seconds). A voltage pulse seemed to destabilize the membrane. The conductance of a channel-like event was most often between $G_p = 25 \pm 10\ pS$ but events resembling channel-like events were found with conductance up to $G_p = 70\ pS$ (see figure 6.11).

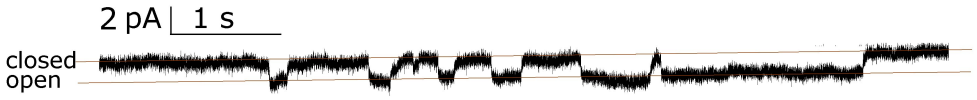

Figure 6.4: *Channel-like events. BLM: DMPC-DLPC 4:1,* 21.6 °*C, U* = −100 *mV*

Figure 6.5: *Channel-like events. BLM: DMPC-DLPC 4:1,* 21.6 °*C, U* = −200 *mV*

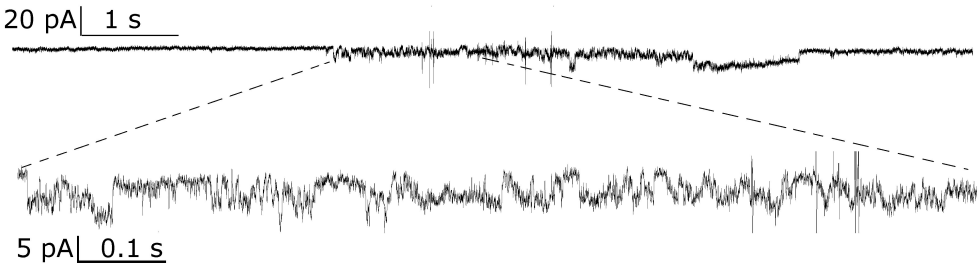

Figure 6.6: *Burst of the order of 4 seconds. BLM: DMPC-DLPC 4:1,* 21.6 °*C, U* = −300 *mV*

- **Bursts**
  The *spikes*, the *channel-like events* and the *baseline jumps* were often found in bursts in connection with each other. The bursts were also associated with an increased noise (see figure 6.6). The onset of a burst could be stimulated by a

voltage pulse ($\sim 500\ mV$ for $\sim 0.1\ s$).

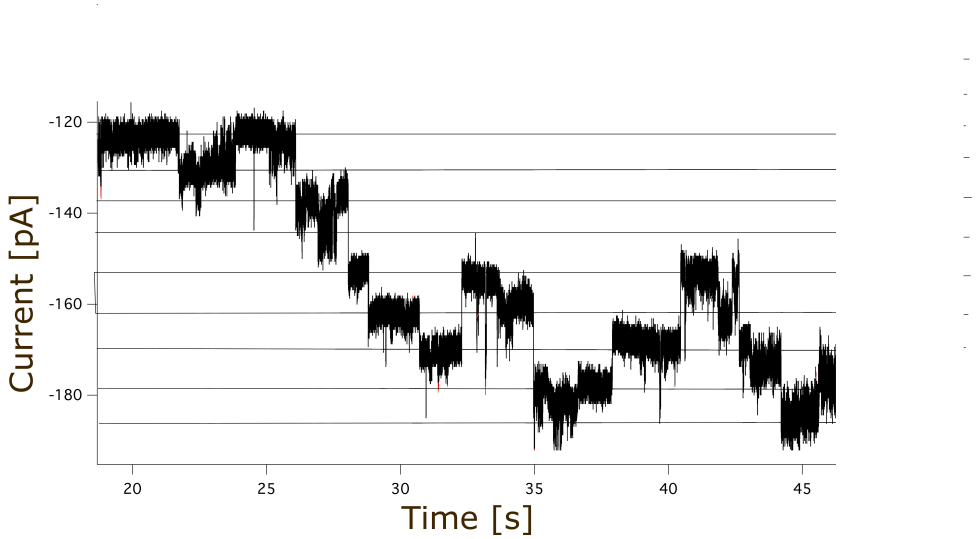

Figure 6.7: *Multilevel conductance. The figure shows the quantized nature of the BLM conductance. Presumably each step of* $G_p \approx 26\ pS$ *corresponds to the opening/closing of a lipid channel. At* $t = 45$ *there are* ~ 7 *more open lipid channels than at* $t = 20$*. BLM: DMPC-DLPC 4:1,* 21.6, $°C$, $U = -300\ mV$

- **Baseline jumps**
  Baseline jumps are drastic shifts in the baseline current when the voltage is kept constant. ($\Delta G_m > 70\ pS$ see figure 6.8).
  The baseline jumps were often from a state of stable baseline to unstable states exhibiting channel-like events and other unstable behavior. The baseline jump could be to higher or lower conductance.
  Other examples of baseline jumps were in connection with *baseline drift*. The conductance increased slowly over a period of seconds to minutes and then suddenly performed a baselinejump back to the initial state of low conductance.

- **Reversible and irreversible electrical breakdown**
  Eventually all membranes rupture. The lifetime can vary from seconds up to hours but it is drastically lowered by a high voltage ($|U| > 300\ mV$).
  Irreversible electrical breakdown is the rupture of the membrane. It can happen quickly ($t < 0.1\ s$) from a low or high conductance state or it can happen slowly ($t > 1\ min$) from a low conductance state through baseline drift and baseline jumps (see figure 6.12). Subsequent to a irreversible electrical breakdown, the conductance can not be restored by lowering the voltage.

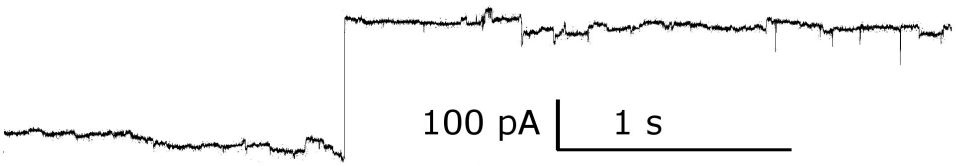

Figure 6.8: *Baseline jump. The conductance makes a baseline jump from a state of high conductance ($G_m \approx 850\ pS$) and CLEs ($G_p \approx 20\ pS$) to a state of low conductance ($G_m \approx 250\ pS$) with CLEs ($G_p \approx 20\ pS$) $DPPC/DMPC - 1:4$, $25°C$, $-400\ mV$*

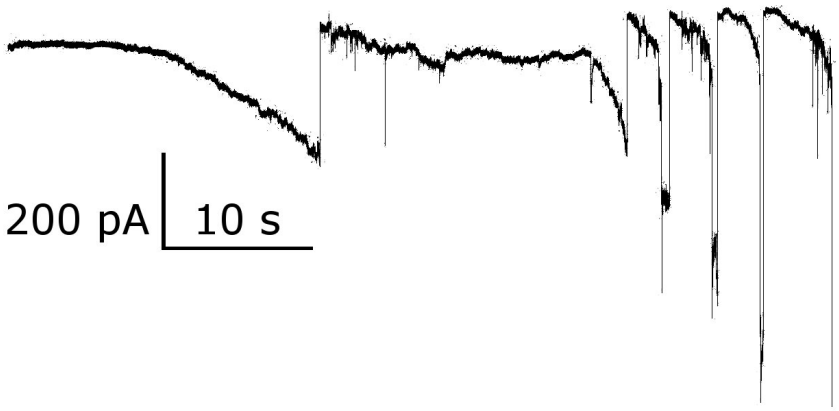

Figure 6.9: . *The conductance starts increasing (baseline drift) until the conductance suddenly jumps back to the original baseline (baseline jump). After a while the baseline starts to drift again and again it falls back. This phenomenon repeats itself 4 times before the membrane ruptures (Irreversible electrical breakdown). $DPPC/DMPC - 1:4$, $25°C$, $U = -200\ mV$*

Reversible electrical breakdown is basically behaves in the same manner as the irreversible breakdown except, the conductance is restored after a few seconds. The reversibility can happen spontaneous, without lowering the voltage or it can be induced by lowering the voltage shortly after the breakdown (see figure 6.13. The conductance is restored spontaneous, without lowering the voltage.).
Reversible electrical breakdown was only found for medium to high voltage ($|U| > 150\ mV$).

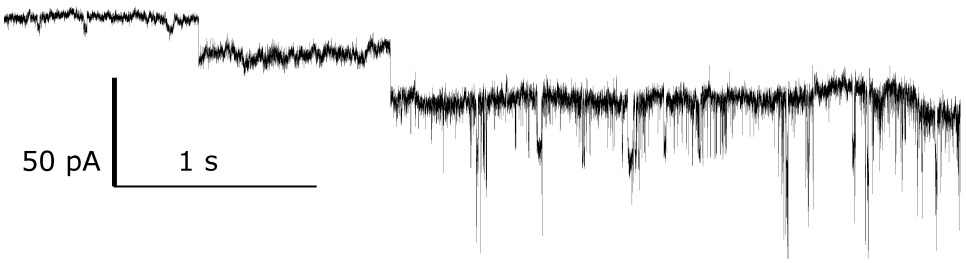

Figure 6.10: *This figure shows channel-like events ~ 20pS and baseline jumps. The baseline jumps are quantized and reversible in some cases. They resemble large channel-like events ~ 70pS. The noise increases with increased conductance. BLM: DMPC-DLPC 4:1,* 21.5 °*C, U* = −300 *mV*.

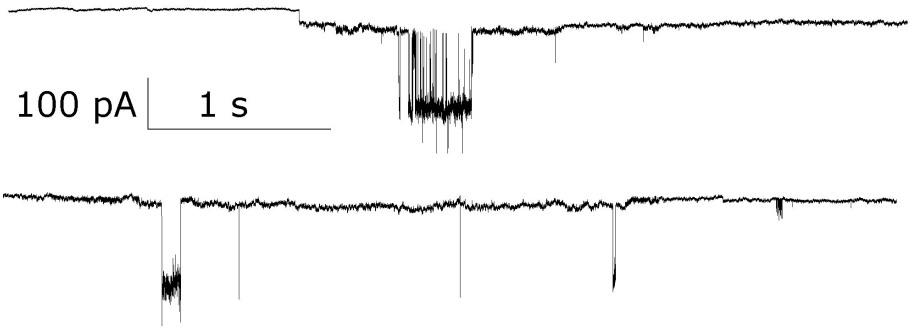

Figure 6.11: *This figure shows channel-like events ~ 20pS and baseline jumps. The baseline jumps are quantized and reversible in some cases. They resemble large channel-like events ~ 70pS. The noise increases with increased conductance. BLM: DMPC-DLPC 4:1,* 21.5 °*C, U* = −300 *mV*.

- **Oscillating reversible electrical breakdown**
  Oscillating reversible electrical breakdown is the repetition of an event involving a drastic conductance change with a fixed time scale under voltage clamp conditions.
  Oscillating reversible electrical breakdown was observed multiple times under various conditions. The time scale of one oscillation was 3 – 10 seconds, the voltage was 150 – 600 *mV* and the conductance oscillated between 150 *pS* and something larger than 4000 *pS* (the apparatus could not record currents higher than 1200 *pA*).
  In the trace of figure 6.15 the time scale was about 2.5 seconds (see figure 6.16). The conductance was stable for ~ 2 seconds whereupon the baseline started drift-

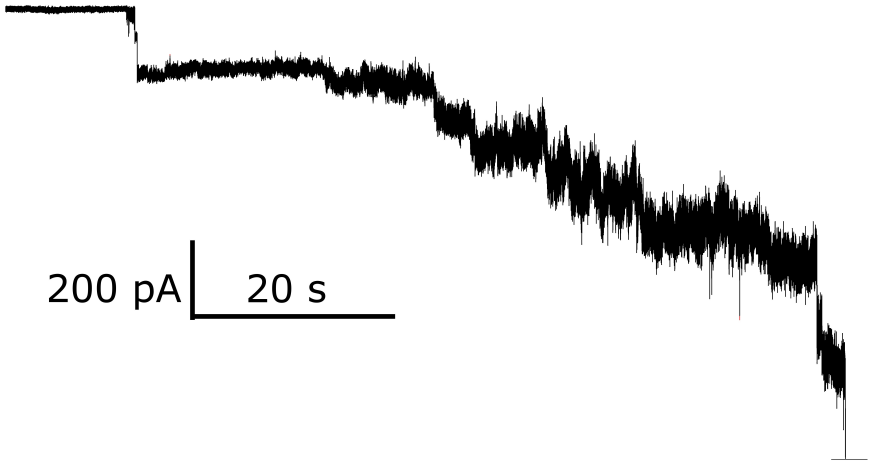

Figure 6.12: *Irreversible electrical breakdown. From a state of low conductance the membrane starts a process of irreversible electrical breakdown through an increase in conductance and noise. The conductance could subsequently not be restored by lowering the voltage.* $DPPC/DMPC - 1:4$, $25°C$, $U = -150\,mV$

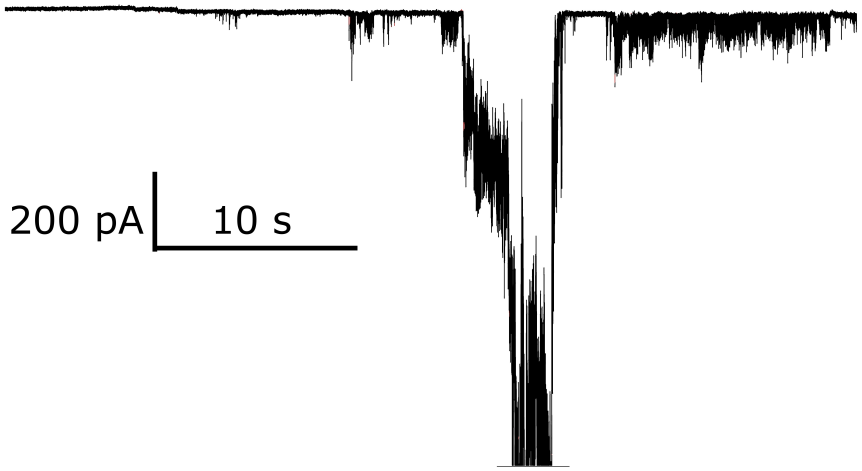

Figure 6.13: *Reversible electrical breakdown. The conductance soars from* $\sim$ 300 pS *to more than* 8000 pS. *Subsequently the conductance was restored without changing the voltage.* $DPPC/DMPC - 1:4$, $25°C$, $U = -150\,mV$

ing with an increasing rate. The system was then short circuited (or reached a conductance state too high to record on our equipment) for a period of $\sim$ 0.5 sec-

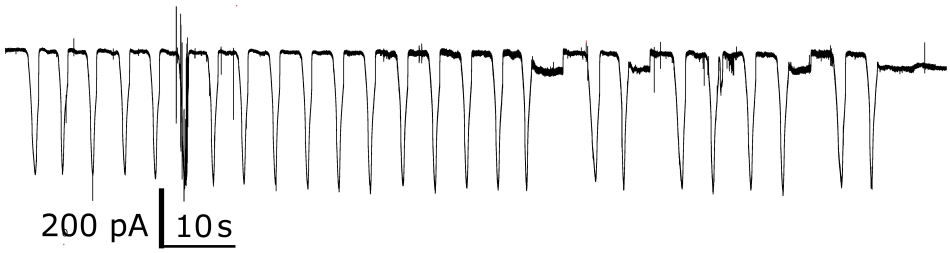

Figure 6.14: *Oscillating reversible electrical breakdown. This oscillation has a timescale of* ~ 5 *seconds.* $DPPC/DMPC - 1:4$, $25°C$, -550 *mV*

onds. Finally, the conductance rapidly returned to its initial state to complete one cycle. The trace continued for ~ 200 seconds.

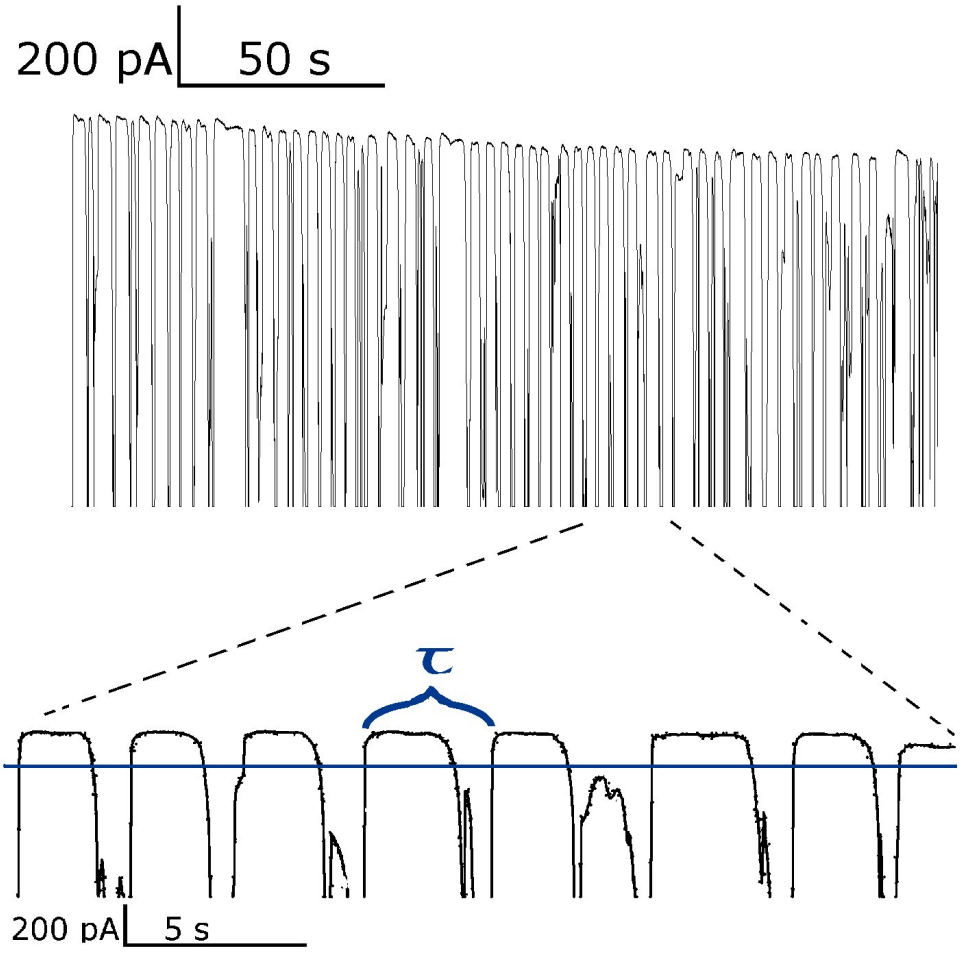

Figure 6.15: *Top: Oscillating reversible electrical breakdown. The conductance changes from* $G_m = 100\ pS$ *to* $G_m > 2000\ pS$. *After* $\sim 0.5\ s$ *the conductance is restored for* $\sim 2.5\ s$. *This phenomenon repeated itself for* $t > 200\ s$ *Bottom: A closeup of the top figure.* $DPPC/DMPC - 1:4$, $25°C$, $-500\ mV$

6.3 Pore size estimation

One of the first methods for estimating pore sizes was based on the permeability of ions of different sizes. The channel diameter was assumed to permeate ions with diameters equal to, or smaller than the diameter of the pore [Cecchi et al., 1982, Hille, 1972]. This model does not take into account the electrostatic interactions between the ions charged parts of, or near the channel. This interaction can effectively change the established value of the radius. This is mainly a problem for biomembranes or BLMs containing lipids with charged head groups.

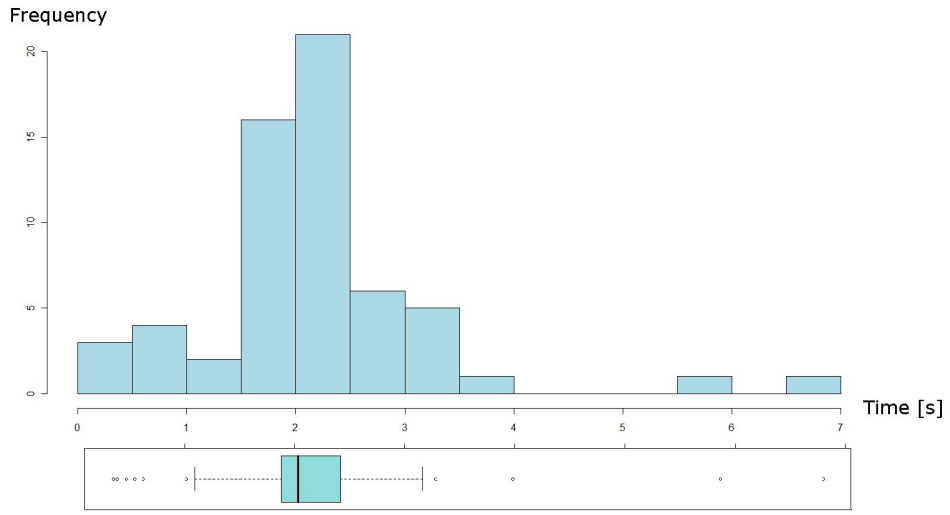

Figure 6.16: *Time scale for the oscillation in figure 6.15. The oscillation was very regular. The time was measured between two oscillations (τ of figure 6.15) and the result is showed in this histogram.*

Another simple method viewed the channel as a water filled cylinder with the length equal to the membrane thickness. The radius could then be calculated directly from the conductivity [Benz and Hancock, 1981, Colombini, 1980].
This model simplifies the problem too much. It does not consider friction or hydrophobic interaction [Antonov, 1982, Krasilnikov et al., 1992].
An improved version of the above model views the cylindrical tube as being filled with electrolyte solution of ohmic resistance, the pore radius r_p can be estimated from the average conductance of a single pore [Freeman et al., 1994, Eldridge and Morowitz, 1978].

$$r_p = \sqrt{\frac{G_p d}{\pi S}} \tag{6.3}$$

Where G_p is the conductance of a single pore and S is the specific conductivity of the electrolyte solution [Antonov et al., 2005]. S can be calculated from Kohlrauschs Law, which states that the molar conductivity of a solution is proportional to the square root of the concentration [Hallock, 1900]. A buffer solution of 150 mM KCl was found to be equal to 75 S/m [Wodzinska, 2008]. The values of the membrane thickness d is dependent on the lipid species and on the state of the membrane. The thickness of the hydrophobic part was found to depend linearly on the number of C-atoms in the tail [Lewis and Engelman, 1983].
From the value reported in 1983 by Lewis and Engelman $d = 4.5\ nm$ [Lewis and Engel-

man, 1983] for a lipid in the gel phase the thickness was taken to be $3,8 - 4.5\ nm$ in the transition.
From the tip-dip experiments the conductance of a pore (channel-like event) was found to be $25 \pm 10\ pS$
From equation 6.3 the pore size was found to be $0,85 \pm 0.15\ nm$.

Chapter 7

Summarizing discussion and perspectives

In chapters 1 and 2 the theory behind membrane properties leading to permeability was described. In chapter 3 the effect of voltage on permeability was examined and two pore theories were presented. In the following I will discuss the findings of chapter 6 in the light of the theoretical considerations.

7.1 Comparison of channel-like events and protein ion channels

In voltage clamp experiments on BLMs studied with the tip-dip method I have found channel-like events with conductance $G_p = 25 \pm 10\ pS$. The channel-like events were observed in protein free membranes in the biological voltage regime ($U < 150\ mV$). The mean lifetimes of channel-like events are similar to the channels observed in protein channels [Wodzinska, 2008].

The behavior resembles protein ion channels and it is therefore interesting that these events can occur in a protein free environment.
The fact that channel-like events can occur without proteins has been pointed out by several authors before [Yafuso et al., 1974, Antonov et al., 1980, Antonov et al., 2005, Wodzinska et al., 2009, Pakhomov et al., 2009, Heimburg, 2010b] but after more than 3 decades the phenomenon remains relatively unknown [Böckmann et al., 2008].
Although the similarities between channel-like events and the quantized conductance of an acetyl choline receptor (see figures 2.3 and 2.4) are striking, the two fields are utterly segregated.

In the field of electroporation, the ability of a membrane to form pores is widely accepted *. The pore models by Winterhalter/Helfrich and Abidor et al. can account for stable pores with $r_p \approx 1\ nm$ but they are not considered in biological processes. This is perhaps due to the fact that the voltage exerted on the membrane during electroporation is out of biological regime and that mechanisms for gating the lipid channels seem unattainable.

The transition of membranes is an important factor in the attempt to make the pore theories of electroporation relevant for biological processes. The transition lowers the voltage required for electroporation phenomena to biological the regime. Both channel-like events and electroporation phenomena can be gated by shifting the state of the membrane in and out of the transition.
Further PEGs have been shown to mechanically block the conductance of specific ions based on the pore sizes of the channels [Antonov et al., 2005].
Other means for gating of channel-like events include anesthetics, which were found to block channel-like events by shifting the transition [Græsbøll, 2006, Blicher et al., 2009, Wodzinska et al., 2009]. There even exists a direct correlation between the strength of the anesthetic and its ability to dissolve in the BLM [Overton, 1901]. This is called the *Meyer-Overton relation* and is the only known relation between different anesthetic compounds.

If the lipids of the membrane alone can account for the voltage driven traffic of ions across the membrane, what purpose does the *protein ion channels* serve?
The membrane and the proteins interact. The proteins in and around the membrane affect the membrane and shift the transition. One purpose of the proteins could be to regulate the state of the membrane. This idea is supported by experiments on E.coli membrane showing that the range of the transition was correlated with the growth conditions (pH, temperature, etc.) in a way so the transition was always in the vicinity of environmental conditions [Heimburg and Jackson, 2007].

Through studies on BLMs I have examined the movement of ions across a protein free membrane. It is much more difficult to construct an experiment in which the functions of the protein ion channels can be studied isolated from lipids. The functions of proteins are closely coupled to their shape and for integral proteins such as ion channels the shape is dependent on the membrane.

An interesting experiment could be to investigate the function of a peripheral protein on the channel-like events of a BLM. A peripheral protein does not penetrate the

*For what it is worth: Pore-theory is the parent mechanism used by the open dictionary *wikipedia.org* to account for the phenomenon of electroporation.

membrane but binds to the surface. Presumably, a peripheral protein could be shown to switch channel-like event activity on/off (by moving the transition). Hereby one could rule out the possibility of ion transport through proteins and show that the proteins affect the permeability of the membrane in an indirect manner.

7.2 Comparison of electroporation and channel-like events

In chapter 6, I found reversible- and irreversible breakdown of the BLM. I found that the triggering voltage could be significantly lowered by shifting the temperature to the transition regime.
Further, I observed baseline jumps, spikes and channel-like events. These events were often found in the same traces as the electroporation phenomenon.
Most models of electroporation builds on the assumption that hydrophilic lipid pores form in the membrane. The pore theories are many and the physics have been thoroughly treated for more than 3 decades.
The same two equations outlined in section 3.1 that are used to describe electroporation, can also account for channel-like events. Further, both phenomena are sensitive to a shift in transition. Channel-like events can be switched on/off and the triggering voltage for electroporation can be lowered.

The manner in which voltage influences the state of the membrane is disputed. It is believed that the work exerted by the electric field on the lipid head groups shifts the transition to higher temperatures. The idea can be pictured as if electrical field has an ordering effect on the polar head groups of the lipids [Stulen, 1981, Dimitrov, 1984].
Further investigation in this field is called for.

The lag-time observed in electroporation following the initial voltage pulse is believed to be a meta state containing non-conducting pre pores. These prepores are qualitatively the same as the hydrophobic pores proposed for both the pore theory of Winterhalter/Helfrich and Abidor et al.

The lag-time clearly precedes the onset of the channel-like events. The origin of this lag-time is most likely the relaxation times of the membrane. The destabilization of the ordered membrane from a stable conductance state to a meta stable state requires a change in conformation.
The relaxation time for this phenomenon was found to be inversely proportional to the applied voltage [Melikov et al., 2001]. It is in the same order as the relaxation times found for domain formations in BLM, which ranges from seconds to minutes. This correlation verifies the result that the lag time of both phenomena were reduced in the transition.

7.3 Oscillating reversible electrical breakdown

In chapter 4 I proposed two different models for an oscillating system composed of two differential equations describing the rate changes $\dot{U}(U,r)$ and $\dot{r}(U,r)$:

$$\dot{U}(r,U) = \kappa_1 - \kappa_2 U - \kappa_3 r^2 \tag{7.1}$$

and the two descriptions of $\dot{r}(U,r)$ derived from the pore models by Abidor and Wintherhalter/Helfrich discussed in chapter 3,

$$\begin{aligned} a) \qquad & \dot{r}(r,U) = (-\kappa_4^{Ab} + \kappa_5^{Ab} r + \kappa_6^{Ab} r U^2) \cdot \kappa_7^{Ab} \\ b) \qquad & \dot{r}(r,U) = (-\kappa_4^{Wi} + \kappa_5^{Wi} r + \kappa_6^{Wi} U^2 - \kappa_7^{Wi} r U^2)\kappa_8^{Wi} \end{aligned} \tag{7.2}$$

I illustrated the trajectories with a vector plot in U,r-space. Both systems were found to produce limit cycles, stable and unstable spirals.
The stable spirals corresponds to a stable pore size. Any starting point (U,r) in the vicinity of the stable spiral ends up in the stable node P_s in the center of the spiral. This point corresponds to a finite stable pore size.
In the case of the unstable spiral, any starting point in the vicinity of the spiral moves away from the unstable point in the center of the spiral.
The constant κ_7^{Wi} acts to close the pore in the Wintherhalter/Helfrich system. It is not included in the Abidor system, hence the Abidor system has some difficulties oscillating. On the other hand it seems more probable, that the system can achieve large radii in the case of unstable spirals which corresponds to irreversible breakdown.
For each of the two systems I have 4 unknown parameters. 3 parameters describing the rate change of the voltage and 1 phenomenological constant for each of the rate changes of the radius. Variation of these parameters can change the system drastically, it would be very interesting to obtain real physical values for these parameters from experiments and compare the results with the obtained oscillations.

I obtained oscillations in the systems of equations (7.1 and 7.2), but the form of the oscillations was not identical to the oscillating reversible electrical breakdowns observed in the experiments. One discrepancy is the time scale of the pore opening/closing. In experiments the conductance change which corresponds to the opening/closing of the pore, happens very fast while the conductance stays constant corresponding to the closed pore for a longer time.
A better description of experimental data could probably be obtained by varying the 4 parameters. I have not examined the parameter space thoroughly but I encourage others to do so.

7.4 Other points

7.4.1 Note about reproducibility in experiments

The natural sciences build on knowledge obtained from experiments. We construct an experiment, look at the outcome and make a general statement about nature. This is the logical method of *induction*.

$$\begin{array}{ll} P & \text{All swans I have observed have been white} \\ \hline & \Downarrow \\ K & \text{All swans are white} \end{array}$$

In this form of logic the conclusion can be false even though the premise is true. We need another premise to make this argument compellingly true:

$$\begin{array}{ll} P_1 & \text{All swans I have observed have been white} \\ P_2 & \text{Nature behaves uniformly in space and time} \\ \hline & \Downarrow \\ K & \text{All swans are white} \end{array}$$

If P_1 and P_2 are true then K must also be true. P_2 is the premise which all natural science relies upon. The outcome of an experiment performed today should have the same outcome as the same experiment performed under the same conditions yesterday. Likewise, experiments performed in Odense and Copenhagen should yield the same result if all other conditions are the same. Scientific experiments should be reproducible.

What I observed in experiments was not always reproducible. What seemed to be the same experiments could have different outcomes. In chapter 6, I have described my results obtained from tip-dip experiments. As described, I observed many different phenomena and have tried to describe my observations as accurate as possible.

Most likely, the problem was that the experiments were not identical. The pipet tip may have differed slightly in shape, the lipid concentration in the buffer may have enhanced the stability of the BLM, the experimental setup may not have been properly isolated from electrical noise of the environment, etc.

The tip-dip technique is potent tool for *quick and dirty* experiments, but for more thorough experiments I would recommend other experimental techniques that can provide uniform measurements.

Chapter 8

Conclusions

The purpose of this thesis was to:

- Confirm the findings of channel-like events in pure black lipid membranes.
- Propose an electrical pore model for the phenomenon of oscillating reversible breakdown.
- Investigate the correlation between the lipid ion channels of electroporation and the channel-like events observed in the phase transition of black lipid membranes.

In response to these objectives, I conclude that channels-like events and electroporation are governed by the same physical mechanisms. I have observed channel-like events and investigated the correlation between these events and electroporation phenomena. Both are purely lipid based phenomena and both are induced by the phase transition of the membrane. Further, the theoretic models used to describe electroporation can also account for channel-like events of the magnitude and time scale observed.

The resemblance between channel-like events and protein ion channels are striking. I believe that lipid ion channels could be responsible for a number of the cross membrane transport processes the literature assigns to proteins.
Aside from the resemblance in lifetime and magnitude, both mechanisms can be gated and seem to behave similarly.
I am not denying that the famous patch clamp recordings by Neher and Sakmann and many others since then was currents through the acetylcholine receptor. What I am saying is that I can achieve the same results in a protein free membrane.
According to the scientific principle of Occam's razor one should always choose the simplest of two models if both have equal explanatory power.
Many issues are still unresolved and more research is required.

Finally, I have proposed a qualitative model for the oscillating reversible electrical breakdown. The oscillating reversible electrical breakdown phenomenon was observed under voltage clamp conditions and described in chapter 6. To my knowledge the phenomenon has not been described before.

The system I have proposed was composed of two differential equations describing the rate changes $\dot{U}(U,r)$ and $\dot{r}(U,r)$.
I have assumed the form of $\dot{U}(U,r)$ to be dependent an a constant positive driving term, a negative term proportional to the voltage and a negative term proportional to the area of the pore.
The form of $\dot{r}(U,r)$ is derived from the pore free energy functions of Abidor et al. and Wintherhalter and Helfrich. This results in two different forms of $\dot{r}(U,r)$ and two systems of differential equations.

I have illustrated the dynamics of the flow in U,r-space by plotting a vector field for the flow. For different parameter values the flow of the systems changed.
For both systems I found oscillations. For certain parameter values the oscillations stabilized in a limit cycle. For other values the flow oscillated in spirals that were either stable or unstable. In the former case the flow equilibrated towards a stable node in U,r-space and in the latter case the spirals escalated towards higher values.

The form of the Wintherhalter/Helfrich pore model made the system more likely to show large limit cycles and stable spirals while it was less likely to show flows towards large r-values.

I must emphasize that 4 parameters were arbitrarily chosen and that a different behaviors could also be produced. I have not made systematic attempts to investigate the parameter space. Presumably some of these parameters could be determined experimentally. If the radius could be kept constant at different values the κ_3 could be determined. The phenomenological constants could probably be obtained from comparison with experimental time constants.

Appendix A

Appendix A

A.1 R-code for U, r-space plots

The following is the code for generating phase plots of voltage/radius correlation (see section 4). I have only included the code for the Abidor-version. The Wintherhalter/Helfrich version can be obtained by exchanging the equations.

```
# By Klaus Bruun Pedersen
library(grid)
setwd('C:/Users/uu4adm/Documents/LEdProjects/Klaus/pics/abiwinther')
xmin=0
xmax=1.2
ymin=0;ymax=10

x1<-as.numeric(0:10000)
U<-xmax*x1/10000

n=10^9

t=2000
dt=1/40
rg=3.5
Uh=0
rh=4.5

#____________________
# starting points:
Ua=0.2;ra=1.8
Ub=0.2;rb=3
# give values for the parameters (k~kappa
k1=2
```

```
k2=2
k3=.12
k7=20
#_____________________

# give output filename
nam=paste("abidor_01.png",sep="")

k4= 1.26*10^(-10)*n
k5= 6.3*10^(-4)
k6= 0.54

nx=30;ny=30

ma=paste("Abidor \n du/dt= k1 -k2*Ui - k3*ri^2 \n dr/dt= (-k4 + k5*ri
+ k6*Ui^2*ri)*k7"," \n k1=",k1, ", k2=",k2,", k3=",k3, ",
k4=",k4,", k5=",k5,", k6=",k6,", k7=",k7, sep="")

png(file=nam,width=2000,height=1500)
par(mar=c(15,15,15,15))
plot(0,0,xlim=c(xmin,xmax),ylim=c(ymin,ymax),main=ma,cex.lab=5,mgp=c(9,3,0),
cex.axis=5,cex.main=4,col="blue",type='l',xlab="Voltage [U]",ylab="Pore radius")

lx=xmax-xmin
ly=ymax-ymin
dx=lx/nx
dy=ly/ny

for(i in 1:nx){
for(j in 1:ny){
Ui=i*dx
ri=j*dy
du= k1 -k2*Ui - k3*ri^2;
dr= (-k4 + k5*ri + k6*Ui^2*ri)*k7
U2=Ui+du*dt
r2=ri+dr*dt
if(r2<0){r2=0}
arrows(Ui,ri,U2,r2, angle = 30, length = .1, code = 2);
}
}
Ui=Ua;ri=ra
t=9000
dt=.03
for(i in 1:t){
du= k1 -k2*Ui - k3*ri^2;
dr= (-k4 + k5*ri + k6*Ui^2*ri)*k7
U2=Ui+du*dt;
```

```
r2=ri+dr*dt
if(r2<0){r2=0}
arrows(Ui,ri,U2,r2, angle = 30, length = .1, code = 2,col="red");
Ui=U2;ri=r2
}
Ui=Ub;ri=rb
for(i in 1:t){
du= k1 -k2*Ui - k3*ri^2;
dr= (-k4 + k5*ri + k6*Ui^2*ri)*k7
U2=Ui+du*dt;
r2=ri+dr*dt
if(r2<0){r2=0}
arrows(Ui,ri,U2,r2, angle = 30, length = .1, code = 2,col="purple");
Ui=U2;ri=r2
}
par(new=T)
plot(c(Ua,Ub),c(ra,rb),cex=2,xlim=c(xmin,xmax),ylim=c(ymin,ymax),
ylab="",xlab="",mgp=c(9,3,0),cex.axis=0.1,col="blue",type='p')
text(Ua,ra,"P1",cex=4)
text(Ub,rb,"P2",cex=4)

dev.off()
```

Appendix B

Appendix B

B.1 Oscillations in U,r for the Abidor pore radius

The equations are (equations 4.4 and 4.6):

$$\begin{aligned} \dot{U}(r,U) &= \kappa_1 - \kappa_2 U - \kappa_3 r^2 \\ \dot{r}(r,U) &= (-\kappa_4 + \kappa_5 r + \kappa_6 r U^2) \cdot \kappa_7 \end{aligned} \tag{B.1}$$

In figures B.1, B.1 and B.1 the variable κ_1 is varied. κ_2 = and κ_3 = are fixed.

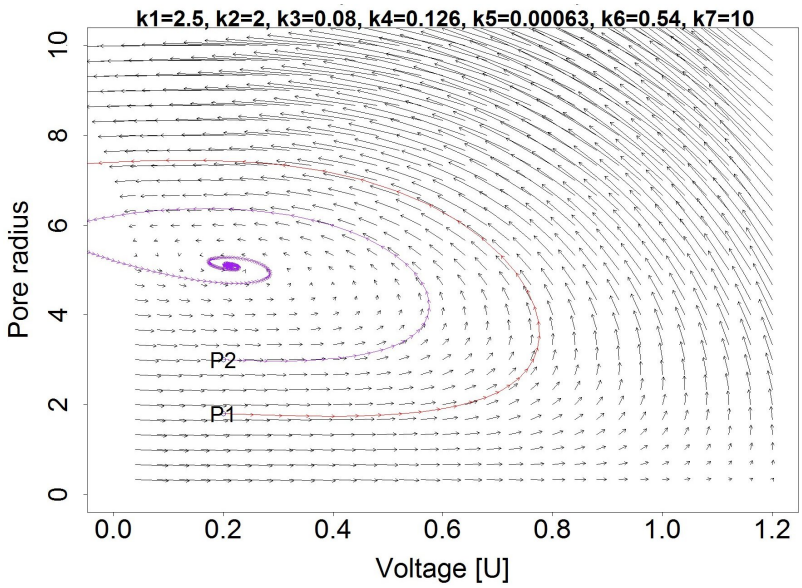

In figures B.1, B.1 and B.1 the variable κ_2 is varied. κ_1 = and κ_3 = are fixed.
In figures B.1, B.1 and B.2 the variable κ_3 is varied. κ_1 = and κ_2 = are fixed.

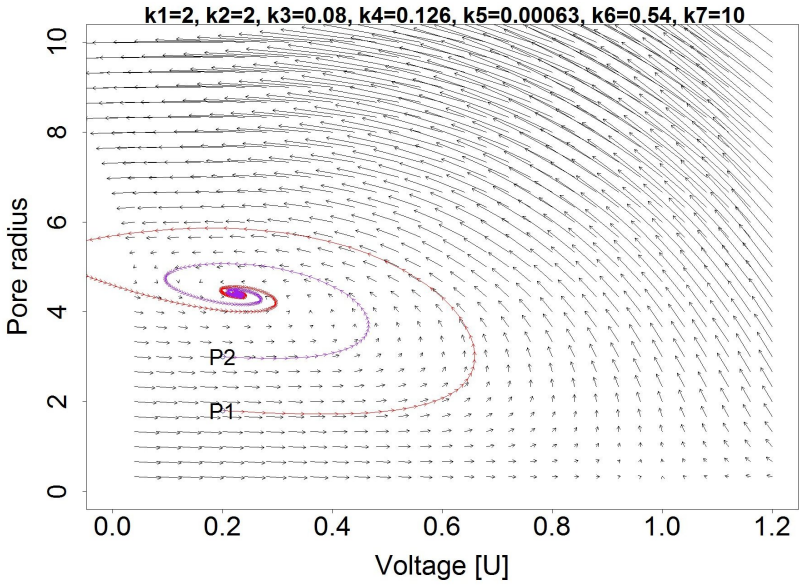

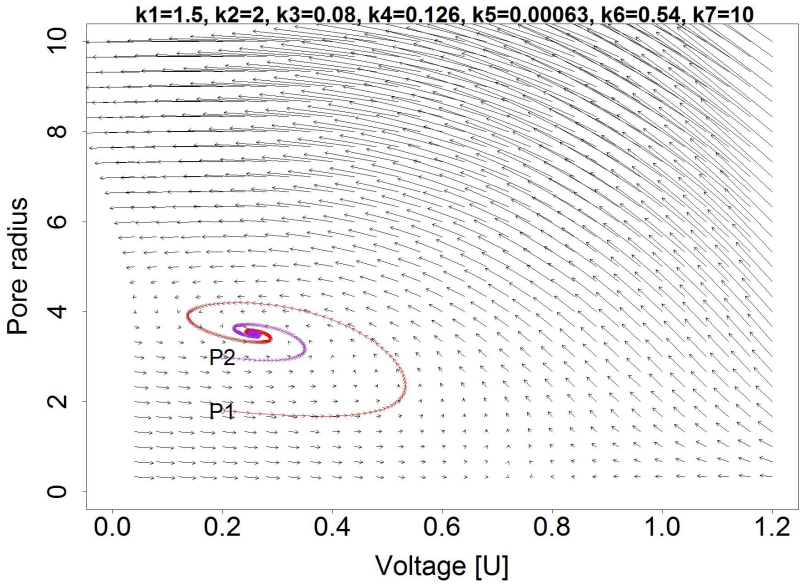

B.2 From stable node to limit cycle

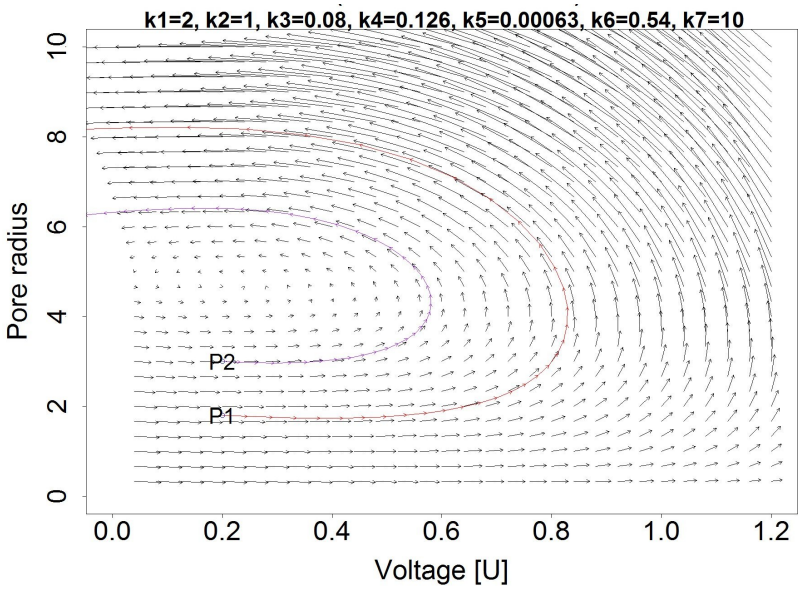
k1=2, k2=1, k3=0.08, k4=0.126, k5=0.00063, k6=0.54, k7=10
Pore radius
Voltage [U]
P2
P1
0
2
4
6
8
10
0.0
0.2
0.4
0.6
0.8
1.0
1.2

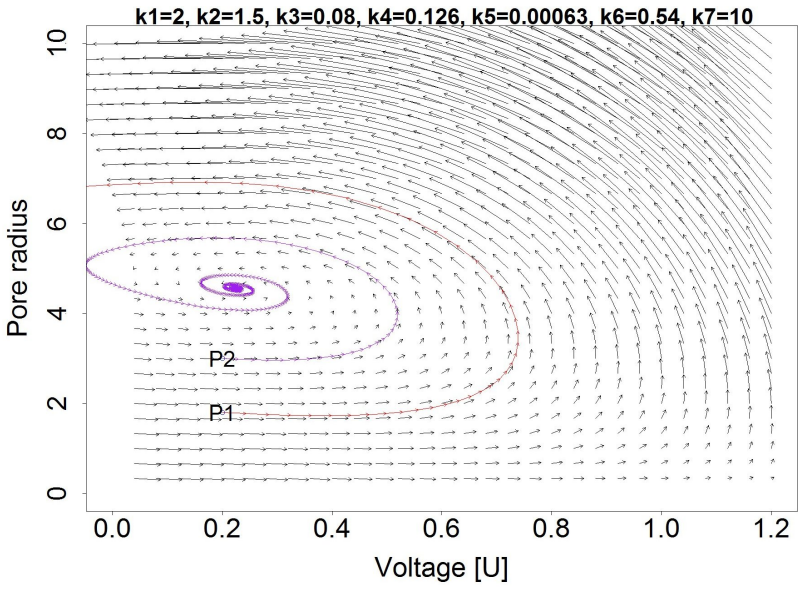
k1=2, k2=1.5, k3=0.08, k4=0.126, k5=0.00063, k6=0.54, k7=10
Pore radius
Voltage [U]
P2
P1
0
2
4
6
8
10
0.0
0.2
0.4
0.6
0.8
1.0
1.2

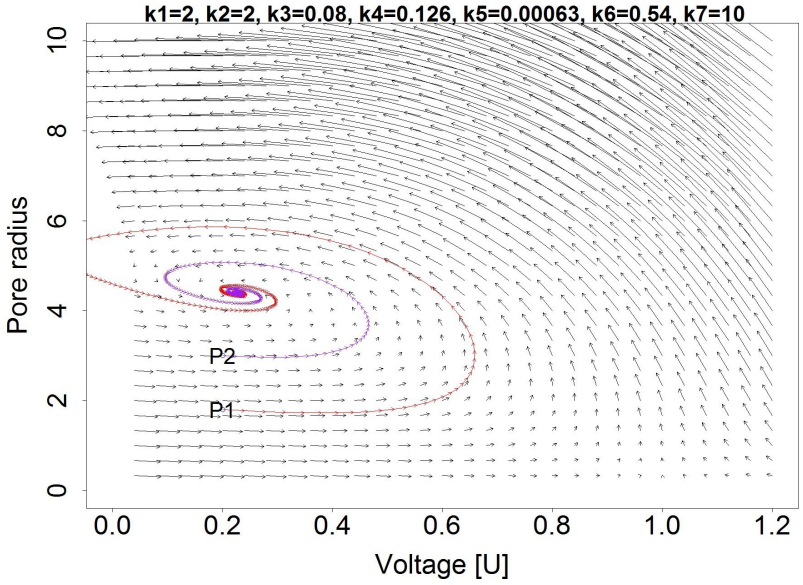
k1=2, k2=2, k3=0.08, k4=0.126, k5=0.00063, k6=0.54, k7=10
Pore radius
0
2
4
6
8
10
P2
P1
0.0
0.2
0.4
0.6
0.8
1.0
1.2
Voltage [U]

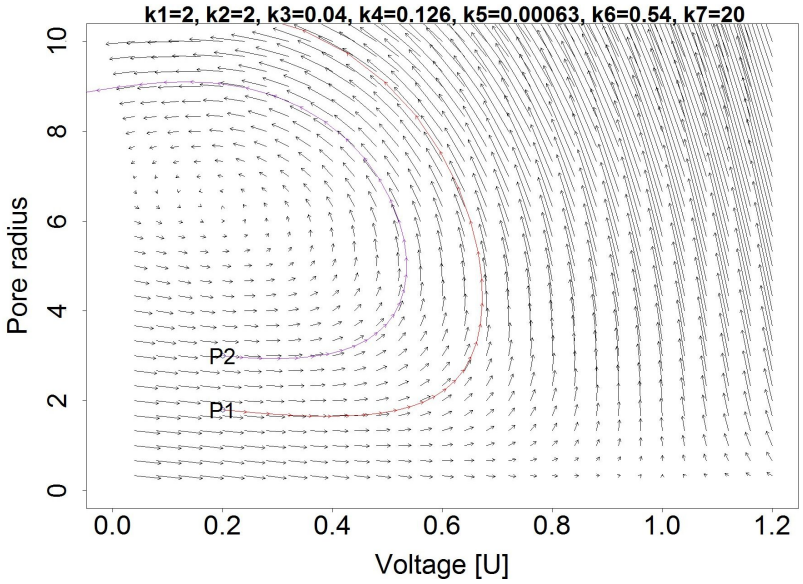
k1=2, k2=2, k3=0.04, k4=0.126, k5=0.00063, k6=0.54, k7=20
Pore radius
0
2
4
6
8
10
P2
P1
0.0
0.2
0.4
0.6
0.8
1.0
1.2
Voltage [U]

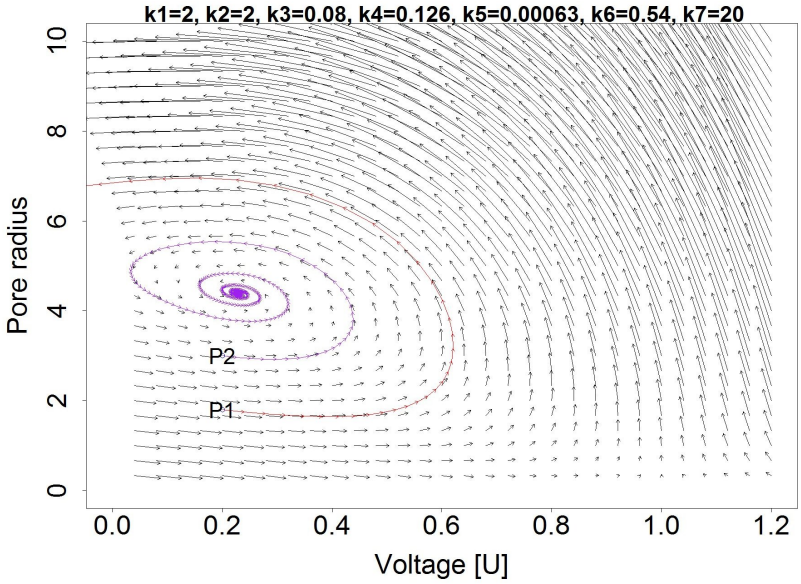
k1=2, k2=2, k3=0.08, k4=0.126, k5=0.00063, k6=0.54, k7=20
Pore radius
Voltage [U]
P2
P1
0
2
4
6
8
10
0.0
0.2
0.4
0.6
0.8
1.0
1.2

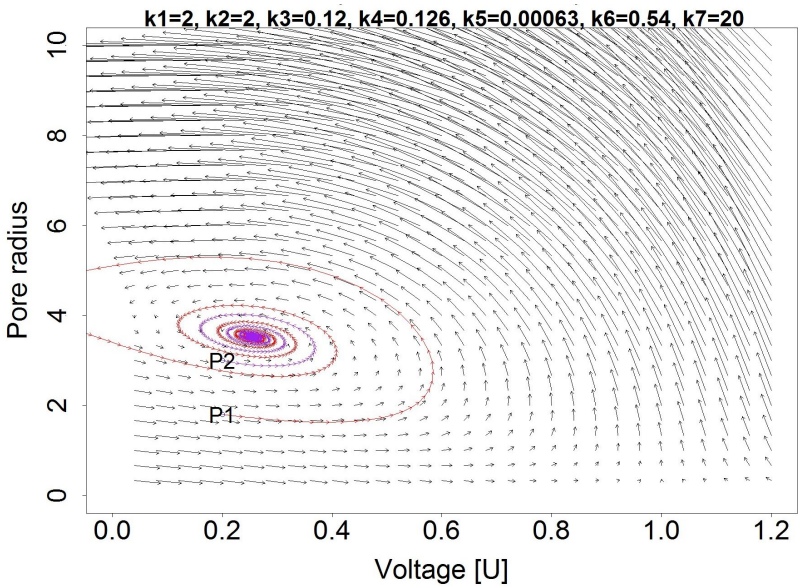
k1=2, k2=2, k3=0.12, k4=0.126, k5=0.00063, k6=0.54, k7=20
Pore radius
Voltage [U]
P2
P1
0
2
4
6
8
10
0.0
0.2
0.4
0.6
0.8
1.0
1.2

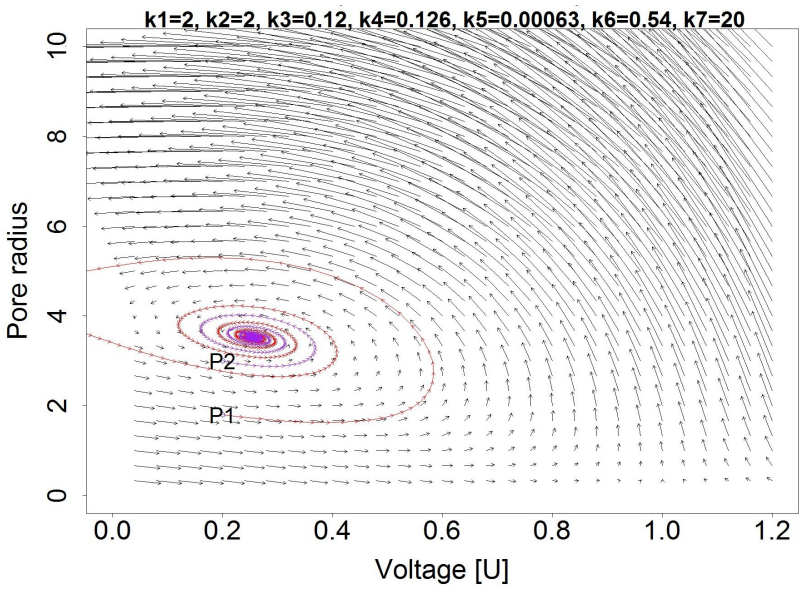
k1=2, k2=2, k3=0.12, k4=0.126, k5=0.00063, k6=0.54, k7=20
Pore radius
0
2
4
6
8
10
P2
P1
0.0
0.2
0.4
0.6
0.8
1.0
1.2
Voltage [U]

Bibliography

[Abidor et al., 1979] Abidor, I. G., Arakelyan, V. B., Chernomordik, L. V., Chizmadzhev, Y. A., Pastushenko, V. F., and Tarasevich, M. R. (1979). Electrical breakdown of bimolecular lipid membranes as an electromechanical instability. *J. Electroanal. Chem.*, 104:37–52.

[Anthony et al., 1981] Anthony, F. H., Biltonen, R. L., and Freire, E. (1981). Modification of a vibrating-tube density meter for precise temperature scanning. *Analytical Biochemistry*, 116(1):161 – 167.

[Antonov, 1982] Antonov, V. F. (1982). Lipids and ionic permeability of membranes. *Nauka, Moscow*. in Russian.

[Antonov et al., 2003] Antonov, V. F., Anosov, A. A., Norik, V. P., Korepanova, E. A., and Smirnova, E. Y. (2003). Electrical capacitance of lipid bilayer membranes of hydrogenated egg lecithin at the temperature phase transition. *European Biophysics J.*, 32:55 – 59.

[Antonov et al., 2005] Antonov, V. F., Anosov, A. A., Norik, V. P., and Smirnova, E. Y. (2005). Soft perforation of planar bilayer lipid membranes of dipalmitoylphosphatidylcholine at the temperature of the phase transition from the liquid crystalline to the gel state. *Biophysical J.*, 34:155–162.

[Antonov et al., 1980] Antonov, V. F., Petrov, V. V., Molnar, A. A., Predvoditelev, D. A., and Ivanov, A. S. (1980). The appearence of single-ion channels in unmodified lipid bilayer membranes at the phase transition temperature. *Nature*, 283:585–586.

[Benz and Hancock, 1981] Benz, R. and Hancock, R. E. W. (1981). Properties of the large ion permeable pore formed by protein f of pseudomonas aeruginosa in lipid bilayer membranes. *Biochim. Biophys. Acta.*, 646:298 – 308.

[Blicher et al., 2009] Blicher, A., Wodzinska, K., Fidorra, M., Winterhalter, M., and Heimburg, T. (2009). The temperature dependence of lipid membrane permeability, its quantized nature, and the influence of anesthetics. *Biophysical J.*, 96:4581–4591.

[Böckmann et al., 2008] Böckmann, R. A., de Groot, B. L., Kakorin, S., Neumann, E., and Grubmüller, H. (2008). Kinetics, statistics, and energetics of lipid membrane electroporation studied by molecular dynamics simulations. *Biophysical J.*, 90:1837–1850.

[Caterina et al., 1997] Caterina, M. J., Schumacher, M. A., Tominaga1, M., Rosen, T. A., Levine, J. D., and Julius, D. (1997). The capsaicin receptor: a heat-activated ion channel in the pain pathway. *Nature*, 389:816–824.

[Cecchi et al., 1982] Cecchi, X., Bull, R., Franzoy, R., Coronado, R., and Alvarez, O. (1982). Probing the pore size of the hemocyanin channel. *Biophysical Chemistry*, 693:173 – 176.

[Chen et al., 2006] Chen, C., Smye, S. W., Robinson, M. P., and Evans, J. A. (2006). Membrane electroporation theories: a review. *Med Biol Eng Comput*, 44:5–14.

[Colombini, 1980] Colombini, M. (1980). Pore size and properties of channels from mitochondria isolated from neurospora crussa. *J. Membr. Biol.*, 53:79 – 84.

[Crowley, 1973] Crowley, J. M. (1973). Electrical breakdown of bimolecular lipid membranes as an electromechanical instability. *Biophysical J.*, 13.

[Dimitrov, 1984] Dimitrov, D. S. (1984). Electric field-induced breakdown of lipid bilayers and cell membranes: A thin viscoelastic film model. *Journal of Membrane Biology*, 78:53 – 60.

[Ebel et al., 2001] Ebel, H., Grabitz, P., and Heimburg, T. (2001). Enthalpy and volume changes in lipid membranes. i. the proportionality of heat and volume changes in the lipid melting transition and its implication for the elastic constants. *J. Phys. Chem.*, 105:7353 – 7360.

[Eldridge and Morowitz, 1978] Eldridge, C. A. and Morowitz, H. J. (1978). A hydrodynamic theory of ion conductance through ohmic pores. *Journal of Theoretical Biology*, 73:539–548.

[Evans, 1974] Evans, E. A. (1974). Bending resistance and chemically induced moments in membrane bilayers. *Biophys. J*, 14:923–931.

[Fidorra, 2004] Fidorra, M. (2004). *Untersuchung des Phasenverhaltens von Membranen durch konfokale Mikroskopie und Kalorimetrie*. PhD thesis, Institut für Schwingungsphysikder Georg-August-Universität zu Göttingen. In german.

[Finkelstein, 1987] Finkelstein, A. (1987). Water movement through lipid bilayers, pores, and plasma membranes. theory and reality. *John Wiley*.

[Freeman et al., 1994] Freeman, S. A., Wang, M. A., and Weaver, J. C. (1994). Theory of electroporation of planar bilayer membranes: predictions of aqueous area, change in capacitance and pore-pore separation. *Biophysical J.*, 67:42 – 56.

[Glaser et al., 1988] Glaser, R. W., Leikin, S. L., Chernomordik, L. V., Pastushenko, V. F., and Sokirko, A. I. (1988). Reversible electrical breakdown of lipid bilayers: formation and evolution of pores. *Biochemica et Biophysica*, 940:275–287.

[Grabitz et al., 2002] Grabitz, P., Ivanova, V. P., and Heimburg, T. (2002). Relaxation kinetics of lipid membranes and its relation to the heat capacity. *Biophysical J.*, 82:299–309.

[Græsbøll, 2006] Græsbøll, K. (2006). Function of nerves - action of anesthetics. *Gamma*, 143:27 – 36.

[Hallock, 1900] Hallock, W. (1900). Kleiner leitfaden der praktischen physik. *Science*, 117:484.

[Hanke et al., 1984] Hanke, W., Methfessel, C., Wilmsen, U., and Boheim, G. (1984). Channel reconstitution into lipid bilayer membranes on glass patch pipettes. *Bioelectrochem Bioenerg*, 12:329–339.

[Haydon, 1971] Haydon, D. A. (1971). In permeability and function of biological membranes. *North Holland Publishing Company,*, 185.

[Heimburg, 1998] Heimburg, T. (1998). Mechanical aspects of membrane thermodynamics. estimation of the mechanical properties of lipid membranes close to the chain melting transition from calorimetry. *Biochimica et Biophysica Chemistry*, 1415:147–162.

[Heimburg, 2008] Heimburg, T. (2008). Biophysics of nerves - biophysics 4. Lecture notes by T. Heimburg for the course: "Biophysics of nerves".

[Heimburg, 2010a] Heimburg, T. (2010a). Biophysics of membranes - biophysics 2. Lecture notes by T. Heimburg for the course: "Biophysics of membranes".

[Heimburg, 2010b] Heimburg, T. (2010b). Review: Lipid ion channels. *arXiv*, 1001.2524v1.

[Heimburg and Jackson, 2007] Heimburg, T. and Jackson, A. D. (2007). The thermodynamics of general anesthesia. *Biophys. J.*, 92:3159–3165.

[Helfrich, 1973] Helfrich, W. (1973). Elastic properties of lipid bilayers: Theory and possible experiments. *Z. Naturforsch.*, 28:693–703.

[Hill, 1960] Hill, T. L. (1960). *An Introduction to Statistical Thermodynamics*. Dover Publications.

[Hille, 1972] Hille, B. (1972). The permeability of sodium channel to metal cations in myelinated nerve. *J. Gen. Physiol.*, 59:637 – 658.

[Hodgkin and Huxley, 1952] Hodgkin, A. L. and Huxley, A. F. (1952). A quantitative description of membrane current and its application to conduction and exitation in nerve. *J. Physiol.*, 117:500–544.

[Israelachvili and Pashley, 1984] Israelachvili, J. N. and Pashley, R. M. (1984). Measurement of the hydrophobic interaction between two hydrophobic surfaces in aqueous electrolyte solutions. *J. Coll. Interface Sci.*, 98:500–514.

[Joshi et al., 2002] Joshi, R. P., Hu, Q., Schoenbach, K. H., and Hjalmarson, H. P. (2002). Improved energy model for membrane electroporation in biological cells subjected to electrical pulses. *PHYSICAL REVIEW E*, 65:041920.

[Joshi and Schoenbach, 2000] Joshi, R. P. and Schoenbach, K. H. (2000). Electroporation dynamics in biological cells subjected to ultrafast electrical pulses: A numerical simulation study. *PHYSICAL REVIEW E*, 62(1):1025 – 1033.

[Krasilnikov et al., 1992] Krasilnikov, O., Sabirov, R., Ternovsky, V., Merzliak, P., and Muratkhodjaev, J. (1992). A simple method for the determination of the pore radius of ion channels in planar lipid bilayer membranes. *FEMS Microbiology Immunolog*, 105:93–100.

[Lee and Kosterlitz, 1991] Lee, J. and Kosterlitz, J. M. (1991). Finite-size scaling and monte carlo simulations of first-order phase transitions. *Phys. Rev. B*, 43:3265–3277.

[Leirer et al., 2009] Leirer, C., Wunderlich, B., Myles, V., and Schneider, M. (2009). Phase transition induced fission in lipid vesicles. *Biophysical Chemistry*, 143(1-2):106 – 109.

[Levitt, 1984] Levitt, D. G. (1984). Kinetic of movement in narrow channels. *Membrane Transport*, 21:181–197.

[Lewis and Engelman, 1983] Lewis, B. and Engelman, D. M. (1983). Lipid bilayer thickness varies linearly with acyl chain length in fluid phosphatidylcholine vesicles. *J. Mol. Biol.*, 166:211–217.

[Litster, 1975] Litster, J. D. (1975). Stability of lipid bilayers and red blood cell membranes. *Physics Letters*, 53A(3):193–194.

[Marcelja, 1977] Marcelja (1977). *Croat. Chem.*, 49:347–350.

[Melikov et al., 2001] Melikov, K. C., Frolov, V. A., Shcherbakov, A., Samsonov, A. V., Chizmadzhev, Y. A., and Chernomordik., L. V. (2001). Voltage-induced nonconductive pre-pores and metastable single pores in unmodified planar lipid bilayer. *Biophysical J.*, 80:1829 – 1836.

[Nagle and Scott, 1978] Nagle, J. and Scott, H. (1978). Lateral compressibility of lipid mono- and bilayers theory of membrane permeability. *Biochimica et biophysica*, 513:236–243.

[Needham and Hochmuth, 1989] Needham, D. and Hochmuth, R. M. (1989). Electromechanical permeabilization of lipid vesicles. *Biophysical Journal*, 55:1001–1009.

[Neher and Sakmann, 1976] Neher, E. and Sakmann, B. (1976). Single-channel currents recorded from membrane of denervated frog muscle fibres. *Nature*, 260:799–802.

[Neumann and Rosenheck, 1972] Neumann, E. and Rosenheck, K. (1972). Permeability changes induced by electric impulses in vesicular membranes. *J. Membrane Biol.*, 10:279–290.

[Neumann et al., 1982] Neumann, E., Schaefer-Ridder, M., Wang, Y., and Hofschneider, P. H. (1982). Gene transfer into mouse lyoma cells by electroporation and electroporative delivery of drugs and genes. *EMBO J.*, 1:841–845.

[Overton, 1901] Overton, A. (1901). Studien über die narkose. *Fischer, Jena*.

[Pakhomov et al., 2009] Pakhomov, A. G., Bowman, A. M., Ibey, B. L., Andre, F. M., Pakhomova, O. N., and Schoenbach, K. H. (2009). Lipid nanopores can form a stable, ion channel-like conduction pathway in cell membrane. *Biochemical and Biophysical Research Communications*, 385(1-2):181 – 186.

[Papahadjopoulos et al., 1973] Papahadjopoulos, D., Jacobson, K., Nir, S., and Isac, T. (1973). Phase transitions in phospholipid vesicles fluorescence polarization and permeability measurements concerning the effect of temperature and cholesterol. *Biochimica et Biophysica*, 311:330–348.

[Parsegian, 1969] Parsegian, A. (1969). Energy of an ion crossing a low dielectric membrane: Solutions to four relevant electrostatic problems. *Nature*, 221:844 – 846.

[Petrov et al., 1980] Petrov, A. G., Mitov, M. D., and Derzhnansky, A. I. (1980). The appearence of single-ion channels in unmodified lipid bilayer membranes at the phase transition temperature. *Nature*, 283:585–586.

[Rand, 1981] Rand, R. P. (1981). Interacting phospholipid bilayers: measured forces and induced structural changes. *Annu Rev Biophys Bioeng*, 10:277 – 314.

[Seeger et al., 2007] Seeger, H. M., Gudmundsson, M. L., and Heimburg, T. (2007). How anesthetics, neurotransmitters, and antibiotics influence the relaxation processes in lipid membranes. *J. of Physical chemistry B*, 111:13858–13866.

[Singer and Nicolson, 1972] Singer, S. J. and Nicolson, G. L. (1972). The fluid mosaic model of the structure of cell membranes. *Science*, 18:720 – 731.

[Sowers, 1986] Sowers, A. E. (1986). A long-lived fusogenic state is induced in erythrocyte ghosts by electric pulses. *J. Cell Biol.*, 102:1358–1362.

[Stulen, 1981] Stulen, G. (1981). Electric field effects on lipid membrane structure. *Biochimica et Biophysica*, 640:621–627.

[Sugar, 1979] Sugar, I. P. (1979). A theory of the electric field-induced phasetransition of phospholipid bilayers. *Biochim Biophys Acta*, 556:72–85.

[Sugar and Neumann, 1984] Sugar, I. P. and Neumann, E. (1984). Stochastic model for electric field-induced membrane pores electroporation. *Biophysical Chemistry*, 19:211–225.

[Taupin et al., 1975] Taupin, C., Dvolaitzky, M., and Sautery, C. (1975). Osmotic pressure-induced pores in phospholipid vesicles. *Biochemistry*, 14:4771–4775.

[Tien and Ottova, 2003] Tien, H. and Ottova, A. (2003). The bilayer lipid membrane (blm) under electrical fields. *Dielectrics and Electrical Insulation*, 10:717 – 727.

[Tsong and Kanehisa, 1977] Tsong, T. Y. and Kanehisa, M. I. (1977). Relaxation phenomena in aqueous dispersions of synthetic lecithins. *Biochemistry*, 16(12):2674–2680.

[Weaver and Chizmadzhev, 1996] Weaver, J. C. and Chizmadzhev, Y. A. (1996). *Handbook of Biological effects of Electromagnetic Fields*, pages 247–256. CRC Press inc., 8. edition.

[Wilhelm et al., 1993] Wilhelm, C., Winterhalter, M., Zimmermann, U., and Benz, R. (1993). Kinetics of pore size during irreversible electrical breakdown of lipid bilayer membranes. *Biophysical J.*, 64:121–128.

[Wintherhalter and Helfrich, 1987] Wintherhalter, M. and Helfrich, W. (1987). Effects of voltage on pores in membranes. *Physical Review*, 36.

[Wodzinska, 2008] Wodzinska, K. (2008). Pores in lipid membranes and the effect of anaesthetics. Master's thesis, Niels Bohr Institute, University of Copenhagen.

[Wodzinska et al., 2009] Wodzinska, K., Blicher, A., and Heimburg, T. (2009). The thermodynamics of lipid ion channel formation in the absence and presence of anesthetics. blm experiments and simulations. *arXiv:09022271v2*.

[Woodbury, 1989] Woodbury, D. J. (1989). Pure lipid vesicles can induce channel-like conductance in planar bilayers. *J. Membrane Biol.*, 109:145–150.

[Wunderlich et al., 2009] Wunderlich, B., Leirer, C., Idzko, A. L., Keyser, U. F., Wixforth, A., Myles, V. M., Heimburg, T., and Schneider, M. F. (2009). Phase-state dependent current fluctuations in pure lipid membranes. *Biophysical J.*, 96:4592–4597.

[Yafuso et al., 1974] Yafuso, M., Kennedy, S. J., and Freeman, A. R. (1974). Spontaneous conductance changes, multilevel conductance states and negative differential resistance in oxidized cholesterol black lipid membranes. *J. Membrane Biol.*, 212:201–212.